

**IMPACT ON THE POWER SYSTEM  
WITH A LARGE PENETRATION OF  
PHOTOVOLTAIC GENERATION**

*A thesis submitted to*

**THE UNIVERSITY OF MANCHESTER INSTITUTE  
OF SCIENCE AND TECHNOLOGY**

*for the degree of*

**DOCTOR OF PHILOSOPHY**

*by*

**YUN TIAM TAN**

Department of Electrical Engineering and Electronics

UMIST

FEBRUARY 2004

## **Declaration**

No portion of the work referred to in this thesis has been submitted in support of an application for another degree or qualification of this or any other university, or institution of learning

## **Dedication**

I dedicate this work to Yen Siang and my parents

## **Acknowledgement**

I wish to express my gratitude to my supervisor, Professor Daniel Kirschen, who gave me valuable advice, excellent guidance and continuous encouragement throughout my research. I wish to extend my thanks to my advisor, Professor Nick Jenkins for his valuable comments and advice during the course of this project.

I wish to express my special thanks to my colleague J.C. Ausin for his valuable suggestion and discussion throughout the project. Special thanks also to Dr. A. Arulampalam, Dr. V. K. Ramachandaramurthy and Dr. C. Prapanavarat for their assistance in running the experiment rig throughout the project.

I wish to acknowledge the ORS for awarding me scholarship for university fee. I wish to extend my acknowledgement to Engineering and Physical Sciences Research Council (EPSRC), National Grid Company (NGC), Department of Trade and Industry (DTI) and Future Energy Solutions (FES) for providing financial support throughout the project.

I would like to express my appreciation to all my friends, and particularly to Dejan Melovic, Predja Djapic, Danny Pudjianto, Soon Kiat Yee and Chee Yong Chen for their encouragement.

Last but not least my gratitude goes to Yen Siang, parents and family members for their love, moral support and understanding.

## **Abstract**

The research investigated the impact on the power system with a large penetration of photovoltaic (PV) generation. The characteristic of photovoltaic generation was first described. Its associated operating behaviour and associated control were explained. A model of PV generation suitable for studying its interactions with the power system was developed. The model of PV generation was built on the basis of experimental results. The results were used to validate the simulation results obtained from the PV generation model that was developed.

The dynamic response of a PV generation system to rapid changes in irradiance was investigated. An aggregated model of grid-connected PV generation was built and it was used for simulating the integration of PV generation on a large-scale.

Voltage control technique was investigated by simulation. The simulation results were carried out in order to mitigate the negative effects caused by rapid changes in irradiance. Different types of voltage control were investigated using once again, simulation.

The dynamic responses of PV generation when subjected to faults were investigated. The responses of the PV generation to faults that occur in the power system were analysed using simulation results obtained with a dynamic model of a widely used dynamic test system. The simulation of the effect of the characteristics of PV generation, fault impedance, protection parameters of PV generation and fault clearing time were performed and discussed.

The capability of the PV generator to provide frequency response for the power system using electronic control was studied. A new control technique was proposed and built in Simulink<sup>TM</sup>. The way the control of PV generation can be modified to contribute to frequency response was described. The control technique was simulated and the results showed a significant improvement in frequency response.

## Table of Contents

### Chapter 1 – Introduction

1.1 Renewable energy .....	1
1.2 PV generation as a source of renewable energy.....	2
1.3 Research objective.....	3
1.4 Research approach.....	4
1.5 Overview of the chapters.....	5

### Chapter 2 – Characteristic of Photovoltaic Generation

2.1 Introduction.....	7
2.2 Solar irradiance.....	8
2.3 Photovoltaic cell characteristic.....	10
2.3.1 Effect of irradiance and cell temperature.....	13
2.4 Inverter.....	14
2.5 Controller.....	16
2.5.1 Maximum power point tracking controller.....	16
2.5.1.1 Simple panel load matching.....	16
2.5.1.2 Voltage feedback method.....	17
2.5.1.3 Power feedback method.....	19
2.5.1.3.1 Perturbation and observation method.....	19
2.5.1.3.2 Incremental conductance method.....	21
2.5.2 Islanding protection.....	23
2.6 Grid.....	26

### Chapter 3 – A Model of Photovoltaic Generation Suitable for Stability Analysis

3.1 Introduction .....	27
3.2 Methodology.....	28
3.3 Experimental setup.....	28
3.4 Experimental results.....	31
3.5 Model description.....	36

3.5.1 General description.....	36
3.5.2 Flow chart.....	38
3.5.3 PV array characteristic.....	39
3.5.4 Effect of changes in irradiance.....	40
3.5.5 Effect of changes in grid ac voltage.....	43
3.5.6 MPPT.....	44
3.5.7 Model validation.....	44
3.6 Conclusion.....	47
<b>Chapter 4 – Dynamic Response to Rapid Changes in Irradiance</b>	
4.1 Introduction.....	48
4.2 Exploring the problem.....	49
4.3 10-bus test system.....	49
4.4 Integration of PV generation into the test system.....	50
4.5 Simplification of aggregate model of grid connected PV generation.....	52
4.5.1 Uniform solar irradiance distribution.....	53
4.5.2 Non-uniform solar irradiance distribution.....	54
4.6 Case studies.....	55
4.6.1 Simulation results.....	56
4.6.2 Analysis.....	59
4.6.3 Tripping of PV generation.....	59
4.7 Conclusion.....	61
<b>Chapter 5 – Mitigating Voltage Fluctuation due to Photovoltaic Generation</b>	
5.1 Introduction.....	62
5.2 Constant power factor control.....	63
5.3 Automatic voltage control from PV inverter.....	64
5.4 Voltage control from SVC.....	64
5.5 Case studies.....	68
5.5.1 Simulation results.....	68
5.5.1.1 Simulation results of constant power factor control.....	70

5.5.1.2 Simulation results of voltage control from PV generator itself.....	76
5.5.1.3 Simulation results of SVC voltage control.....	78
5.6 Conclusion.....	80

## **Chapter 6 – Impact of Photovoltaic Generation on Transient Stability**

6.1 Introduction.....	82
6.2 Transient stability.....	82
6.3 Response of PV generation to disturbance.....	83
6.3.1 Mechanism causing instability.....	84
6.4 Case studies.....	85
6.4.1 Test system preparation.....	85
6.4.1.1 Steady state load flow.....	86
6.4.1.2 Dynamic modeling.....	87
6.4.2 Simulation results.....	88
6.4.2.1 Level of PV penetrations.....	88
6.4.2.2 Fault impedance.....	95
6.4.2.3 Protection parameters.....	101
6.4.2.1 Fault clearing time.....	105
6.4.3 Analysis of the simulation results.....	111
6.5 Conclusion.....	113

## **Chapter 7 – Frequency Response from Photovoltaic Generation**

7.1 Introduction.....	114
7.2 Frequency control.....	115
7.3 De-loading of PV generator.....	117
7.4 Methodology.....	118
7.5 Implementation of electronic control circuit of frequency response.....	120
7.5.1 $P_{pv}^{freq}$ control block.....	120
7.5.1.1 S&H block.....	121
7.5.1.2 Power-frequency curve block.....	122
7.5.2 $\Delta I_{pv}^{frequency}$ control block.....	123

7.5.3 Implementation of relay with timer.....	124
7.6 Simulation results.....	125
7.7 Case studies.....	126
7.8 Conclusion.....	128
<b>Chapter 8 – Conclusions</b>	
8.1 Summary.....	129
8.2 Further work.....	131
8.2.1 PV generator with different MPPT controller.....	131
8.2.2 Simulation studies with UK system.....	132
8.2.3 Incorporate of the frequency response controller to power system model..	132
8.3 Research impact and benefits to society.....	133
<b>References</b> .....	134
<b>List of publications</b> .....	143
<b>Appendix A1</b> .....	144
<b>Appendix B1</b> .....	147
<b>Appendix B2</b> .....	149
<b>Appendix B3</b> .....	150
<b>Appendix B4</b> .....	151

# Chapter 1

## INTRODUCTION

### 1.1 INTRODUCTION

As a result of human activities, greenhouse gases are increasing in the earth's atmosphere. Many in the scientific community now believe that this increase in carbon dioxide (CO<sub>2</sub>), methane (CH<sub>4</sub>) and other greenhouse gases is causing the earth's temperature to rise, and that this increase in greenhouse gases will lead to even greater global warming during this century.

Renewable energy resources are clean and environmental friendly. They can provide many immediate environmental benefits by avoiding the emission of greenhouse gases and can help conserve fossil resources as electricity supply for future generations. Therefore, the UK government is encouraging the development of renewable energy in the anticipation that it will provide 10% of electrical energy by 2010. The government also aims for a 60% reduction in CO<sub>2</sub> emission by 2050.

## 1.2 PV GENERATION AS A SOURCE OF RENEWABLE ENERGY

One technology to generate electricity in a renewable way is to use solar cells to convert the energy delivered by the solar irradiance into electricity. PV energy generation is the current subject of much commercial and academic interest. Recent work indicates that in the medium to longer term PV generation may become commercially so attractive that there will be large-scale implementation in many parts of the developed world. The European White Paper on Renewable Energy includes a target of 500,000 roofs and facades within Europe in the “Campaign for take off”. In the UK. The Department of Trade and Industry (DTI) has recently announced a major industrial initiative to support photovoltaic energy systems and components. The consultation document issued earlier by the DTI “New and renewable energy, prospects for the 21<sup>st</sup> century” considers building-integrated photovoltaic to be one of the technologies that has longer term potential (after 2010) in the UK if supported by appropriate R&D programmes.

The integration of a large number of embedded PV generators will have far reaching consequences not only on the distribution networks but also on the national transmission and generation system. If the PV generators are built on the roof and sides of buildings, most of them will be located in urban areas and will be electrically close to loads. On the other hand, these PV generating units may be liable to common mode failures that might cause the sudden or rapid disconnection of a large proportion of operating PV capacity. The following modes of failures have been identified: -

- Embedded generation (such as PV units) is normally equipped with protection schemes designed to disconnect it from the network in the even of loss of mains. If the system is affected by a large disturbance (e.g. tripping of the DC link with France or of a large conventional generator), such protection schemes could cause the sudden disconnection of a large proportion of the PV generation. Since this disconnection would be compounded with the original disturbance, its consequence could be severe.
- Similarly, a large disturbance could also temporarily perturb the voltage seen by the PV generating units. The controller of the inverters interfacing these PV units to the

grid system may not be able to cope with this perturbation. Consequently they may fail or trigger a shutdown of the inverter.

- It is likely that a large majority of the PV generating units will be located in dense urban areas. A rapidly moving weather front can, in a matter of a few minutes, reduce the irradiance over such an area from its maximum value to value below the minimum required for operating the PV units. If such a meteorological event were to affect three of Britain's largest metropolitan areas almost simultaneously during a period of rapid load pick up, the grid system would be subjected to a disturbance that it may have difficulties to overcome.

Since all these phenomena involve an interaction between conventional and PV generation through the transmission network, their analysis requires system studies using power system models. Through these studies it will be possible to determine whether credible disturbances could lead to voltage collapse over parts of the system or to steady state instabilities.

### **1.3 RESEARCH OBJECTIVE**

This thesis investigates the impact of PV generation on the steady state and dynamic behaviour of power systems. The aim of the research can be summarized as:

*To investigate the impact on the power system of a large penetration of grid- connected PV penetration and to develop measures to mitigate the negative effects, if any.*

In order to achieve the aim, a number of objectives have been defined and each of these objectives has its own sub-objectives.

The first objective of this research is to clarify the characteristics of grid connected PV generation by analysing qualitatively their behaviour. A better understanding of the operating characteristic of the solar cell, of the inverter and of their associated controller should be the outcomes of this task.

The second objective is to investigate whether dynamic models of PV generators that can be incorporated into models of a power system suitable for dynamic simulation are available. If no suitable model is found, then a new model should be developed.

The third objective of this research is to incorporate the PV generator model into a power system model to investigate the impact of sudden changes in irradiance, e.g. a change due to a passing cloud. The objective could be met by carrying out simulation studies and analysing the results obtained.

The fourth objective is very dependent on the results obtained from the third objective. If any negative effects due to the sudden change in irradiance are observed, suggestions and measures to mitigate these effects should be identified.

The fifth objective is to apply the developed model to draw more quantitative conclusions with respect to the impact of PV generator on power system dynamics. The transient studies on power system model are carried out and the objective is achieved by acquiring and analyzing the simulation results obtained.

The sixth objective is to investigate the possibility of the PV generators involving themselves in the operation of power system by contributing to frequency control.

#### **1.4 RESEARCH APPROACH**

The overall approach taken to reach the research objectives was to investigate the behaviour of the PV generation, to develop models of PV generation, to connect these PV generation model to models of a power system, to compare the responses of power system with various penetration of PV generation and to explain the observations from the working principle of the PV generation types and the characteristics of their interaction with the power system.

It proved necessary to investigate the various types of control of PV generation on the market separately, because it turned out that the impact of an increasing PV penetration on the dynamics of the power system was not identical for all PV generation types, but

varied between them due to the differences in the operation of their controller. It was hence impossible to draw conclusions with respect to the impact of an increasing PV power penetration in general and the conclusions had to be qualified by the type of PV generator control being used.

The widely used power system dynamics simulation program Eurostag<sup>TM</sup> (version 4.1) was used for a large part of this research. At the start of research project, it was quickly found that no PV generator models were included in the standard model library of this program. Further study showed that at that time, this also applied to other dynamics simulation packages, and that PV generator models complying with the assumptions and approaches on which power system dynamics simulation software packages are based, could not even be found in the literatures. It was therefore inevitable to develop a PV generator model suitable for use with power system dynamic simulation packages.

## 1.5 OVERVIEW OF THE CHAPTERS

**Chapter 2** describes the characteristic of photovoltaic generation. Its operating behaviour and associated control are discussed.

**Chapter 3** describes a model of PV generation suitable for studying its interactions with the power system. The methodology of developing the model of PV generation is described. Experiments were performed and the results were used to validate the PV generation model that was developed.

**Chapter 4** discusses the dynamic response of a PV generation system to rapid changes in irradiance. An aggregate model of grid-connected PV generation was built and was used for simulating the integration of PV generation on a large-scale.

The voltage control technique is investigated by simulation in **chapter 5**. The simulation results are carried out in order to mitigate the negative effects caused by rapid changes in irradiance as described in Chapter 4. Different types of voltage control technique were investigated using once again, simulation.

**Chapter 6** explains the dynamic responses of PV generation when subjected to faults. The responses of the PV generation to faults that occur in the power system were analysed using simulation results obtained with a dynamic model of a widely used dynamic test system. The simulation of the effect of the characteristics of PV generation, fault impedance, protection parameters of PV generation and fault clearing time were performed and discussed.

In **chapter 7** the capability of the PV generator to provide frequency response for the power system using electronic control is studied. A new control technique was proposed and built in Simulink<sup>TM</sup>. This chapter describes how the control of PV generation can be modified to contribute to frequency response. The control technique was simulated and the results showed a significant improvement in frequency response.

In **chapter 8**, the conclusions from the research project are summarized and topics for further research are outlined.

# Chapter 2

## CHARACTERISTIC OF PHOTOVOLTAIC GENERATION

### 2.1 INTRODUCTION

Photovoltaic (PV) systems convert light energy into electricity. The term photo is from the Greek which mean “light”. “Volt” is named for Alessandro Volta (1745-1827), a pioneer in the study of electricity. PV is then could literally mean “light-electricity”. [1]

A grid connected PV system converts sunlight directly into ac electricity. The main purpose of the system is to reduce the electrical energy imported from the electric utility. Figure 2.1 shows a functional diagram of the basic configuration of a grid-connected PV system. The dc output current of the PV array  $I_{pv}$  is converted into ac and injected into the grid through an inverter. The controller of this inverter implements all the main control and protection functions:- Maximum Power Point Tracking (MPPT), protection relay and detection of islanding operation.

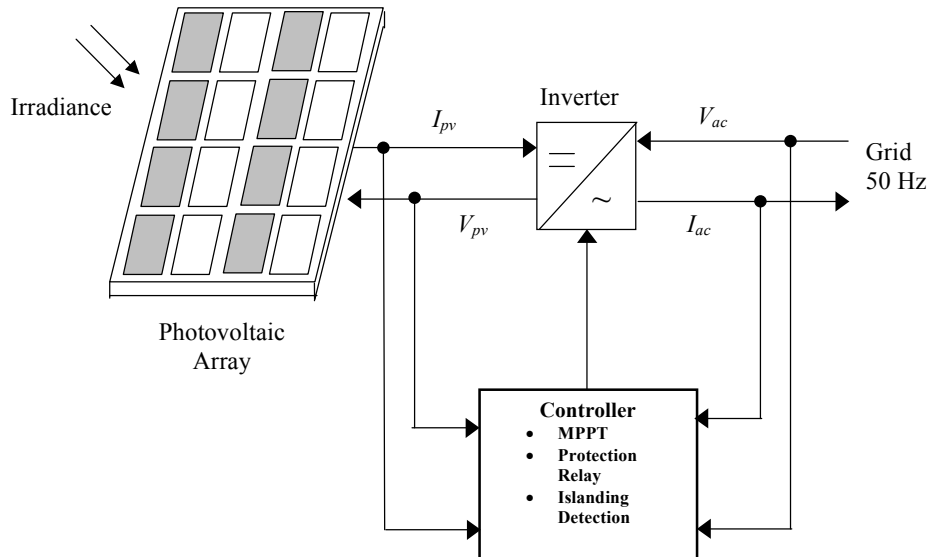


Figure 2.1: Basic configuration of grid connected PV generation

## 2.2 SOLAR IRRADIANCE [2,3]

Solar irradiance is the radiant power incident per unit area upon a surface. It is usually expressed in  $\text{W}/\text{m}^2$ . Radiant power is the rate of flow of electromagnetic energy. Sunlight consists of electromagnetic waves composed of photons at different energies, which travel at constant speed. Solar radiation has a wave like characteristic with the wavelength ( $\lambda$ ) inversely proportional to the photon energy (E).

$$\lambda = \frac{hc}{E} \quad (2.1)$$

where  $c$  = velocity of light  
 $h$  = Planck's constant

The spectrum of the sunlight is shown in Figure 2.2. The light from the sun has a spectrum close to the light from a black body at a temperature of 5762K. The dotted line shows black body radiation at this temperature. This is in good agreement with the AM0 curve which shows the spectrum outside the earth's atmosphere on a plane perpendicular to the sun at the mean earth-sun distance. The power density outside the earth's atmosphere is  $1367 \text{ W}/\text{m}^2$  and this is known as the solar constant. Air mass refers to the relative path length of the direct solar beam through the atmosphere. The path of the light through the atmosphere is shortest when the sun is at its zenith (perpendicular to

the earth's surface), the path length is 1.0 (AM 1.0) and this gives rise to the AM1 spectrum. Obviously, the sun is not always at the zenith. When the angle of the sun from zenith increases, the air mass increases so that at an angle of  $48.2^\circ$  the air mass is 1.5 and at an angle of  $60^\circ$  the air mass is 2.0 (see Figure 2.3). AM 1.5 has been adopted as the standard sunlight spectrum for terrestrial arrays.

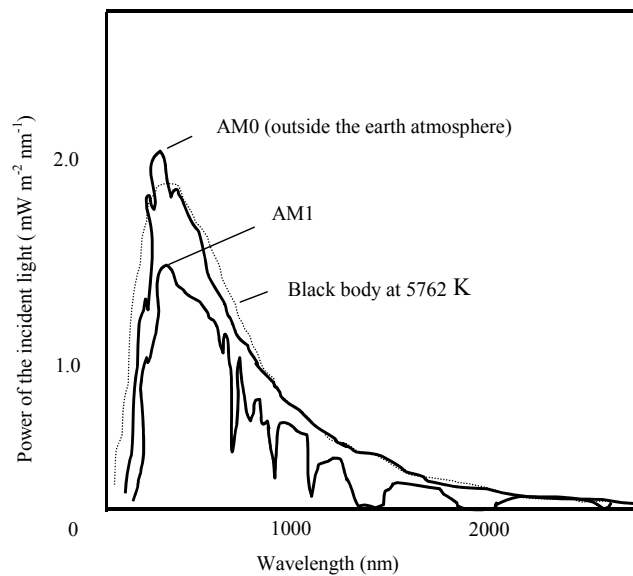


**Figure 2.2: The spectrum of sunlight**

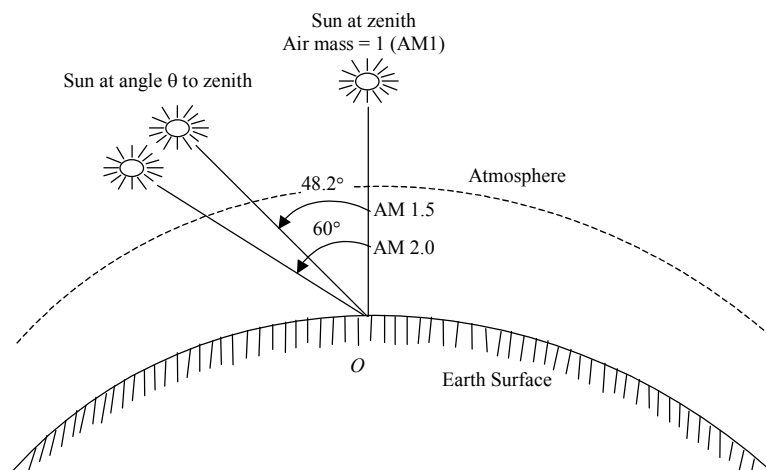


**Figure 2.3: Air mass concept**

Usually, the peak power output of a PV inverter is measured under AM1.5 ( $1\text{kW}/\text{m}^2$ ) sunlight with a junction temperature of  $25^\circ\text{C}$ . This is the so-called standard test condition (STC).

### 2.3 PV CELL CHARACTERISTIC [1, 2]

The equivalent circuit shown in Figure 2.4 and described by Equation 2.2 represents a PV cell:

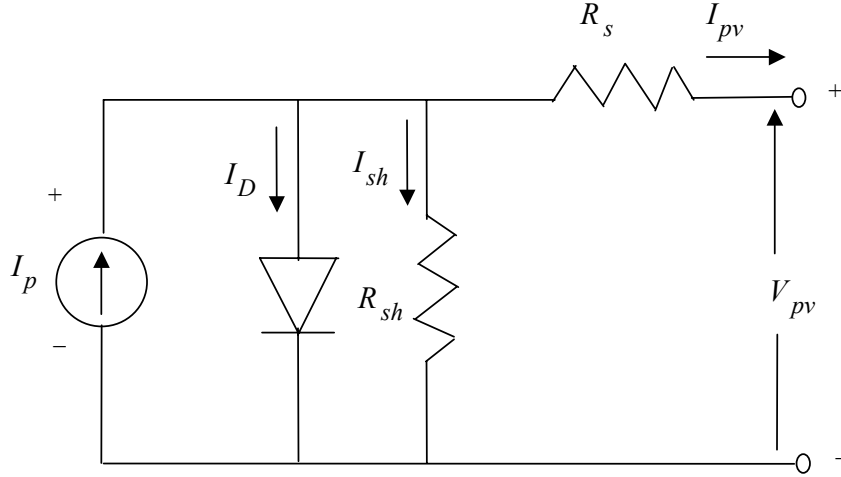


Figure 2.4: PV cell equivalent circuit

$$\begin{aligned}
 I_{pv} &= I_p - I_D - I_{sh} \\
 &= I_p - I_o \left[ e^{\frac{q(V_{pv} + R_s I_{pv})}{NkT}} - 1 \right] - \frac{V_{pv} + R_s I_{pv}}{R_{sh}} \quad (2.2)
 \end{aligned}$$

- where
- $I_p$  = Photocurrent [A]
  - $V_{pv}$  = Terminal voltage of the cell [V]
  - $I_D$  = Diode current [A]
  - $I_o$  = Saturation current [A]
  - $I_{sh}$  = Shunt current [A]
  - $N$  = Ideality factor
  - $q$  = Electron charge [C]
  - $k$  = Boltzmann's constant
  - $T$  = Junction temperature [K]
  - $R_s$  = Series resistance [ $\Omega$ ]
  - $R_{sh}$  = Shunt resistance [ $\Omega$ ]

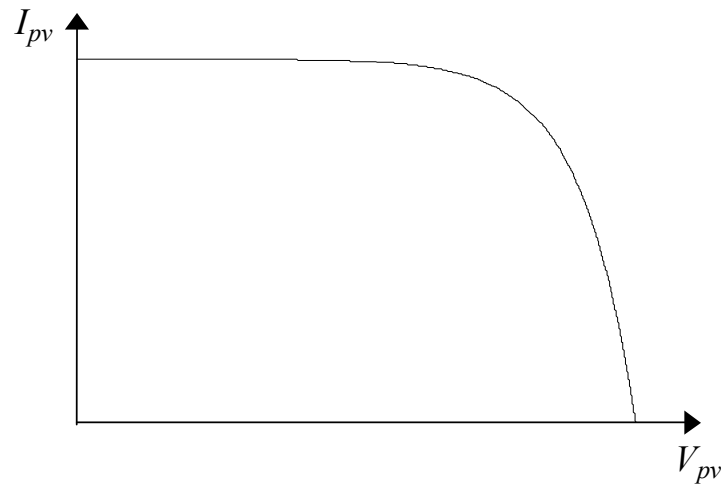


Figure 2.5: Characteristic of PV cell

Figure 2.5 shows the  $I_{pv}$ - $V_{pv}$  operating characteristic of a solar cell. The PV array consists of a number of individual PV cells that are connected together to obtain a unit with a suitable power rating. The characteristic of the PV array can be determined by multiplying the voltage of an individual cell by the number of cells connected in series and multiplying the current by the number of cells connected in parallel. Three important operating points should be noted on Figure 2.6.

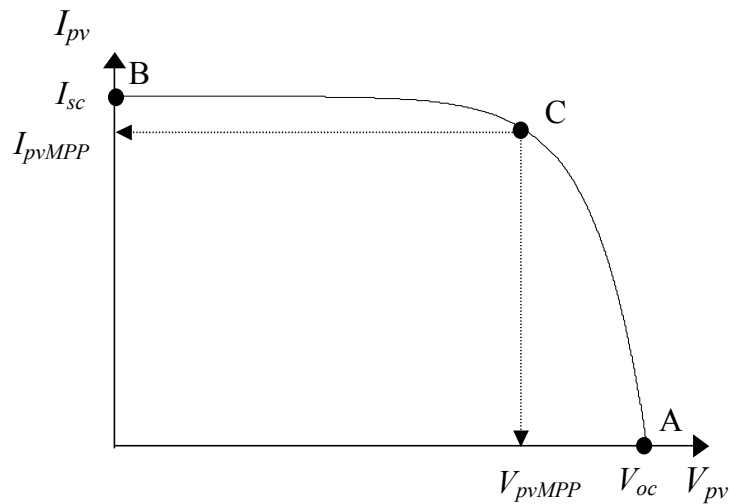


Figure 2.6: PV cell operating point

### Open Circuit Voltage

Voltage at the operating point A on Figure 2.6 is the open circuit voltage. Figure 2.7 shows an open circuit condition with shunt current  $I_{sh}$  neglected. It can be represented by the equation as shown in Equation 2.3.

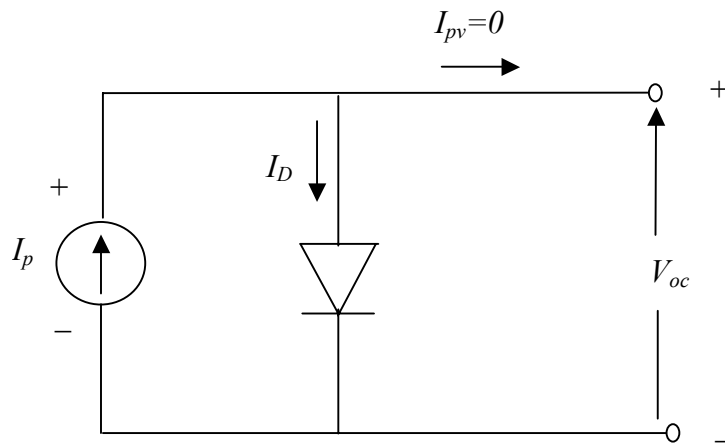


Figure 2.7: Open circuit condition

$$I_p - I_o \left[ e^{\frac{qV_{oc}}{nkT}} - 1 \right] = 0$$

$$V_{oc} = \frac{nkT}{q} \ln \left[ \frac{I_p + I_o}{I_o} \right] \quad (2.3)$$

### Short Circuit Current

Current at the operating point B as shown in Figure 2.6 is the short circuit current. Figure 2.8 shows a short circuit condition with the series resistance  $R_s$  neglected. It can be represented by Equation 2.4.

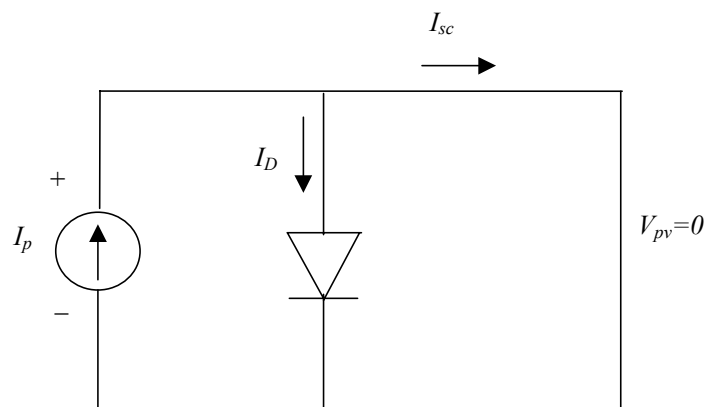


Figure 2.8: Short circuit condition

$$I_{sc} = I_p \quad (2.4)$$

### Maximum Power Point

Under constant irradiance and cell temperature, the operating point of a PV array is determined by the intersection of the  $I_{pv}$ - $V_{pv}$  characteristic and the load characteristic as shown in Figure 2.9. The load characteristic is represented by a straight line with a gradient  $M = I/R = I_{Load}/V_{Load}$ . The system operating point moves along the  $I_{pv}$ - $V_{pv}$  characteristic curve of the PV panel from B to A as the load resistance increase from zero to infinity. Position C is the maximum power operating point. At this point, the area under the  $I_{pv}$ - $V_{pv}$  characteristic curve, which is equivalent to the output power is maximum. If the load resistance is too high, the operating points would be in the CA regions. If the load resistance is too low, the operating points would be in the CB regions. Therefore, the maximum power point can be obtained by matching the load resistance to the PV array characteristics.

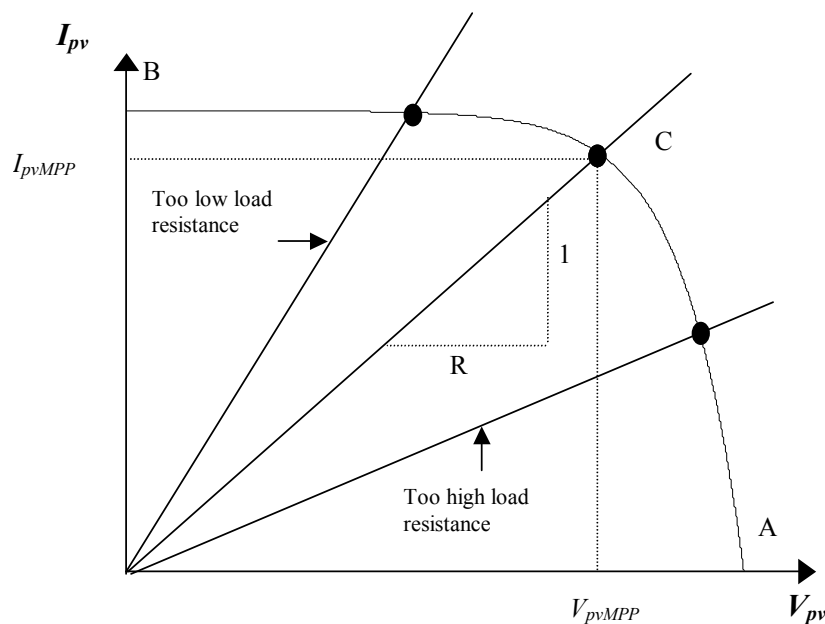
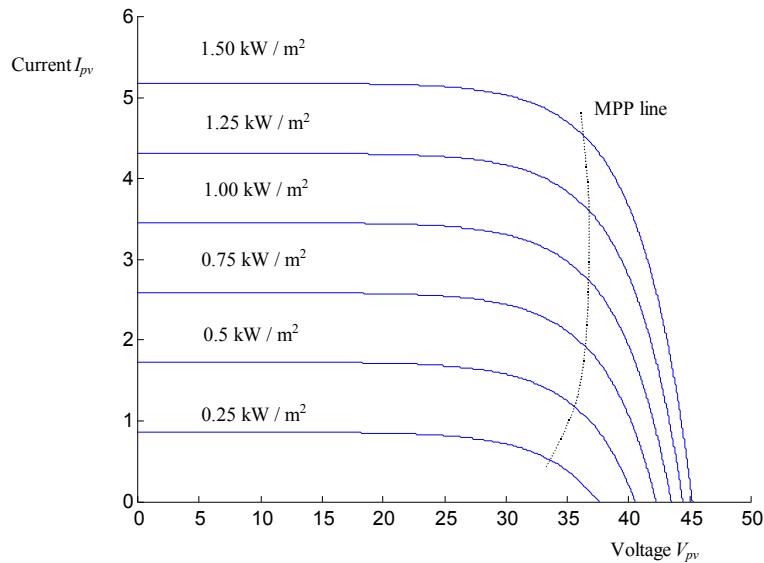


Figure 2.9: Intersection of the  $I_{pv}$ - $V_{pv}$  characteristic curve and the load characteristic

#### 2.3.1 Effect of Irradiance and Cell Temperature[4]

The effect of irradiance and cell temperature on  $I_{pv}$ - $V_{pv}$  characteristic curve is shown in Figure 2.10 and Figure 2.11 respectively. Figure 2.10 shows that the maximum power output varies linearly with the irradiance. Figure 2.11 shows that the maximum output power from the array decreases as the temperature increases.



**Figure 2.10: Effect of irradiance on the I-V characteristic at constant cell temperature**

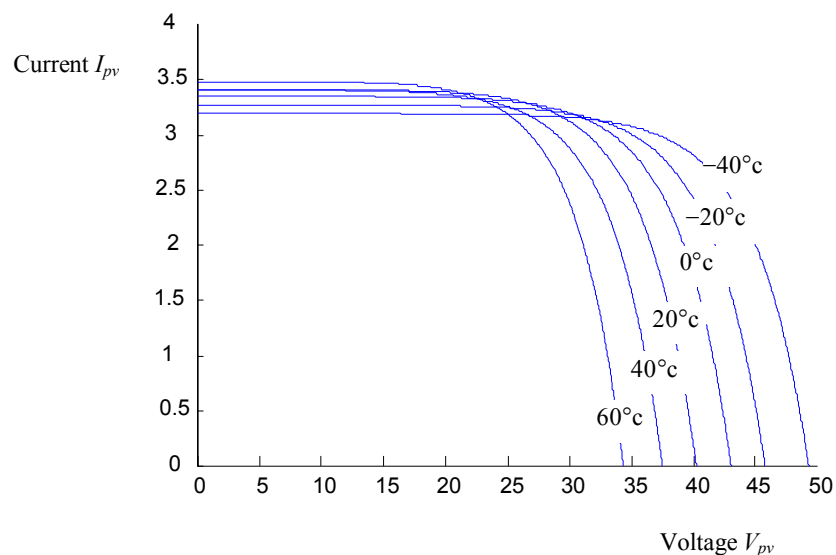


**Figure 2.11: Effect of temperature on the I-V characteristic at constant irradiance**

## 2.4 INVERTER [5]

An essential part of a grid connected PV systems is the means of converting the dc output of the PV array into ac power to supply to the utility network. Inverters are used to perform this task. The two basic types of inverters are thyristor based line-commutated inverters (TLCI) and pulse width modulated (PWM) voltage source inverters. These two types of inverter are shown in Figure 2.12 and Figure 2.13 respectively.

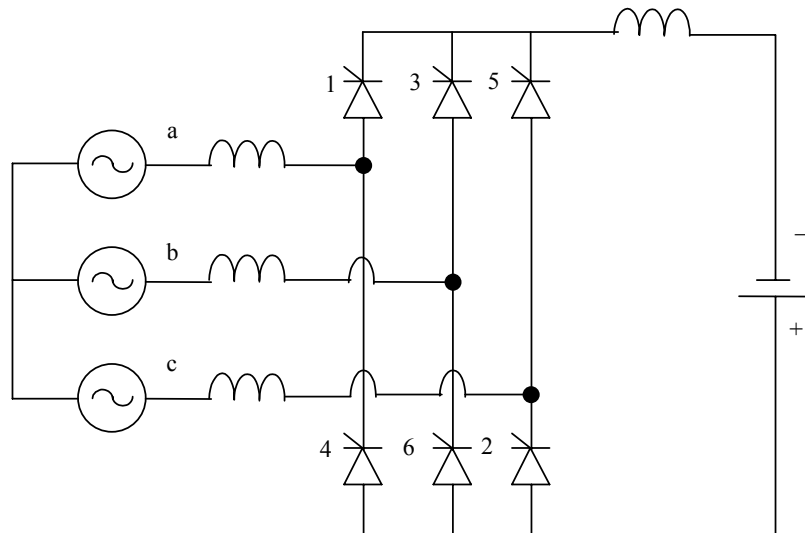


Figure 2.12: TLCI inverter

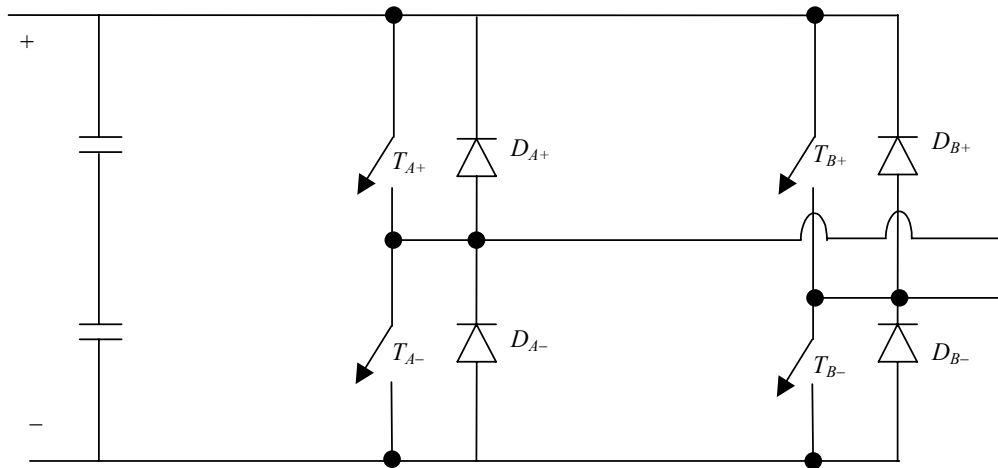


Figure 2.13: PWM voltage source inverter

Many existing PV systems make use of TLCI-type inverters because of its modest cost, availability for even higher power levels and familiarity with the technology. If this inverter connects directly to the PV array, the current drawn from the array can be controlled by varying the firing angle. This type of inverter commonly use in grid connected PV systems.

Development in IGBT (Insulated Gate Bipolar Transistor) and MOSFET (Metal Oxide Semiconductor Field Effect Transistor) toward considerably higher power ratings, together with fast real time digital control have resulted in the use of high quality sinusoidal PWM voltage source inverter in PV systems. The greater flexibility of these inverters and the use of microprocessors provide the opportunity to configure the inverter for particular application easily and appropriately. In these inverters the

magnitude of the input dc voltage is essentially constant in magnitude and it is possible to control both the output voltage and frequency of the inverters. This is achieved by Pulse Width Modulation of the inverter switches and hence such inverters are called PWM inverters.

## 2.5 CONTROLLER

### 2.5.1 Maximum Power Point Tracking Controller [2]

As illustrated in section 2.3.1, the  $I_{pv}$ - $V_{pv}$  characteristic of a PV cell varies with the irradiance and operating temperature of the cell. Consequently the maximum power point varies. A directly connected fixed voltage, fixed current or fixed resistance load therefore cannot extract maximum power from the PV system. To get maximum power output, the PV array should be operated at the maximum power point at all time. A controller capable of tracking the maximum power point must therefore be implemented.

There are a number of Maximum Power Point Tracking (MPPT) techniques. All of these methods require an algorithm to specify the location of the operating point with respect to the maximum power point. Some of them deliver only a sub-optimum power output. A good MPPT technique should produce a high efficiency at low cost because PV systems will have to be mass-produced.

#### 2.5.1.1 Simple Panel Load Matching

To operate the PV cell close to the maximum power operating point, the simple panel load matching technique can be used. In this method, the maximum power operating point of PV cell is determined either in theory or under average operating conditions using a series of measurements. A matching load is designed after the corresponding values for the maximum power current and voltage ( $I_{pv,mpp}$  and  $V_{pv,mpp}$ ) are obtained.

This technique is simple and inexpensive because no additional circuitry is used. The risk of component failure is kept low. However, this system does not take into consideration any changes in irradiance and temperature. In addition, the aging of the

PV cell material and the accumulation of dust and dirt on the panel surface may also cause a variation in the maximum power point and efficiency.

### 2.5.1.2 Voltage Feedback Method

A simple control system can be applied to tie the panel voltage to an almost constant level. The control system implements a feedback loop to the panel voltage and compares it with a constant reference voltage. This loop continuously adjusts the inverter to operate the PV panel at a predefined operating point close to the maximum power point. This method makes it possible to operate a PV array under unknown or changing load and at a desirable but sub-optimal operating point for the panel.

The drawbacks of this configuration are the same as the simple load matching method. It cannot adjust to the changing environment conditions such as irradiance and temperature.

An improved version of the voltage-feedback method is the *Measurement of  $V_{pv,oc}$  Method*. The panel voltage at the maximum power point  $V_{pv,mpp}$  can be considered to be a constant fraction of the panel's open circuit voltage,  $V_{pv,oc}$ . This relation is used to get information about the current position of the panel's maximum power point. It utilizes the fact that the voltage at the maximum power point of an array at any condition is about 65% to 80% of the open circuit voltage at that condition. In this method, the open circuit voltage of the array is monitored periodically by switching off the load for a short period of time (10-50ms) every minute [6]. The new operating voltage of the array will be set at a fixed percentage of this voltage once a new open circuit voltage is known. The block diagram of this control and the locus of the array terminal voltage are shown in Figure 2.14 and Figure 2.15 respectively.

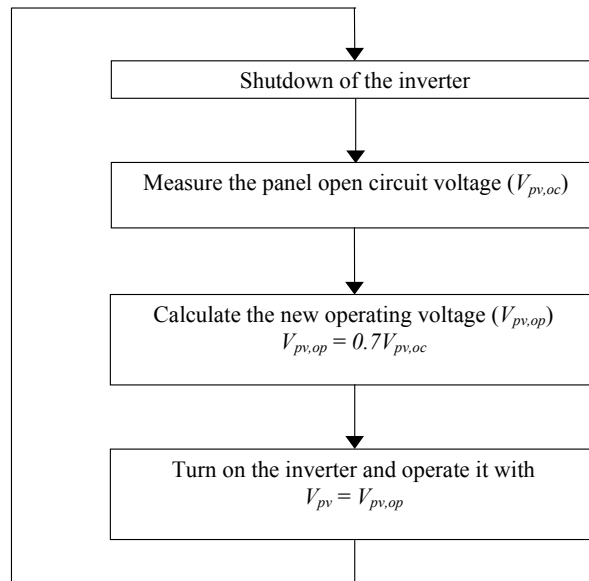


Figure 2.14: Block diagram of measurement of  $V_{pv,oc}$  control

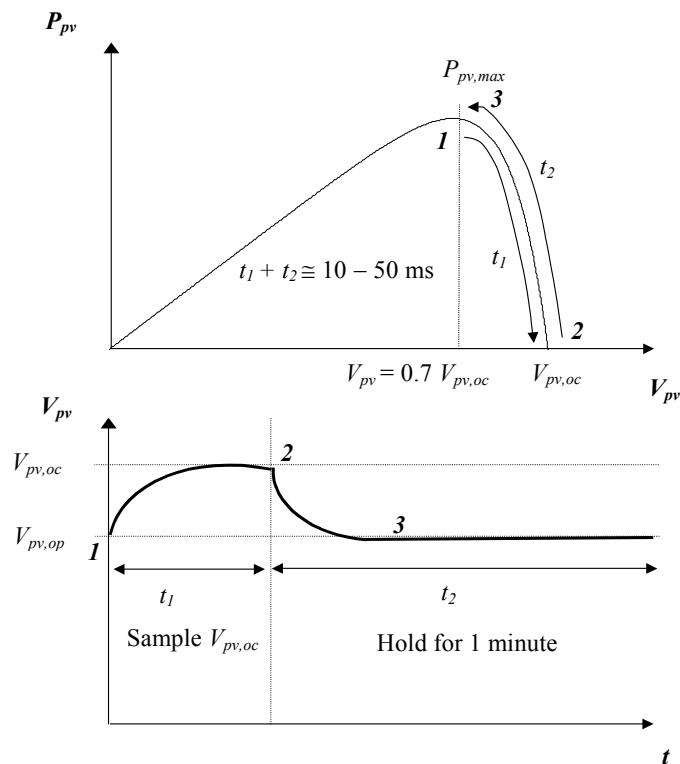


Figure 2.15: PV array voltage locus during sampling

This approach to the control of the PV panel operating voltage takes into consideration important factors such as irradiance and temperature. In addition, the method is simple and inexpensive. However, since the adjustment of the reference voltage to a fraction of the open circuit voltage is always fixed, this method only gives a sub-optimum performance. The accuracy of the adjustment of the operating voltage to the maximum

power voltage,  $V_{pv,mpp}$  depends on the choice of this fraction compared to the real ratio of  $V_{pv,mpp}$  to  $V_{pv,oc}$ .

The response time of the sampling system shown in Figure 2.15 is determined by the input capacitance and the effective load resistance. The higher the capacitance, the longer the sampling time is. To achieve a fast sampling response, the input capacitance should be kept as low as possible. Hence, this method is suitable for a load which draws a constant power from the PV inverter. For a grid connected PV inverter application where a decoupling capacitor is required between the panel and the inverter, a high-speed switch should be inserted to isolate the panel from the capacitor during the open circuit voltage monitoring process.

### 2.5.1.3 Power Feedback Method

If the actual maximum power point is to be found, information about the actual power must be extracted from the PV array. This can be done by measuring the panel output voltage,  $V_{pv}$  and the panel output current,  $I_{pv}$  and multiplying these two parameters to get the actual value for the panel output power  $P_{pv}=V_{pv}\times I_{pv}$ . With these values, there are various methods of tracking the actual maximum power point of the array.

#### 2.5.1.3.1 Perturbation and Observation (P&O) Method [6, 7]

The P&O method is a widely used approach in MPPT because it is simple, it requires only measurements of  $V_{pv}$  and  $I_{pv}$ , and it can track the maximum power point quite accurately through variations in irradiance and temperature.

As its name indicates, the P&O method works by perturbing  $V_{pv}$  and observing the impact of this change on the output power of the PV array. Figure 2.16 is a flow chart of the P&O algorithm. At each cycle,  $V_{pv}$  and  $I_{pv}$  are measured to calculate  $P_{pv}(k)$ . This value of  $P_{pv}(k)$  is compared to the value  $P_{pv}(k-1)$  calculated at the previous cycle. If the output power has increased,  $V_{pv}$  is adjusted further in the same direction as in the previous cycle. If the output power has decreased,  $V_{pv}$  is perturbed in the opposite direction as in the previous cycle.  $V_{pv}$  is thus perturbed at every MPPT cycle. When the

maximum power point is reached,  $V_{pv}$  oscillates around the optimal value  $V_{pv,mppt}$ . This causes a power loss that increases with the step size of the perturbation. If this step width is large, the MPPT algorithm responds quickly to sudden changes in operating condition. On the other hand, if the step size is small the losses under stable or slowly changing conditions will be lower but the system will not be able to respond quickly to rapid changes in temperature or irradiance.

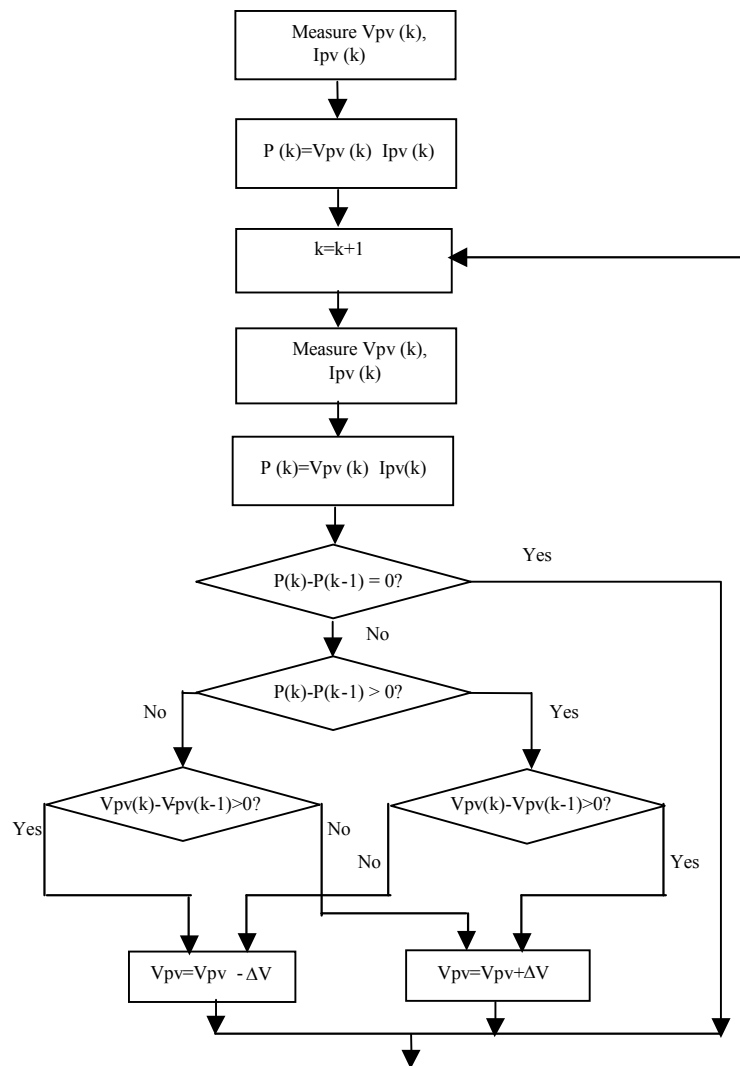


Figure 2.16: Perturbation and Observation method flow chart

The drawback of the P&O MPPT technique is that in case of a rapid change in atmospheric conditions, such as a moving cloud, this method may move the operating point in the wrong direction as shown in Figure 2.17. Initially, the inverter operating voltage is at point 1, which is the maximum power point. Suppose that a perturbation moves the operating point towards point 2. During this perturbation period, the

irradiance has increased from  $I_{r1}$  to  $I_{r2}$ . This leads to an increase in the inverter output power measure from  $P_{pv1}$  to  $P_{pv2}$ . However, the maximum power point at this irradiance is at point 4, which corresponds to a maximum power  $P_{pv,max}$ ,  $I_{r2}$ . In the following perturbation, the P&O algorithm will increment the inverter operating voltage further right to point 3, and again an increase in the inverter power will be measured if the irradiance has increased from  $I_{r2}$  to  $I_{r3}$  with the new maximum power point at point 5. In this way, the P&O algorithm will continue to move the operating point of the inverter further away from the actual maximum power point, and more power will be lost. This incorrect adjustment will continue until the change in irradiance slows or settles down.

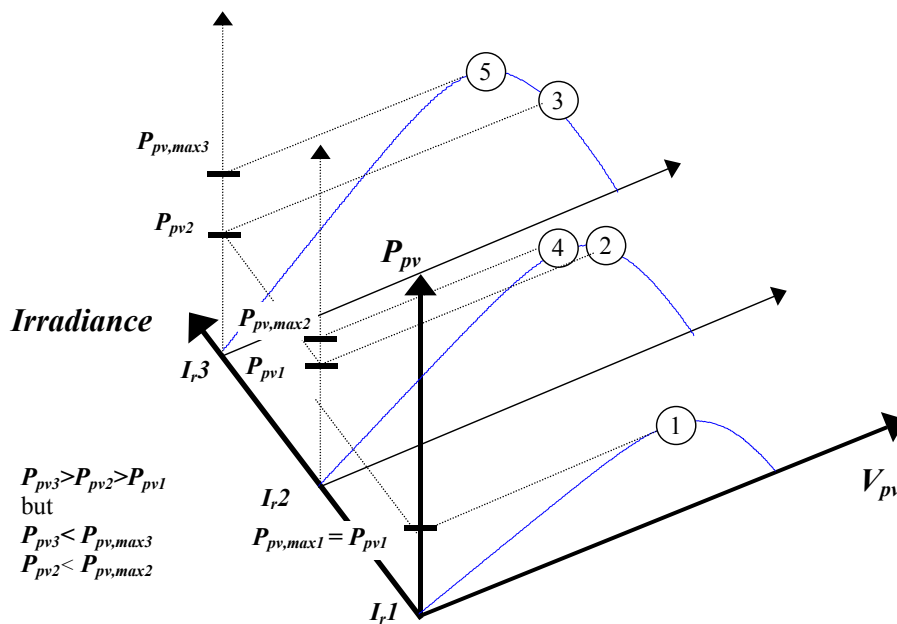


Figure 2.17: Deviation of the P&O method from MPP

The first solution to this problem is to increase the execution speed by using a faster micro controller. The second solution is to check for any fast change in irradiance by checking the value of  $dI_{pv}/dt$  and disabling the voltage adjustment if the change in  $dI_{pv}/dt$  exceeds a limit.

### 2.5.1.3.2 Incremental Conductance Method [7]

The Incremental Conductance method has been proposed to avoid the drawbacks of the P&O MPPT method. It is based on the fact that the derivative of the output power  $P_{pv}$  with respect to the panel voltage  $V_{pv}$  is equal to zero at the maximum power point. The

PV panel  $P_{pv}$ - $V_{pv}$  characteristic in Figure 2.18 shows further that this derivative is positive to the left of the maximum power point and negative to the right of maximum power point.

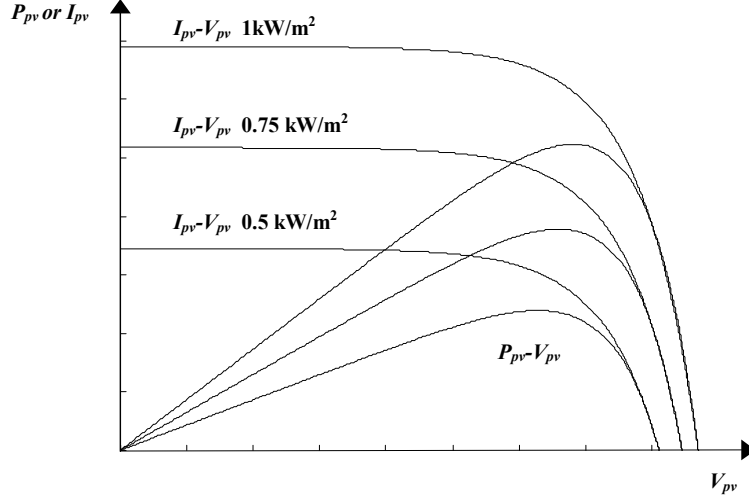


Figure 2.18:  $P_{pv}$ - $V_{pv}$  characteristic curve

This leads to the following set of equations:

$$\frac{dP_{pv}}{dV_{pv}} = \frac{d(I_{pv}V_{pv})}{dV_{pv}} = I_{pv} + V_{pv} \frac{dI_{pv}}{dV_{pv}} = 0 \quad \text{at MPP} \quad (2.5)$$

$$\frac{dP_{pv}}{dV_{pv}} = \frac{d(I_{pv}V_{pv})}{dV_{pv}} = I_{pv} + V_{pv} \frac{dI_{pv}}{dV_{pv}} > 0 \quad \text{to the left of MPP} \quad (2.6)$$

$$\frac{dP_{pv}}{dV_{pv}} = \frac{d(I_{pv}V_{pv})}{dV_{pv}} = I_{pv} + V_{pv} \frac{dI_{pv}}{dV_{pv}} < 0 \quad \text{to the right of MPP} \quad (2.7)$$

These equations can be written as:

$$\frac{dI_{pv}}{dV_{pv}} = -\frac{I_{pv}}{V_{pv}} \quad \text{at MPP} \quad (2.8)$$

$$\frac{dI_{pv}}{dV_{pv}} > -\frac{I_{pv}}{V_{pv}} \quad \text{to the left of MPP} \quad (2.9)$$

$$\frac{dI_{pv}}{dV_{pv}} < -\frac{I_{pv}}{V_{pv}} \quad \text{to the right of MPP} \quad (2.10)$$

The equations above can be used as a control algorithm to control the inverter operating point by measuring the incremental and instantaneous inverter conductance ( $dI_{pv}/dV_{pv}$  and  $I_{pv}/V_{pv}$  respectively). The flowchart of the control algorithm is shown in Figure 2.19. This method may be more difficult to implement than the previous methods because it involves divisions in which the denominators may be equal to zero.

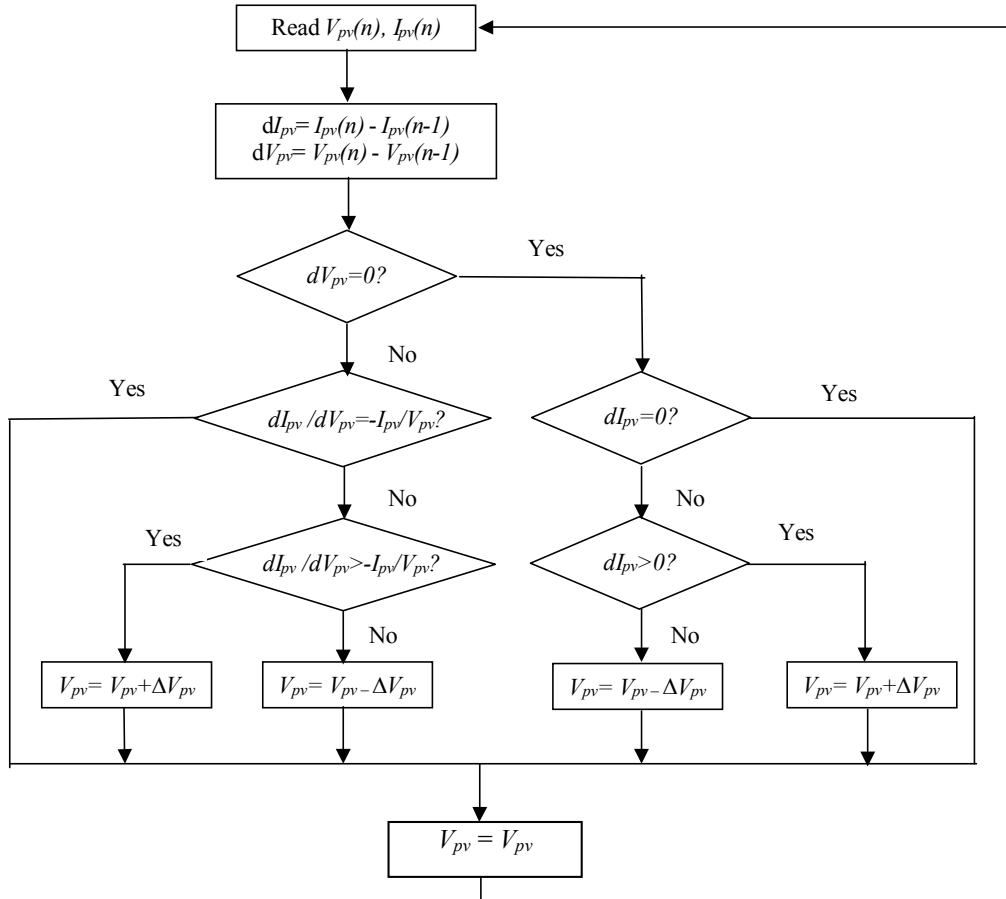


Figure 2.19: Flow chart of incremental conductance MPPT algorithm

### 2.5.2 Islanding Protection

Islanding of grid-connected PV inverters refers to their independent operation when the utility is disconnected. Concern about such a phenomenon is raised because it can be dangerous because of the potential lack of earthing. It puts uninformed maintenance personnel in danger. As a consequence of the disturbed power balance in the grid section that becomes isolated from the main power supply, frequency and voltage obtain new values, often beyond the allowed limits. Over/under voltage and frequency protection is essentially an islanding protection measure. The grid voltage and grid frequency are

checked continuously to detect loss of grid. In case of loss of grid, the inverter is shut down within 0.1s to prevent island operation.

However, in very rare instances, if the local load matches the power delivered by the local PV generator, the power balance can be in equilibrium in the isolated grid section. Voltage and frequency remain constant and the inverter keeps operating. In order to prevent such a potentially dangerous situation, most inverter manufacturers implement additional islanding prevention measures beside frequency and voltage monitoring. The most common types of additional islanding prevention method is *Active Frequency Drift Method* [8]

*Active Frequency Drift (AFD) Method* is easily implemented in a PV inverter with a microprocessor-based controller [9]. In this method, the waveform of the current injected into node “a” as shown in Figure 2.20 by the inverter is slightly distorted such that there is a continuous trend to change the frequency. When connected to the utility it is impossible to change the frequency.

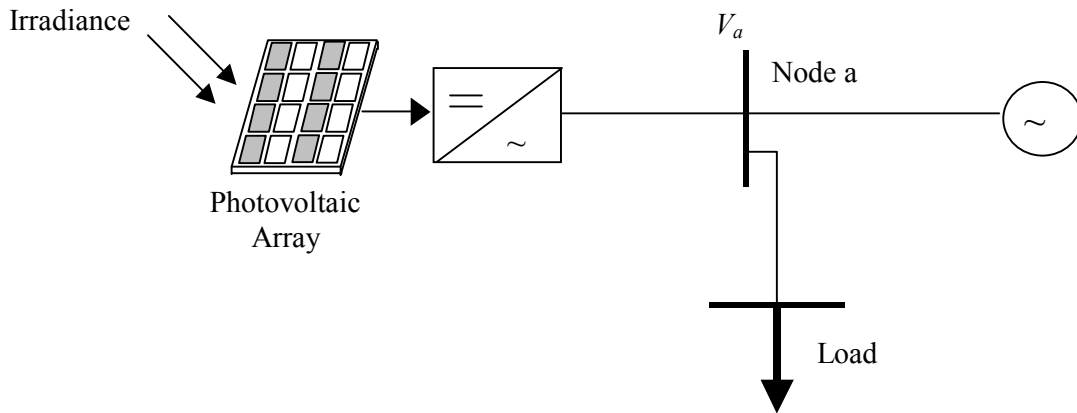


**Figure 2.20: PV system / utility configuration**

When disconnected from the utility, the frequency of  $V_a$  is forced to drift up or down, augmenting the “natural” frequency drift caused by the system seeking the load’s resonant frequency. An example of a PV inverter output current  $I_{pv}$  waveform that implements upward AFD is shown in Figure 2.21, along with an undistorted sine wave for comparison.  $T_{util}$  is the period of the utility voltage,  $T_{pv}$  is the period of the sinusoidal portion of the current output of the inverter, and  $T_z$  is a dead or zero time. The ratio of the zero time  $T_z$  to half of the period of the voltage waveform,  $T_{util}/2$ , is referred to as the “chopping fraction”(cf).

$$cf = \frac{2T_z}{T_{Vutil}} \quad (2.11)$$

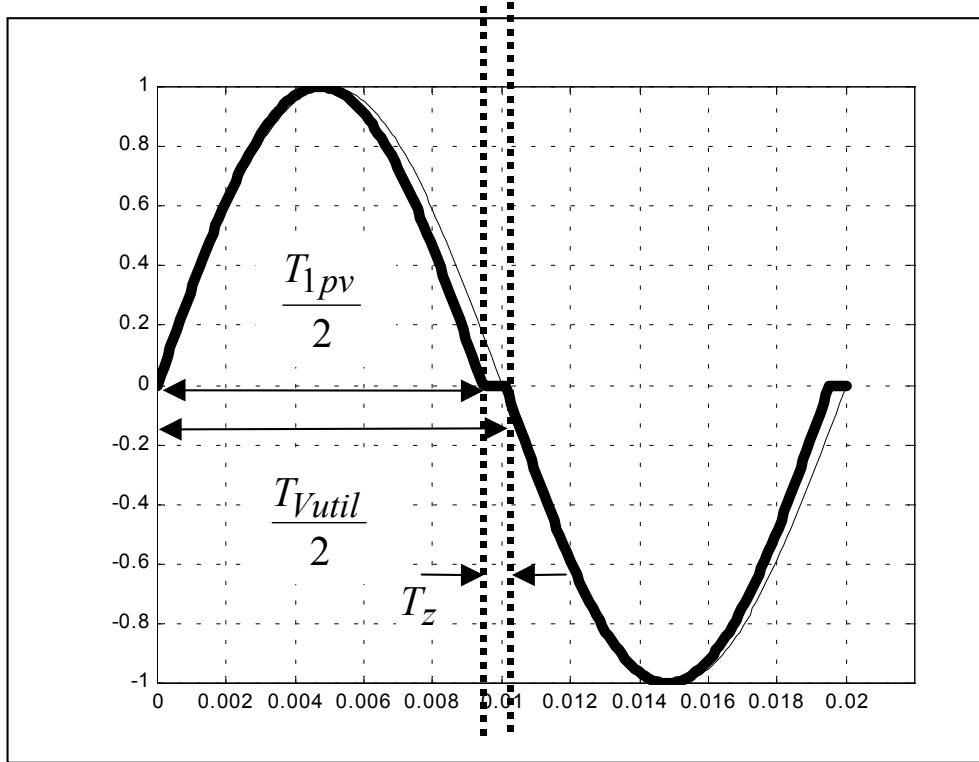


**Figure 2.21: Example of a waveform used to implement the *Active Frequency Drift Method* of islanding protection**

During the first portion of the first half-cycle, the PV inverter current output is a sinusoid with a frequency slightly higher than that of the utility voltage. When the PV inverter output current reaches zero, it remains at zero for time  $T_z$  before beginning the second half cycle. For the first part of the second half-cycle, the PV inverter output current is the negative half of the sine wave from the first half-cycle. When the PV inverter current again reaches zero, it remains at zero until the rising zero crossing of the utility voltage. It is important to note that the zero time in the second half cycle is not fixed and need not equal  $T_z$  if the grid frequency has altered in that time.

When this current waveform is applied to a resistive load in an island situation, its voltage response will follow the distorted current waveform and go to zero in a shorter time ( $T_{Vutil}-T_z$ ) than it would have under purely sinusoidal excitation. This causes the rising zero crossing of  $V_a$  to occur sooner than expected, giving rise to a phase error

between  $V_a$  and  $I_{pv}$ . The PV inverter then increases the frequency of  $I_{pv}$  to attempt to eliminate the phase error. The voltage response of the resistive load again has its zero crossing advanced in time with respect to where it was expected to be, and the PV inverter still detects a phase error and increases its frequency again. This process continues until the frequency has drifted far enough from  $\omega_0$  to be detected by the over/under frequency protection.

The strength of this method is this method is that it relatively easy to implement in micro-controller-based inverters. The weakness of this method is that it requires a small degradation of the PV inverter output power quality. In addition, in order to maintain effectiveness in the multiple-inverter case, there would have to be agreement between all manufacturers of inverters in the direction of the frequency drift.

### **2.6 GRID**

The load of grid connected PV inverters is the utility network. As seen from the inverter, this network looks like an infinite energy sink. The requirements for the grid connected PV system are dictated by the electric utility and each utility may impose a unique set of requirements. These requirements can be divided into protection, power quality, operation and safety.

# Chapter 3

## A MODEL OF PHOTOVOLTAIC GENERATION SUITABLE FOR STABILITY ANALYSIS

### 3.1 INTRODUCTION

As the concern over global warming increases, renewable energy source become a more significant source of energy. Among these renewable energy sources, PV generation is attracting a growing amount of political and commercial interest. For example, the European Commission's White Paper on renewable energy sets an indicative objective of 3GW of installed PV generation in Western Europe by 2010 [10]. Such a large penetration of PV generation would have far reaching consequences not only on the distribution network but also on the transmission grid and the rest of the generators. The effect of a large penetration of PV generation on the stability and security of the power system must therefore be considered carefully. In particular, the response of PV generators to disturbances could aggravate these incidents. The development of a model of PV generator capable of simulating their response to changes in irradiance and grid ac voltage is the subject of this chapter.

In contrast with the approach adopted in published papers on this subject, this model was built on the basis of experimental results. These experiments demonstrated that the maximum power point tracking (MPPT) controller used to maximize the efficiency of the PV cell dictates the dynamic behavior of the PV generator.

### 3.2 METHODOLOGY

The development of dynamic models of PV generation has been the object of only a few scientific publications. References [11]-[13] develop detailed models of the dynamic behavior of the inverter connecting the PV array to the grid. In [11] this inverter is self-commutated while in [12] and [13] this inverter is line commutated. In all these references, the voltage reference signal  $V_{ref}$  of the inverter is assumed to be equal at all times to the maximum power point for the current irradiance level. The operation of the MPPT controller is thus not represented in these models. Simulation results obtained with these models suggest that PV generating units should respond to disturbances in irradiance and line voltage within milliseconds. Experiments carried out with commercial inverter contradict these simulations. These results, indicate that the response time of PV generating units is considerably longer. It was therefore decided to develop an empirical model based on experimental results rather than on analytical manipulations. This model should reflect accurately the dynamic behavior of the PV generating unit following small or slow changes in irradiance, sudden large increases and decreases in irradiance, as well as sudden changes in ac grid voltage. This approach is also well suited to the modelling of commercial PV systems for which no information regarding the control algorithms is available. A PV system was thus subjected to a number of such disturbances in a laboratory environment. An analysis of the response of the PV system to these disturbances led to the identification of various response modes and the development of a model capable of representing this complex dynamic and non-linear behavior.

### 3.3 EXPERIMENT SETUP

Figure 3.1 shows the test rig used to test the PV generating unit. The dimensions of the test unit were 1.5(W)×1.5(H)×0.75(D) meters. The box can accommodate a PV

module of the size up to 1.40×0.70 meters. A bank of 60 low voltage, tungsten halogen lamps installed into their sockets mounted under the ceiling plate of the rig. The ceiling plate is a reinforced 6mm-thick aluminium sheet.



**Figure 3.1: The test unit**

The layout of the location of the lamps over the top plate is shown in Figure 3.2. All the lamps are equally divided into twelve lamp strings. Each string is composed of five lamps connected in series and can be switched on or off independently by its circuit breaker. When the test unit is operating at its maximum power, it dissipates three kilowatts of heat. There are three fans under the PV module. On the top of the test unit, there are two smaller fans blowing the air horizontally over the surface of the top plate to cool the lamps. The fans and a magnetic contactor in the test unit are mains powered. The low-voltage tungsten halogen lamps are powered by a 3kW, 70V, 50A switching dc power supply. The switching power supply requires a single phase 20A mains. The circuit diagram of the test unit is shown in Figure 3.3. The rated supply voltage for each string is 60 volts.

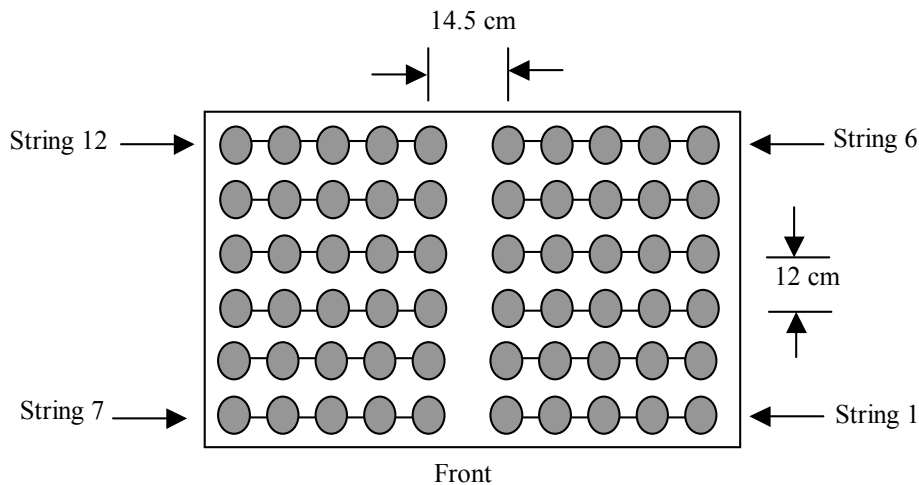


**Figure 3.2: Lamps layout over the top plate of the test cell**

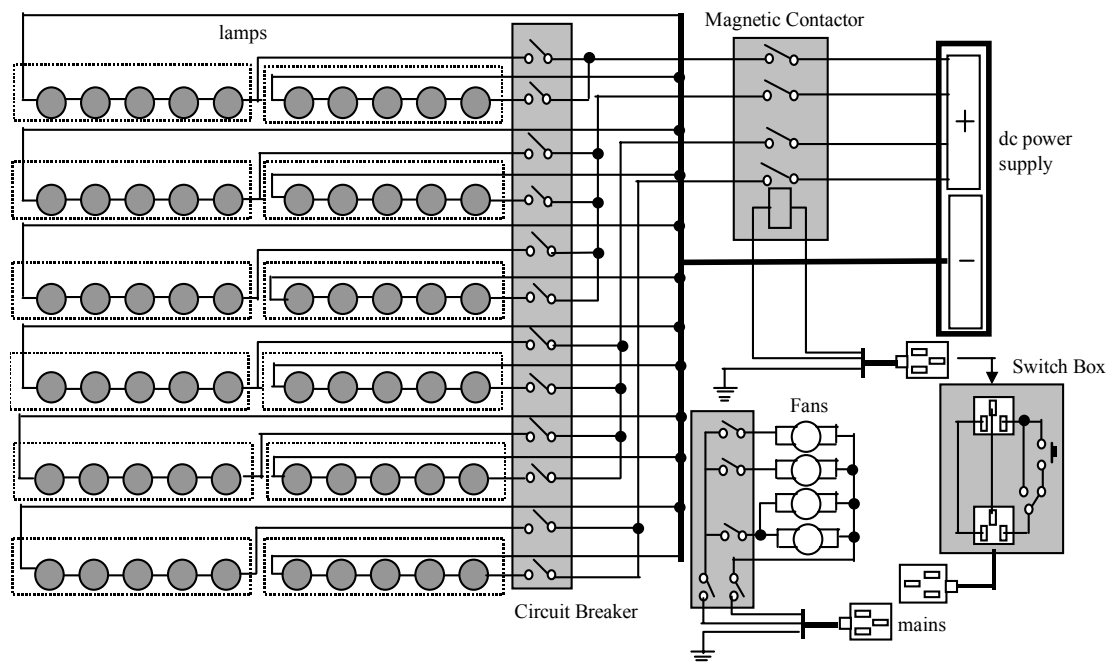


**Figure 3.3: Circuit diagram of the test unit**

Figure 3.4 shows the schematic diagram of the experimental set-up used to test the PV generating unit. Switching on or off some of the twelve-lamp strings simulates sudden large changes in irradiance. Slow changes in irradiance are achieved by adjusting the voltage applied to the lamps. The PV array used has a rated power of 110W, a rated current of 3.15A, a rated voltage of 35V, a short circuit current of 3.45A and an open circuit voltage of 43.5V. These parameters are for standard condition ( $1000 \text{ W/m}^2$ ,  $25^\circ\text{C}$ ). A commercially available inverter, which used the P&O technique for maximum power point tracking, connects the output of the PV array to the grid. This connection is made through a transformer. Changing the tap connection of this

transformer using a relay generates sudden  $\pm 10\%$  changes in the 230V ac grid voltage.

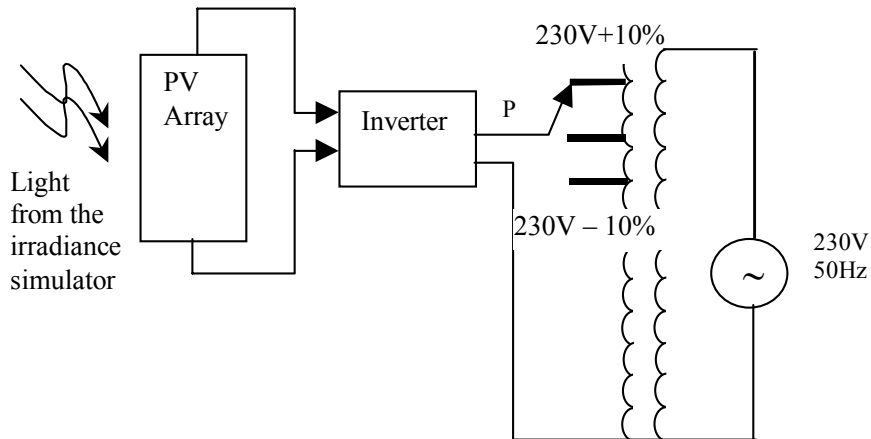


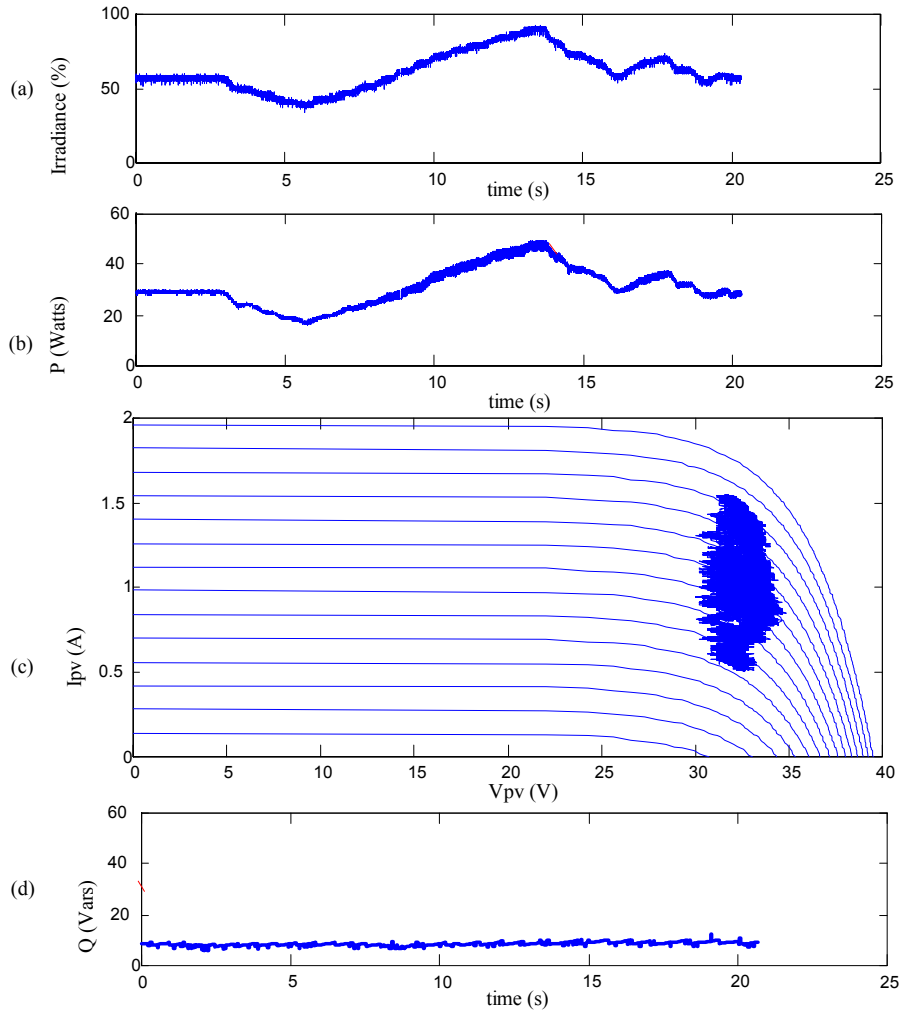
Figure 3.4: Set-up of the PV experiment test rig

In this experiment, LABVIEW is the instrumentation used to measure the  $V_{pv}$ ,  $I_{pv}$ ,  $V_{ac}$  and  $I_{ac}$  from the PV system at a sampling rate of 3200 samples per second.

### 3.4 EXPERIMENT RESULTS

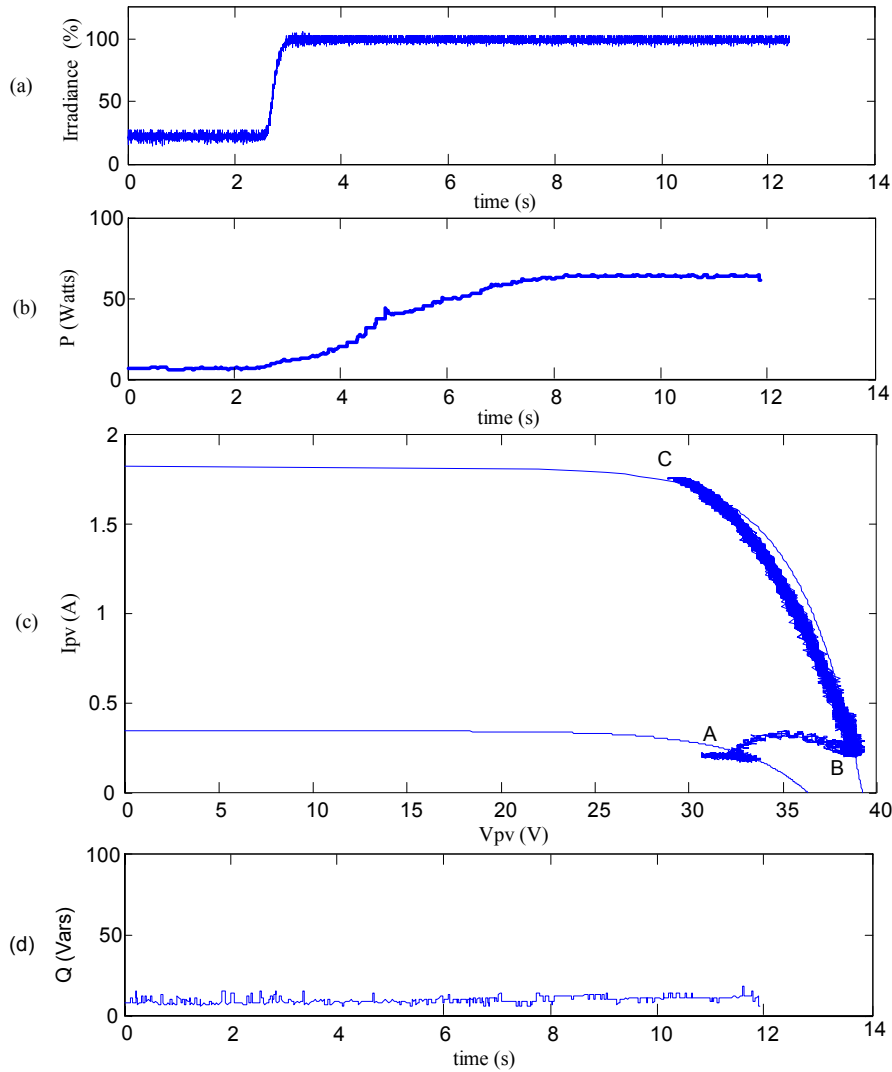
Figure 3.5, Figure 3.6, Figure 3.7, Figure 3.8 and Figure 3.9 show the experimental results of the PV generation response to disturbances. Part (a) of each figure shows the disturbances. Part (b) of each figure shows the active power injected by the PV generating unit into the grid. Part (c) of each figure shows the operating path superimposed on the I-V characteristic of the PV array. Part (d) of each figure shows the response of reactive power by the PV generating unit.

Figure 3.5 illustrates the response of the PV generation system to slow changes in irradiance. Figure 3.5(a) shows the evolution of the irradiance with time while Figure 3.5(b) shows the resulting variation in active power delivered to the grid. Since the irradiance changes slowly, the active power response follows closely the pattern of change in irradiance. On Figure 3.5(c) the time dimension has been made implicit and the dc current and voltage that deliver this output power have been superimposed on the calculated  $I_{pv}$ - $V_{pv}$  characteristic of the PV array. This figure 3.5(d) shows that the operating point of the array always operates around the MPP as irradiance varies. The fuzziness of the trace is due to the operation of the P&O-based MPPT technique.



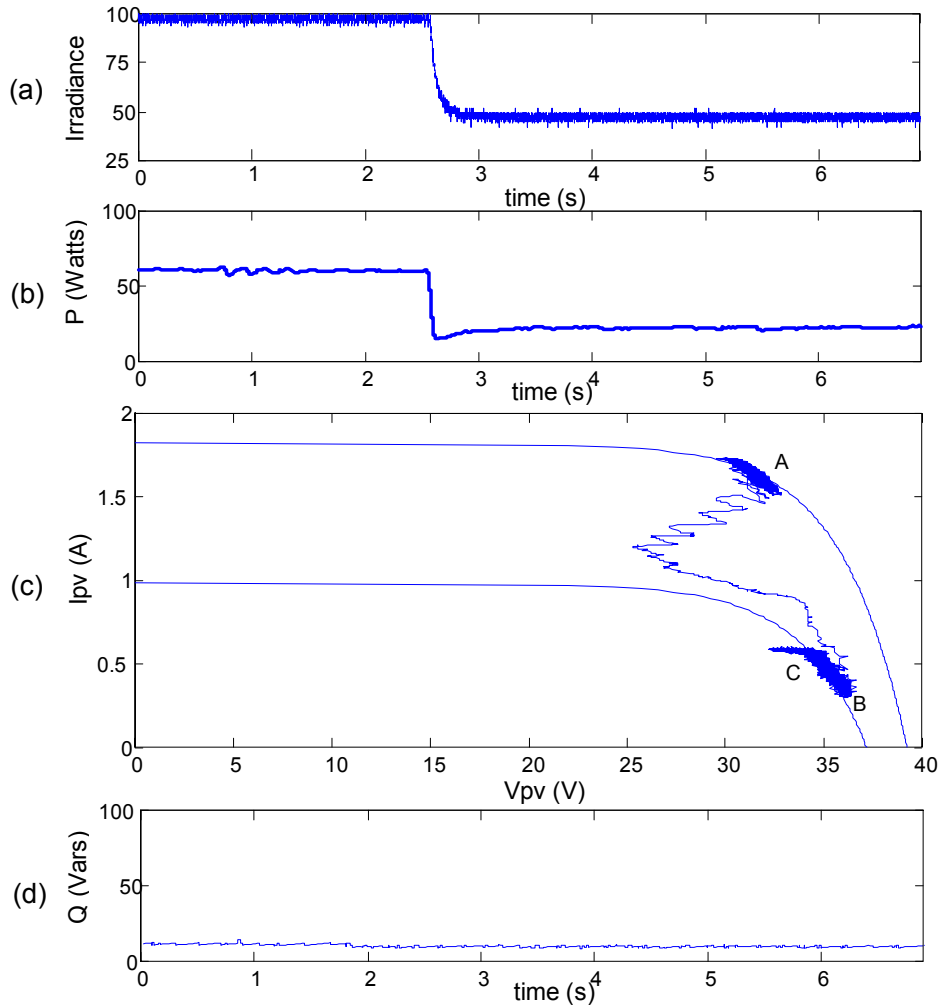
**Figure 3.5: Response of the PV generator to slow change in irradiance**

Figure 3.6 illustrates the response of the system following a sudden increase in irradiance from 20% to 100% of rating at  $t = 2.6\text{s}$ . Figure 3.6(b) shows that the active power delivered to the grid increases from 12W to 60W in approximately 5.5 seconds. Figure 3.6(c) shows the path of the operating point on the calculated  $I_{pv}$ - $V_{pv}$  characteristics of the array. Before the disturbance, the operating point oscillates around point A. Immediately after the increase in irradiance, the operating point moves rapidly from point A (on the 20% irradiance curve) to point B (on the 100% irradiance curve). Then, the P&O MPPT technique gradually decreases  $V_{pv}$  in search of the MPP, which it reaches at point C.



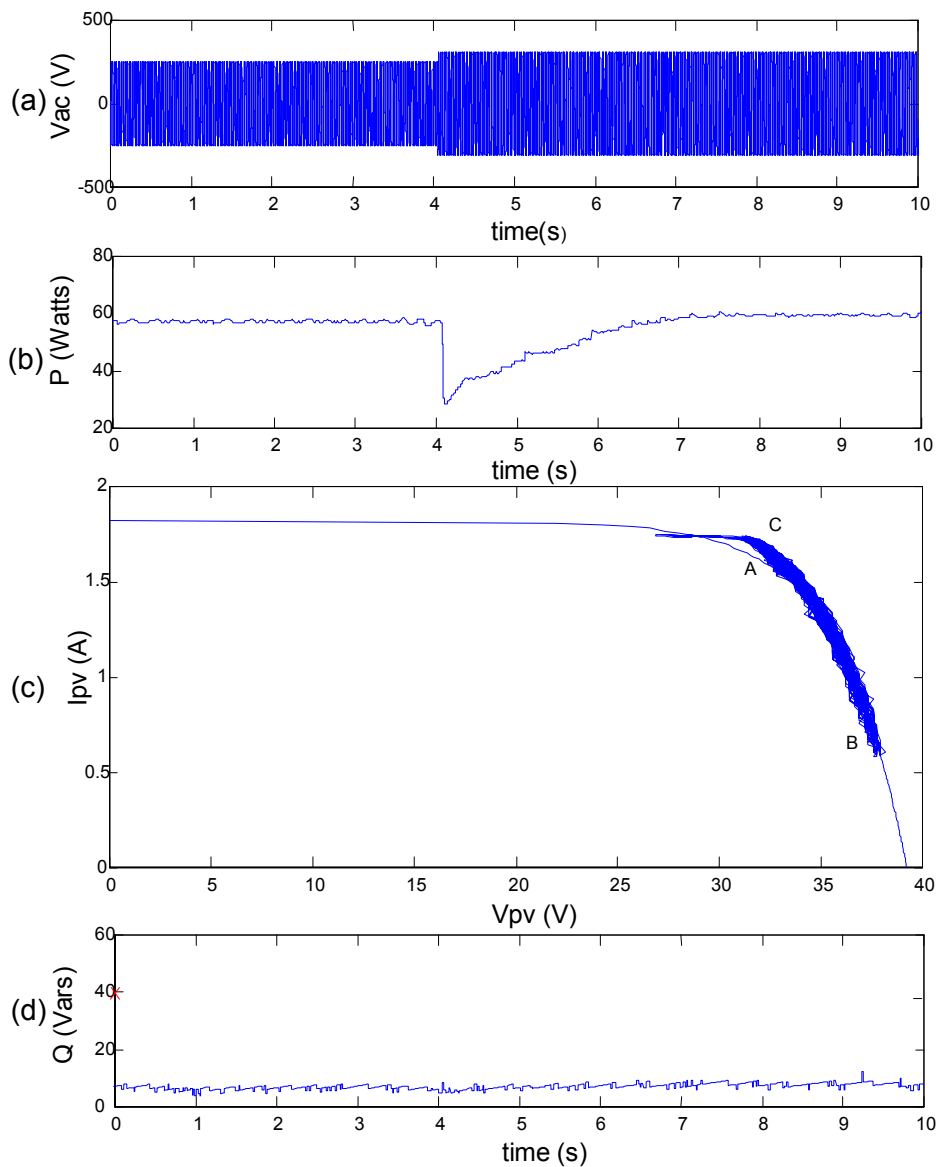
**Figure 3.6: Response of PV generator to sudden large increase in irradiance**

Figure 3.7 illustrates the response of the system following a sudden decrease in irradiance from 100% to 40% of nominal at  $t = 2.6\text{s}$ . As shown on Figure 3.7(b), the active power drops instantly from 60W to 15W and then increases back to 25W in approximately 0.5 second. On Figure 3.7(c) this response has been plotted on the  $I_{pv}$ - $V_{pv}$  characteristic of the array. Until the disturbance occurs, the operating point oscillates around point A. It then quickly drops to point B on the 40% irradiance curve. The MPPT controller then gradually decreases  $V_{pv}$  until the MPP is found in the vicinity of point C.



**Figure 3.7: Response of PV generator to sudden large decrease in irradiance**

The response of the PV generating unit following a sudden 10% increase in ac grid voltage is illustrated on Figure 3.8. When the ac grid voltage increases from 210 V to 230 V at  $t=4s$ , the active power injected by the inverter into the grid drops from 60W to 28W and then increases back to 60W in approximately 3.5 seconds time. Figure 3.8(c) illustrates this response on the  $I_{pv}-V_{pv}$  characteristic of the PV array. Initially, the array operates in the vicinity of point A. The sudden increase in grid ac voltage shifts the operating point to B. The MPPT controller then gradually moves the operating point to C, which is very close to the original operating point A because the irradiance has not changed.



**Figure 3.8: Response of PV generator to sudden increase in grid ac voltage**

Figure 3.9 shows that the system's response following a sudden 10% decrease in the ac grid voltage is very similar. However, the operating point does not move as much following a sudden decrease in ac voltage than it does following a sudden increase in ac voltage. The active power injected by the inverter returns to a value which is slightly lower than the original value because the inverter works less efficiently when the grid voltage is less than  $230 V_{ac}$

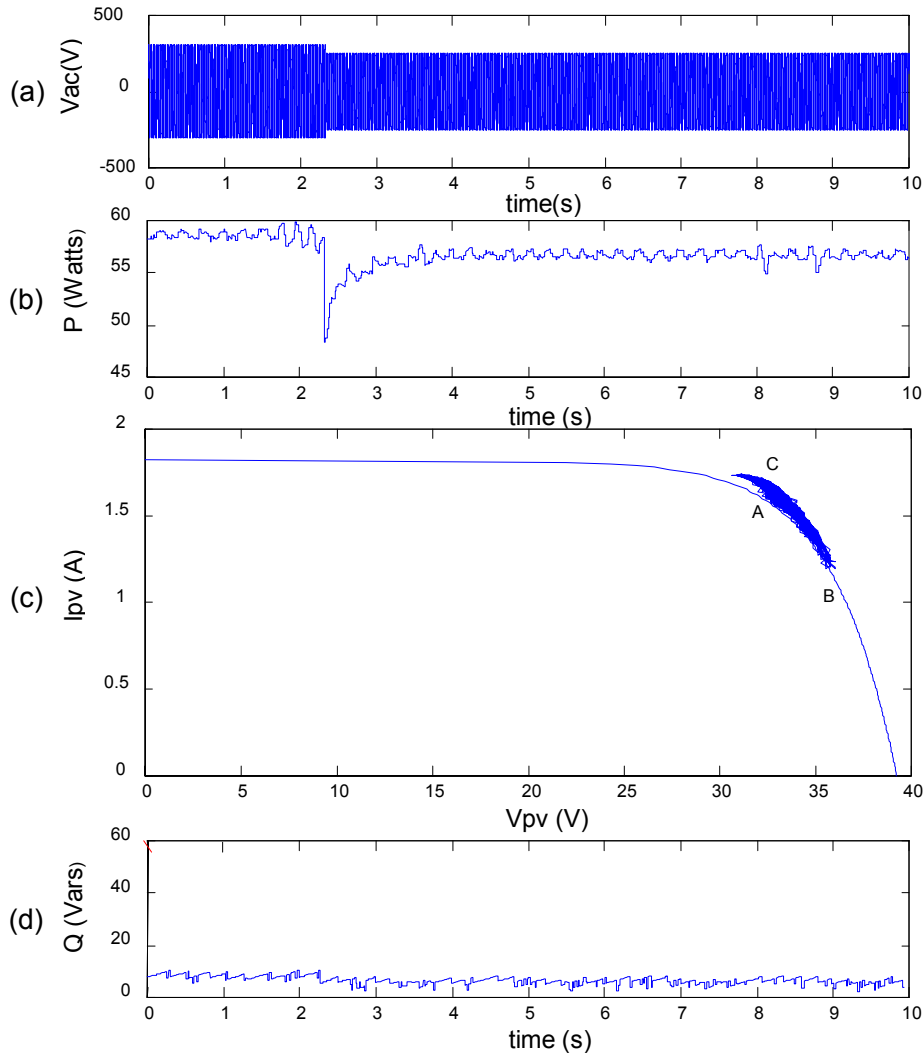


**Figure 3.9: Response of PV generator to sudden decrease in grid ac voltage**

All these results demonstrate that the MPPT controller dominates the dynamic behaviour of a PV generating unit and that the response of such a unit to disturbances in irradiance or grid voltage is measured in seconds rather than milliseconds. Graphs (d) of each of these figures show that these disturbances do not significantly affect the reactive power injection of the PV generating unit.

### 3.5 MODEL DESCRIPTION

#### 3.5.1 General Description

The experimental results discussed in the section 3.4 shows that the P&O MPPT controller makes steps changes in  $V_{pv}$  when searching for the maximum power point. Enlarging a trace of this search suggests that the size of the step is increased or

decreased depending on the “success” of the last step. Modelling the details of such an adaptive search strategy is pointless because the success of a step is often affected by the inevitable noise in the measurements. It turns out that it is much easier to make the model match the experimental results if  $I_{pv}$  is used as the control variable in the model rather than  $V_{pv}$ .

Figure 3.10 gives an overview of the proposed model.  $I_{pv}$  is the control variable and is calculated at each time step as the sum of four components:

- The value of  $I_{pv}$  at the previous step
- A change  $\Delta I_{pv}^{MPPT}$  to reflect the actions of the MPPT
- A change  $\Delta I_{pv}^{Ir}$  to represent the effect of variations in irradiance
- A change  $\Delta I_{pv}^{Vac}$  to represent the effect of sudden variations in ac grid voltage

$I_{pv}$  is one of the inputs to the block representing the non-linear characteristic of the PV array. The other input to this block is the irradiance  $I_r$  and the output is  $V_{pv}$ . The block representing the MPPT has two inputs,  $V_{pv}$  and  $I_{pv}$ , and one output,  $\Delta I_{pv}^{MPPT}$ . Finally, two blocks are used to represent the effect of sudden changes in irradiance and voltage. They take the magnitude of these sudden changes as their input and produce  $\Delta I_{pv}^{Ir}$  and  $\Delta I_{pv}^{Vac}$  respectively

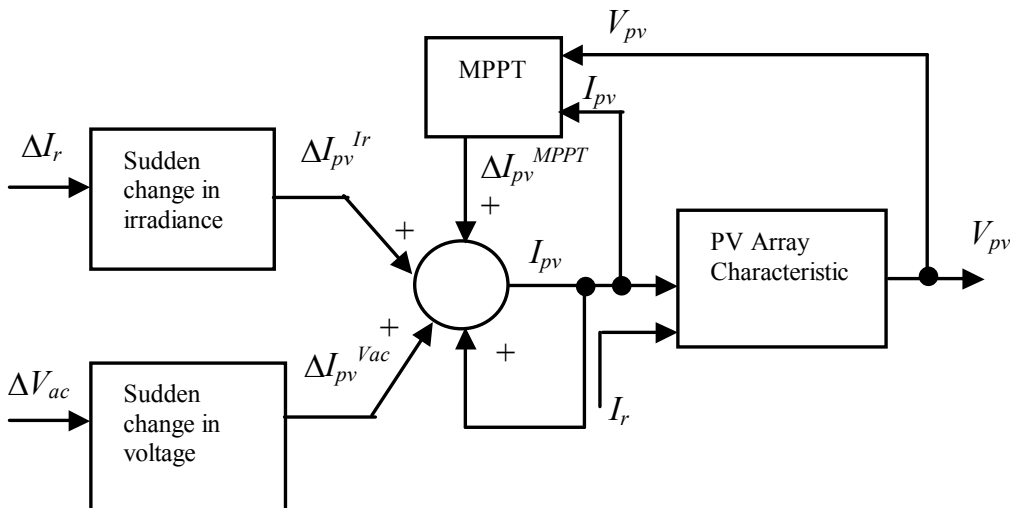


Figure 3.10: Model of PV generation system

### 3.5.2 Flow Chart

While Figure 3.10 represents the interactions of the different parts of the model, the flow chart of Figure 3.11 illustrates the software implementation of this model. Following the initialization of the variables  $I_{pv}$ ,  $I_r$ , and  $V_{pv}$ , the model enters into a loop with a cycle time of 0.2s. The first step in this loop is to determine whether there has been a sudden change in irradiance and the magnitude of the change  $\Delta I_{pv}^{Ir}$ . The magnitude of the change  $\Delta I_{pv}^{Vac}$  is then calculated if necessary. The new value of  $I_{pv}$  is calculated by adding these changes to the current value of  $I_{pv}$  and this new value is fed into the PV array equation to determine  $V_{pv}$  and  $P_{pv}$ . Finally,  $\Delta I_{pv}^{MPPT}$  is calculated by comparing the current and previous values of  $P_{pv}$

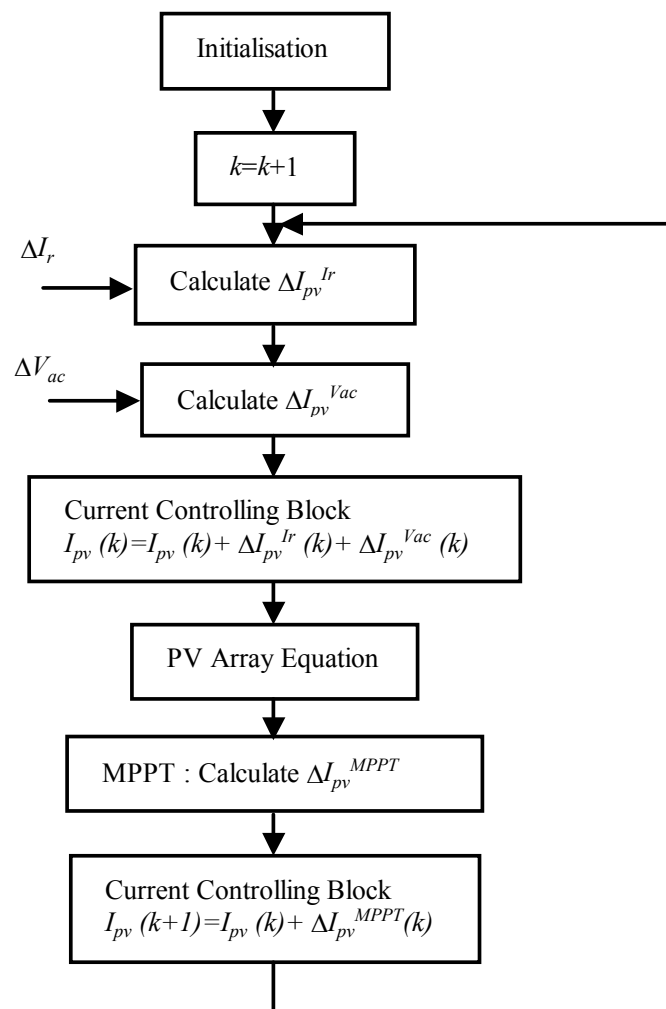


Figure 3.11: Flow Chart of PV generation model

### 3.5.3 PV Array Characteristic

The simple equivalent circuit shown on Figure 3.12 and described by Equation 3.1 represents a photovoltaic cell:

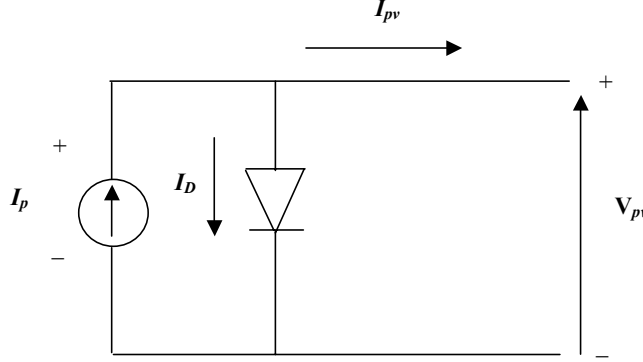


Figure 3.12: PV cell equivalent circuit

$$\begin{aligned}
 I_{PV} &= I_p - I_D \\
 &= N_p I_{sc} \left( \frac{I_r}{100} \right) - N_p I_o \left[ e^{\frac{qV_{PV}}{nkTN_s}} - 1 \right]
 \end{aligned} \tag{3.1}$$

$$\therefore V_{PV} = \frac{N_s nkT}{q} \ln \left[ \frac{N_p I_{sc} \left( \frac{I_r}{100} \right) - I_{PV}}{N_p I_o} + 1 \right] \tag{3.2}$$

where

$I_p$	=	Photocurrent [A]
$I_{sc}$	=	Short circuit current [A]
$I_r$	=	Irradiance in [%]
$V_{pv}$	=	Terminal voltage of the cell [V]
$I_D$	=	Diode current [A]
$I_o$	=	Saturation current [A]
$n$	=	Ideality factor
$q$	=	Charge of the electron [C]
$k$	=	Boltzmann's constant
$T$	=	Junction temperature [°K]
$N_p$	=	Number of cells in parallel
$N_s$	=	Number of cells in series

The PV array used in this study consists of 72 cells in series, such that the overall volt-ampere characteristic is given by  $V_{pv}$  and  $I_{pv}$ , which are the PV generator terminal voltage and current. The photocurrent  $I_p$  is directly proportional to the irradiance ( $I_p=1.82A$  at 100% irradiance). The saturation current and ideality factor of the array are  $1.2987 \times 10^{-4}$  and 1.8405 respectively. This model neglects series and shunt resistances. A change in irradiance will ultimately cause a change in the operating temperature of the PV cells. This change, however, is much slower than the other effects considered and is thus not considered explicitly in the proposed model. The P&O MPPT controller is indeed designed to compensate automatically for the effect of changes in temperature.

### 3.5.4 Effect of Changes in Irradiance

Figure 3.13 shows the flow chart for the calculation of  $\Delta I_{pv}^{Ir}$ . This calculation depends on whether there has been a small change in irradiance, a sudden large decrease in irradiance or a sudden large increase in irradiance.

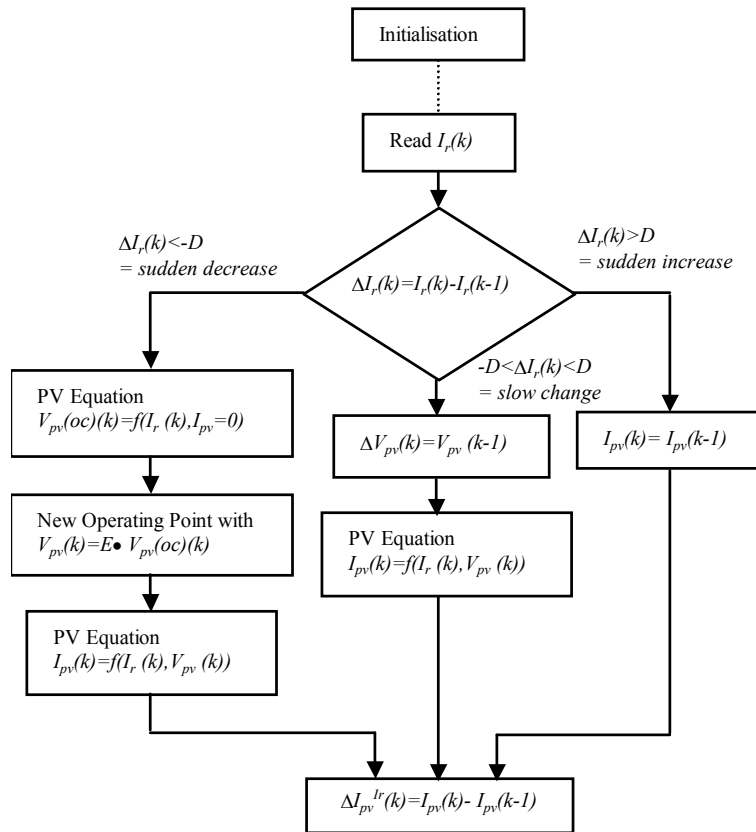


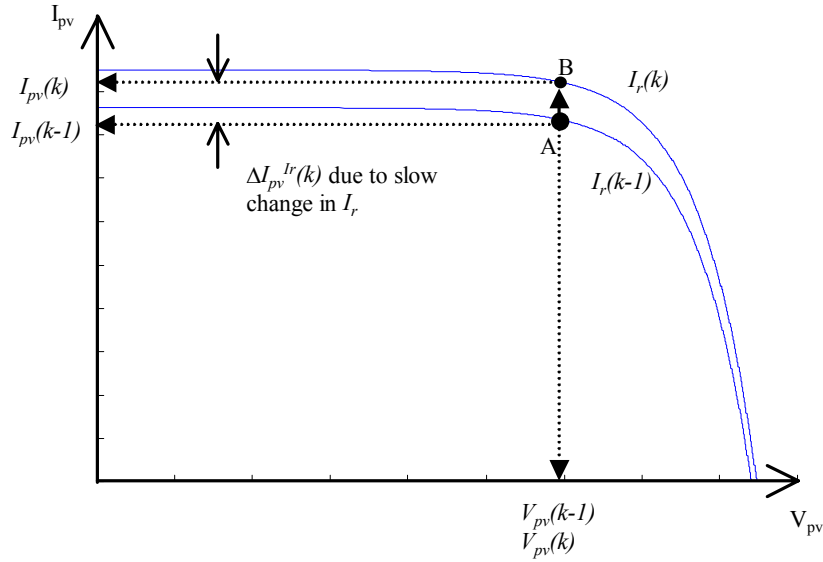
Figure 3.13: Flow chart of  $\Delta I_{pv}^{Ir}$  calculation

Figure 3.14 shows the path of the operating point during small change in irradiance. The operating point of the PV array is assumed to be initially at A on the curve corresponding to  $I_r(k-1)$ . If  $|I_r(k-1)-I_r(k)|$  is sufficiently small (e.g.  $|I_r(k-1)-I_r(k)| < D$ ), the operating point is assumed to move from point A to point B. The dc voltage across the PV array is assumed to remain constant:

$$V_{pv}(k) = V_{pv}(k-1)$$

$I_{pv}(k)$  is calculated using Equations (3.1) and (3.2) with  $I_r(k)$  and  $V_{pv}(k)$  as the inputs. Hence, for a small change in irradiance:

$$\Delta I_{pv}^{I_r}(k) = I_{pv}(k) - I_{pv}(k-1)$$



**Figure 3.14: Path of operating point for slow change in  $I_r$**

Figure 3.15 shows the assumed path of the operating point following a sudden large increase in irradiance. This figure should be compared with Figure 3.6. Immediately after the sudden large increase in irradiance from  $I_r(k-1)$  to  $I_r(k)$ , the operating point moves from point A to point B. Hence, the model assumes that for a large increase in irradiance:

$$I_{pv}(k) = I_{pv}(k-1) \text{ or } \Delta I_{pv}^{I_r}(k) = 0$$

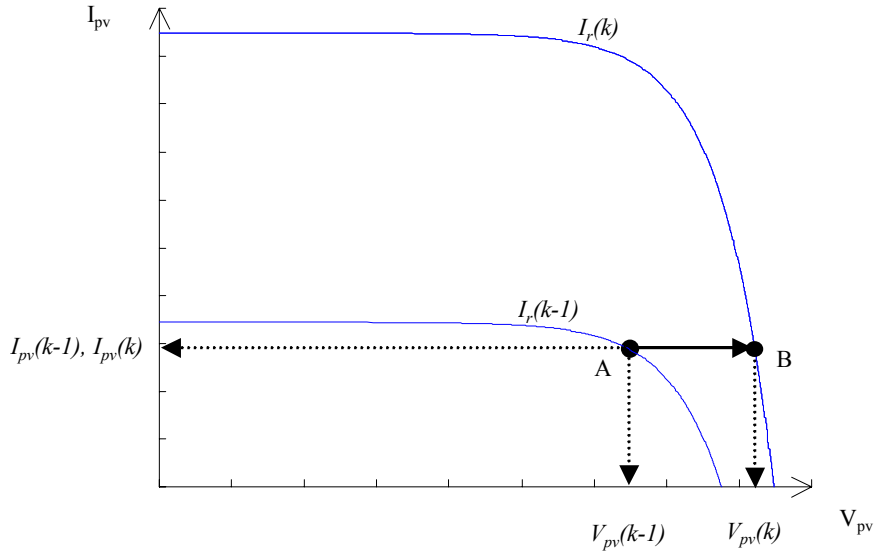


**Figure 3.15: Path of operating point for sudden increase in  $I_r$**

Figure 3.16 shows the assumed path of the operating point following a sudden large decrease in irradiance. This figure should be compared with Figure 3.7. Immediately after the sudden large decrease in irradiance from  $I_r(k-1)$  to  $I_r(k)$ , it is assumed that the operating point moves from point A to point B along a straight line. Point B is such that

$$V_{pv}(k) = E \times V_{pv}(oc)$$

where  $V_{pv}(oc)$  is the open circuit voltage of the PV array for these conditions, i.e. the value of  $V_{pv}$  for  $I_r(k)$  when  $I_{pv}(k)=0$ .  $I_{pv}(k)$  is then calculated using the characteristics of the PV array with  $V_{pv}(k)$  and  $I_r(k)$  as input. Hence, for a large decrease in irradiance:

$$\Delta I_{pv}^{I_r}(k) = I_{pv}(k) - I_{pv}(k-1)$$

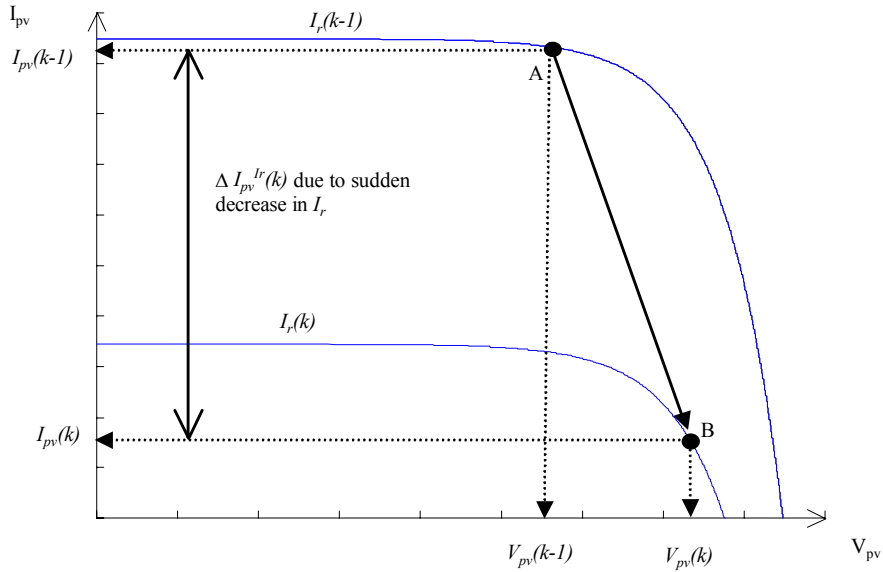


Figure 3.16: Path of operating point for sudden decrease in  $I_r$

### 3.5.5 Effect of Changes in AC Grid Voltage

Figure 3.17 illustrates the modelling of the effects of changes in the ac grid voltage. It should be compared to Figure 3.8 and Figure 3.9, which show the experimental results for a sudden increase and a sudden decrease in ac grid voltage. If A is the operating point before the voltage disturbance, B is assumed to be the operating point immediately after a decrease in voltage and C the operating point immediately after an increase in voltage. While the behaviour of the system is qualitatively similar for both cases, experimental results suggest that the quantitative effects are different. The changes in PV array currents are:

$$\Delta I_{pv}^{Vac} = -G \times \Delta V_{ac} \text{ for an increase in voltage}$$

$$\Delta I_{pv}^{Vac} = -F \times G \times \Delta V_{ac} \text{ for a decrease in voltage}$$

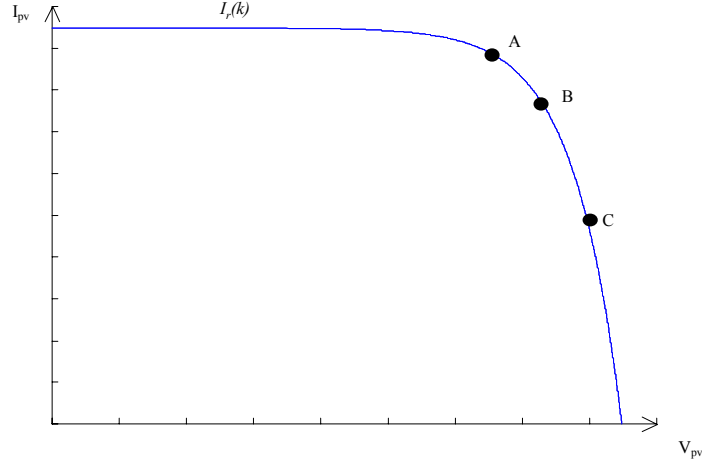


Figure 3.17: Path of operating point for sudden increase and decrease in  $V_{ac}$

### 3.5.6 MPPT

As mentioned above, this PV generation model assumes that the MPPT technique used is the P&O method. However, instead of monitoring and controlling  $V_{pv}$ , this model adjusts  $I_{pv}$  in its search for the MPP. The input of the MPPT are  $I_{pv}$  and  $V_{pv}$ . These two quantities are multiplied to obtain  $P_{pv}(k)$ , which is compared to  $P_{pv}(k-1)$ , i.e. the value obtained during the previous cycle. If the dc power delivered by the array has increased since the last measurement, the output of the MPPT will have the same sign as in the last cycle. On the other hand, if the power has decreased, the output of the MPPT will have the opposite sign to the last cycle. This output (+1 or -1) is multiplied by the  $I_{pv}$  step value,  $\Delta I_{pv}^{MPPT}$  and added with the other components of the current  $I_{pv}$ . The value of  $I_{pv}^{MPPT}$  was determined by trial and error. If the cycle time is small, the  $\Delta I_{pv}^{MPPT}$  will be relatively small. If the cycle time is big, the  $\Delta I_{pv}^{MPPT}$  will be relatively big. In this model, the cycle time used is 0.2s.

The following values of the parameters give a good agreement between the predictions of the model and the experimental results:  $D=0.08$ ,  $E=0.92$ ,  $F=0.25$ ,  $G=2.875$ ,  $\Delta I_{pv}^{MPPT}=0.085A$ .

### 3.5.7 Model Validation.

In order to validate the structure of the proposed model and to evaluate its accuracy, an extensive set of tests was performed on the laboratory PV system. These

experimental results were compared with simulation runs performed using an implementation of the model developed using the Simulink™ tool.

Figure 3.18, Figure 3.19, Figure 3.20, Figure 3.21 and Figure 3.22 show both the actual response of the system (depicted by a solid line) and the simulated response obtained using the model (depicted using a sequence of cross marks). These figures show that the model accurately represents the response of the PV generating unit to small changes in irradiance, large increases or decreases in irradiance, and sudden increases or decreases in ac grid voltage.

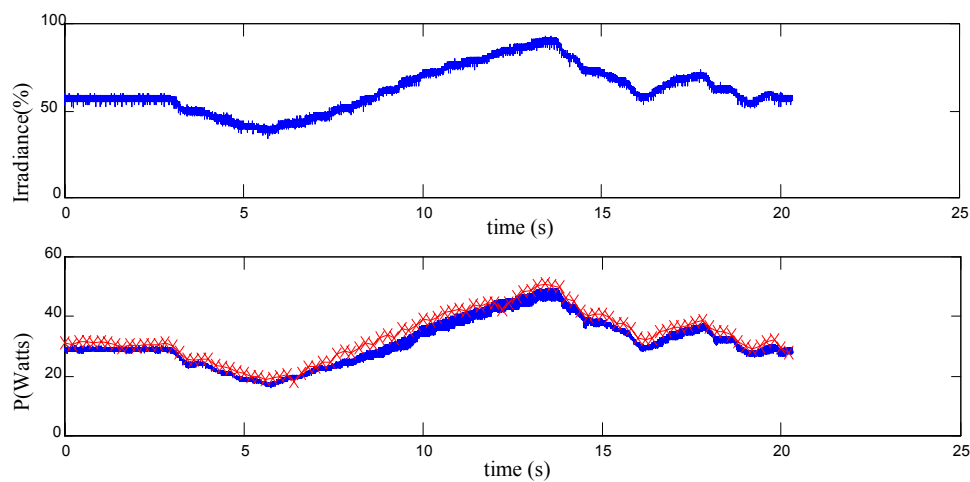


**Figure 3.18: Comparison of the response to slow change in irradiance of the PV generator and of the proposed model**

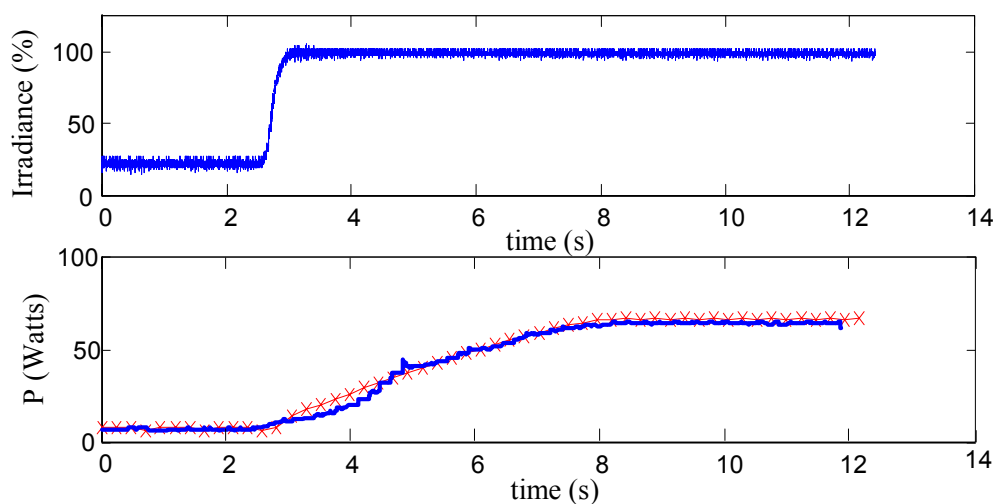


**Figure 3.19: Comparison of the response to a sudden large increase in irradiance of the PV generator and of the proposed model**

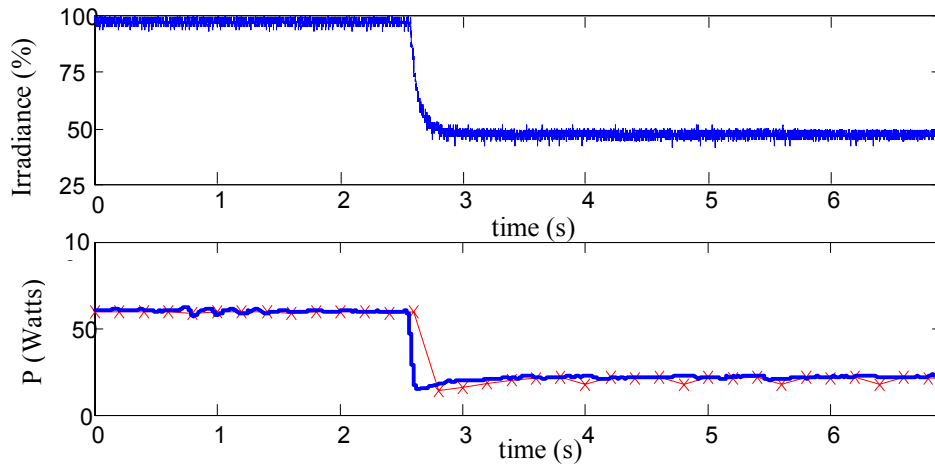


**Figure 3.20: Comparison of the response to a sudden large decrease in irradiance of the PV generator and of the proposed model**

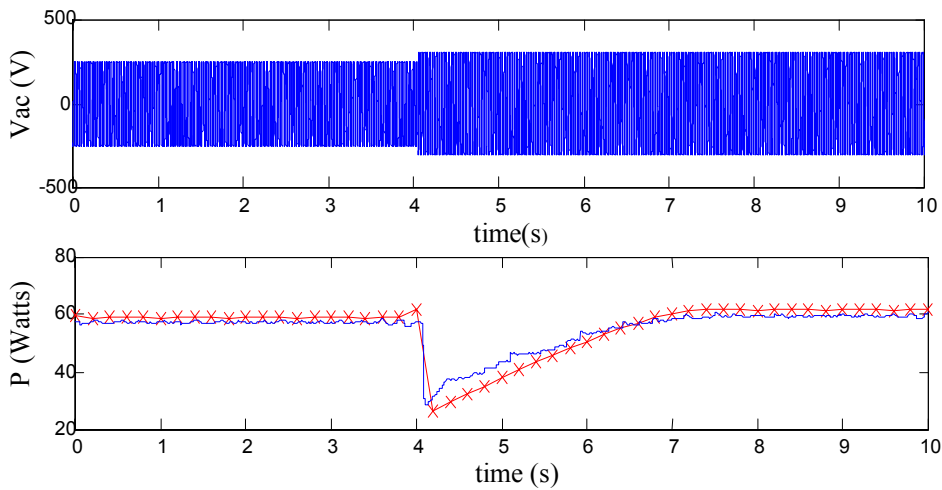


**Figure 3.21: Comparison of the response to a sudden increase in grid ac voltage of the PV generator and of the proposed model**

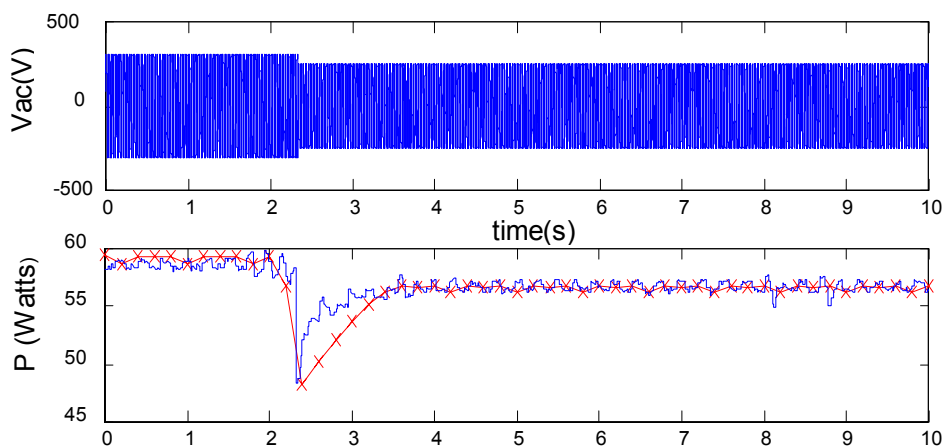


**Figure 3.22: Comparison of the response to a sudden decrease in grid ac voltage of the PV generator and of the proposed model**

### **3.6 CONCLUSIONS**

A significant increase in the penetration of PV generation could have a significant impact on the stability of the transmission network. An accurate model of the dynamic behaviour of PV generating units will therefore be needed to study the security of the power system under these conditions. This chapter proposes such a model. This model was developed on the basis of experimental results. These experimental results show that the MPPT controller plays a critical role in the dynamic response of the PV system. The proposed model is capable of representing the system's response to both small and large changes in irradiance and ac grid voltage. The accuracy of the model is demonstrated by comparing the simulated response with experimental results.

# Chapter 4

## **DYNAMIC RESPONSE TO RAPID CHANGES IN IRRADIANCE**

### **4.1 INTRODUCTION [22, 23]**

The connection of a large amount of PV generation to the grid could have far reaching consequences not only on the distribution networks but also on the transmission grid and the rest of the generators. The most severe disturbance in the output of PV generation would probably be encountered when a band of clouds sweeps over an area with a large concentration of PV generators. This could result in a fairly large and sudden variation in the PV output. The condition would be aggravated if this change in irradiance occurred during a period of rapid increase in load.

This chapter describes how the PV generation model described in the previous chapter has been used to analyse this type of event. The analysis is carried out on a 10-bus test system but the conclusions should be generally applicable to other power systems. It discusses the transient changes in bus voltages resulting from fluctuations in photovoltaic generation. The purpose of this investigation was to determine if these fluctuations were large enough to have serious consequences and place a limit on the amount of PV generation that can be connected to a power system.

## **4.2 EXPLORING THE PROBLEM [26, 31]**

PV power generation depends on solar irradiance. Unlike conventional generation, photovoltaic generators do not have rotating parts, have thus no inertia and changes in output can occur extremely rapidly. This potentially causes a problem for the utility when the output power of the photovoltaic generation changes rapidly due to the irradiance changes caused by the random movement of the cloud cover over a clear sky. As the cloud shadows pass over a PV array, the PV output decreases. The PV system then resumes production when the shadows have moved beyond the array. An accurate prediction of PV power generation is thus difficult.

The impact of PV generation on a power system will vary from one power system to another depending on the intensity of the PV input relative to the power system and the geography of the PV input in relation to the power system geography. Each power system is characterized by its own generation mix. This mix determines the limits on ramping rates, and the ability to respond to imbalances between load and generation. The penetration level, the size of the service area and the distribution (central or dispersed) of the photovoltaic generators over the service area are additional factors that determine the effect of passing clouds on the system. Depending on the percentage of PV penetration and its degree of concentration, these variations in irradiance may cause undesirable voltage fluctuations and may affect the operation of the voltage regulating equipment. These fluctuations are thus likely to give rise to operational problems.

## **4.3 10-BUS TEST SYSTEM [34]**

Figure 4.1 shows the one-line diagram of the test system used for this analysis. The system consists of a local area connected to a remote area by five 500 kV transmission lines. All the loads (6655 MW, 1986 MVars) are in the local area. The local generator at bus 3 generates 1154 MW, and the remaining power is supplied by the two remote generators (bus-1 and bus-2). Shunt capacitors are connected at various buses in the local area. The details of the system data are given in appendix 1.

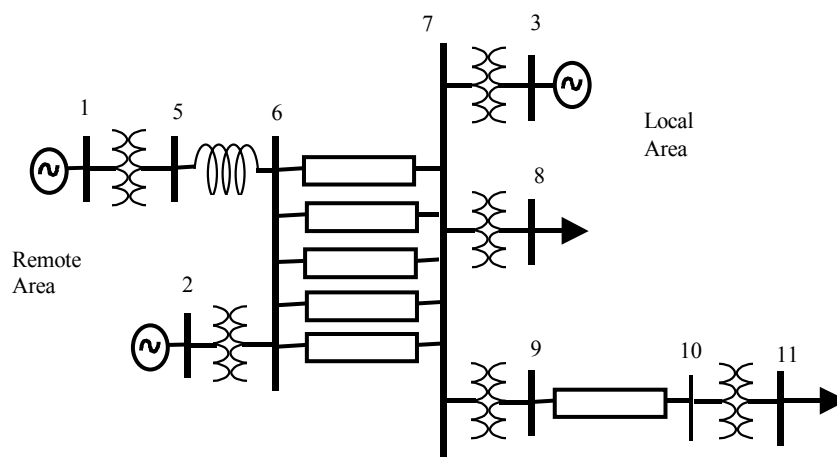


Figure 4.1: Test System

Table 4.1 shows the load flow results for this test system. The table shows that the voltages for every bus are within the acceptable range for load level 1 and load level 2, i.e. between 0.95 p.u and 1.05 p.u except for bus-10. For load level 3, both the bus-10 and bus-11 are below 0.95 p.u.

Table 4.1: Bus voltages for the three different load levels

Bus	$V$ (p.u) (load level 1)	$V$ (p.u) (load level 2)	$V$ (p.u) (load level 3)
1	0.980	0.980	0.980
2	0.965	0.965	0.965
3	1.040	1.040	1.040
5	1.043	1.040	1.038
6	1.031	1.023	1.017
7	1.026	1.006	0.992
8	0.983	0.960	0.946
9	1.013	0.988	0.972
10	0.937	0.908	0.889
11	0.992	0.960	0.939

#### 4.4 INTEGRATION OF PV GENERATION INTO THE TEST SYSTEM

PV penetrations of 5% and 10% of the total loads have been tested. It is assumed that the PV generators can be located at any bus shown on Figure 4.1. Figure 4.2 shows the bus voltage value in the test system in the presence of PV generators with 5% and 10% PV

penetration at each bus considered separately. These are compared to the base case where no PV power is present in the system.

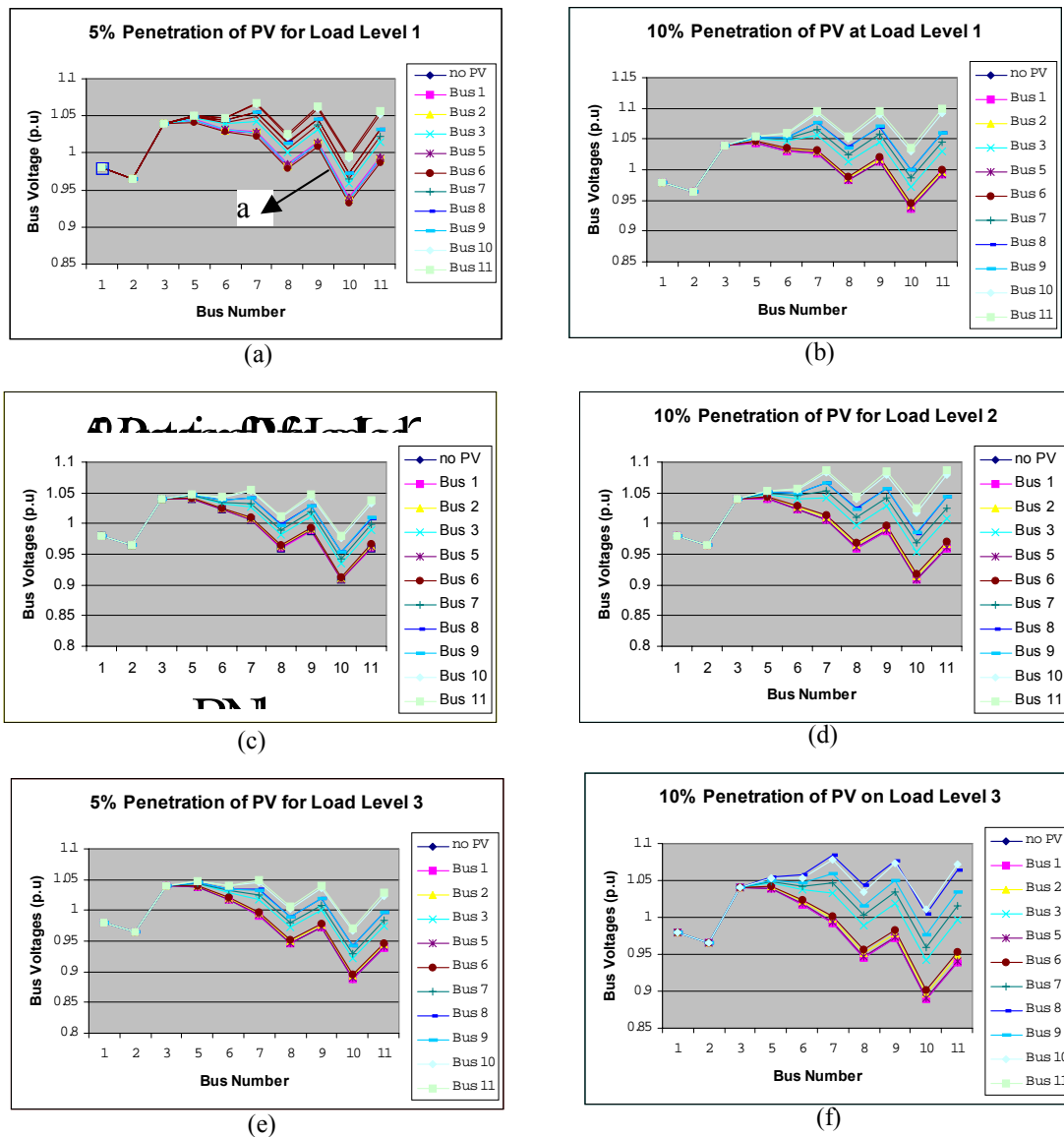


**Figure 4.2: Bus voltages with 5% and 10% of PV penetration at each bus**

Each graph shown in each figure represents the voltages of every bus when the PV generator is located at different bus as identified by the x-axis of each graph, at 5% and 10% PV penetration for the three different load levels. E.g. graph “a” as shown in Figure 4.2(a) represent the voltages at each bus when the PV generator is located at bus-6 with 5% of PV penetration for load level 1. The Y-axis of each graph in Figure 4.2 shows the bus voltages in p.u and the X-axis shows the bus number in the test system. From these figures, it was found that there were no significant effects on the bus voltages when the

PV generators are located at the remote generation area (e.g. bus-1 and bus- 2). When the PV generators are integrated in the local area such as bus-11 and bus-8 where no conventional generator is attached, the buses experience voltage increases. The effect becomes more significant when the penetration of PV generation at the local area is higher as shown in the right hand graphs. The location of the substation where the PV generators are connected is thus very important. This approach helps to identify static voltage problem caused when PV is integrated at different buses and helps to determine the maximum PV penetration that does not cause static voltage problems.

#### 4.5 SIMPLIFICATION OF AGGREGATE MODEL OF GRID-CONNECTED PV GENERATION [34]

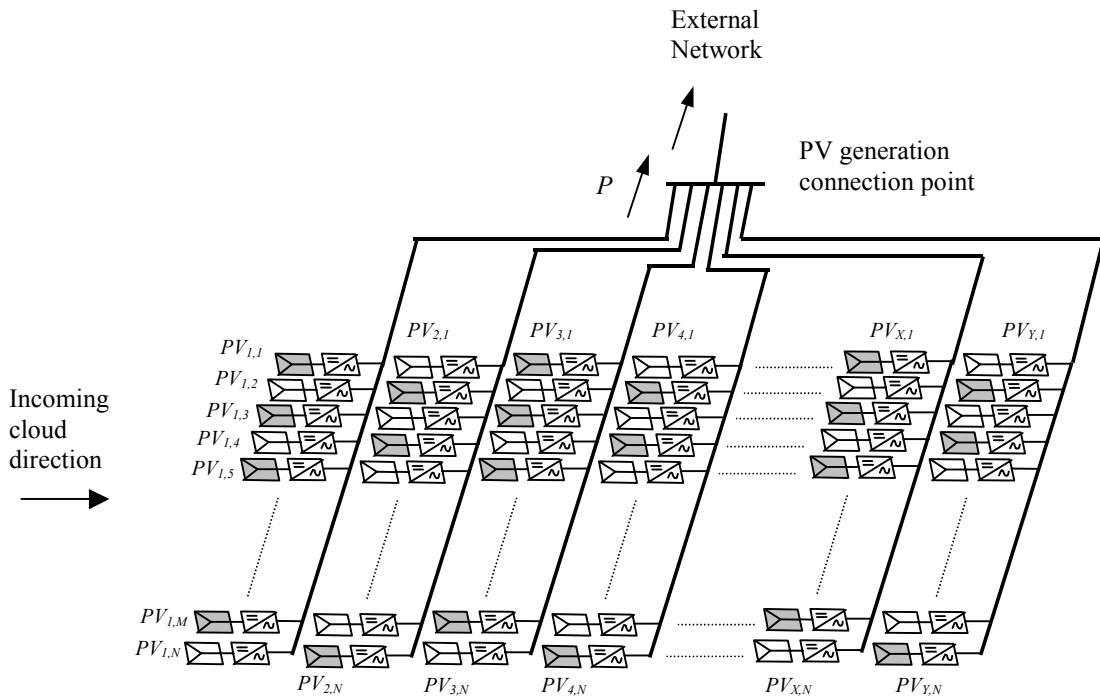


**Figure 4.3: The aggregate model of large PV plant connected to the power grid**

Commonly, grid-connected PV generation consist of a large number of relatively small PV units. This distributed generation can be represented by an equivalent PV generation plant whose rating is equal to the sum of the ratings of the individual PV generating units. The operational points of the individual PV generating units are determined by the irradiance value and MPPT control algorithm.

The aggregate model of the large-scale PV plant thus comprises  $N \times Y$  PV generating units of  $G$  kW power capacity each where  $N$  is the number of PV generating unit in row and  $Y$  is the number of PV generating unit in column. The installed capacity of the equivalent PV plant is thus  $N \times Y \times G$  kW. The model is shown in Figure 4.3.

#### 4.5.1 Uniform Solar Irradiance Distribution

In this case the PV generating units within the plant are assumed to have the same operating points. When reducing the aggregate model of the large PV plant, the following assumptions are made: -

- The MVA rating of the large PV plant equivalent,  $S_{\Sigma, \Sigma}$ , is the sum of the MVA ratings of the PV generating units:

$$S_{\Sigma, \Sigma} = \sum_{i=1}^Y \sum_{j=1}^N S_{i,j} \quad (4.1)$$

where  $S_{i,j}$  is the MVA-rating of the PV generating unit  $j$  being in the column  $i$ .

- The equivalent PV generating plant supplies the same amount of electric power to the grid:

$$P_{\Sigma, \Sigma} = \sum_{i=1}^Y \sum_{j=1}^N P_{i,j} \quad (4.2)$$

where  $P_{i,j}$  is the electric power supplied by the PV generating unit  $j$  being in the column  $i$  and  $P_{\Sigma, \Sigma}$  is the electric power supplied by the whole PV plant.

Equation 4.1 and 4.2 imply that the equivalent PV plant can be defined by a simple addition of the MVA ratings and an addition of the electric power output of the individual generating units. Figure 4.4 shows this one-PV generator equivalent. The incoming cloud shown in Figure 4.3 is assumed to cover all the individual PV generating units in the equivalent plant at the same time.

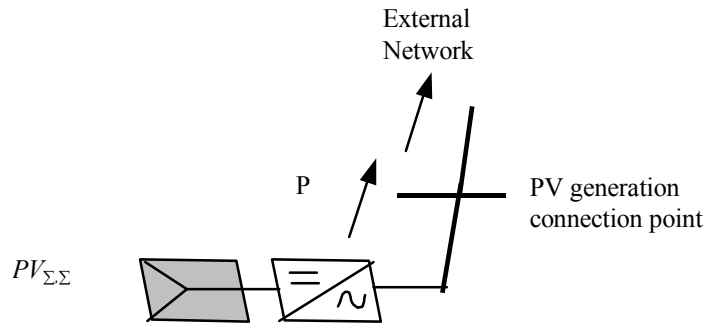


Figure 4.4: One-PV generator equivalent

### 4.5.2 Non-uniform Solar Irradiance Distribution

In this case the incoming cloud is such that:

- Its direction is as shown in Figure 4.3.
- The cloud takes  $k$  seconds time to move from the first column to the second column of the PV generating units. In other words, the irradiance is shifted by  $k$  seconds for each column of PV generating units.

Since the operating points of the PV units in each column are identical, the outputs of the PV units in each column are added and a multi-machine equivalent comprising of  $Y$  PV generating units is obtained. This multi-generators equivalent is shown in Figure 4.5

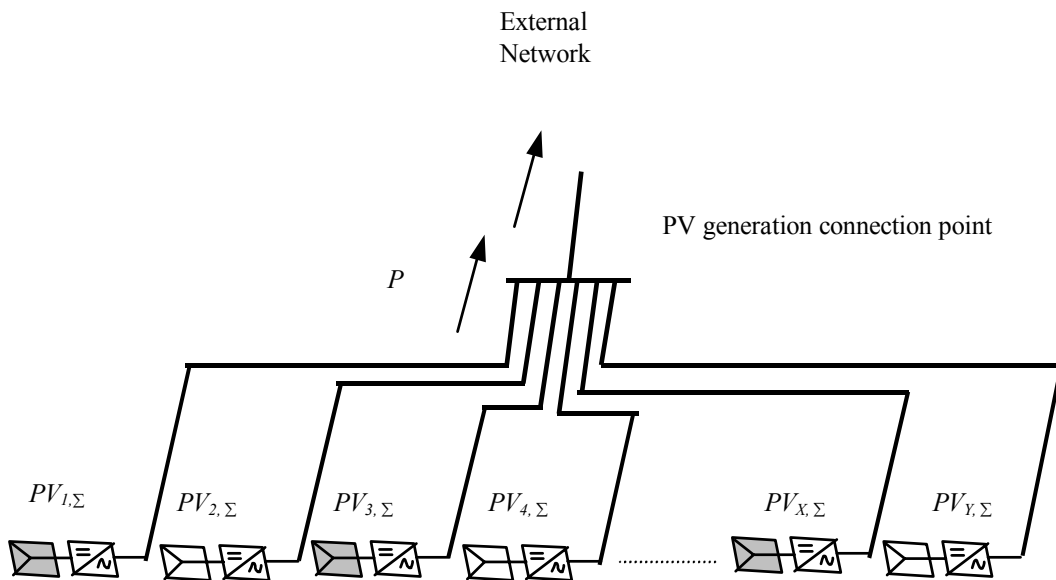


Figure 4.5: The multi-PV generator equivalent

The MVA ratings,  $S_{\Sigma,\Sigma}$ , the electric powers,  $P_{\Sigma,\Sigma}$  of the equivalent PV plants are given by:

$$S_{\Sigma,\Sigma} = \sum_{i=1}^Y S_{i,\Sigma} \quad P_{\Sigma,\Sigma} = \sum_{i=1}^Y P_{i,\Sigma} \quad (4.3)$$

#### 4.6 CASE STUDIES

These case studies illustrate the response of the system when subjected to sudden changes in irradiance caused by a passing cloud. Different amounts of PV penetrations are considered. In section 4.4, it was found that the integration of the PV generation in the local area caused the most impact on the bus voltages in the system of Figure 4.1. Therefore, the PV generators have been connected to bus-11 for simulation studies. The shunt capacitors at the local buses are adjusted so that the initial operating voltage of bus-11 is 0.992 p.u, i.e. the same as the voltage of bus-11 for the base case.

Table 4.2 shows both the power produced by the conventional generators and the peak power of the PV generators for 5%, 10% and 15% penetration of PV generation. Figure 4.6 shows the irradiance data on a typical cloudy day from 7am to 4pm. The system of Figure 4.1 system was simulated over a 60 seconds period from 11:50am to 11:51am on that day. The sampling rate of the irradiance data is 1 sample/second. Both uniform and non-uniform solar irradiance distribution (see sections 4.5.1 and section 4.5.2) are considered.

**Table 4.2: Generation at specific busses by both the conventional and PV generation in the case of 5%, 10% and 15% level of PV penetration**

Bus of Generation	P (MW)		
	5% Penetration	10% Penetration	15% Penetration
1	3633	3268	2905
2	1736	1736	1736
3	1154	1154	1154
11	333	665	998

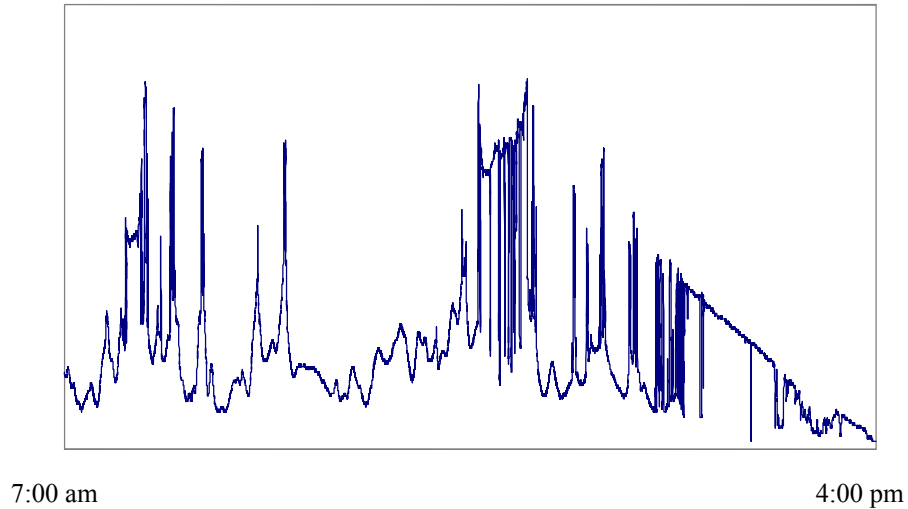
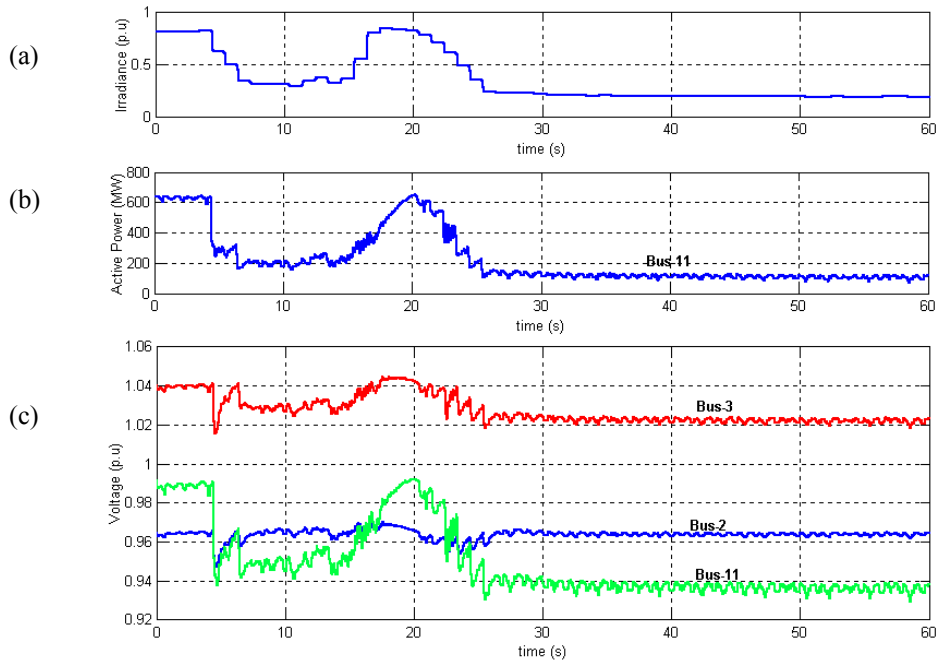


**Figure 4.6: Irradiance data on a partly cloudy day**

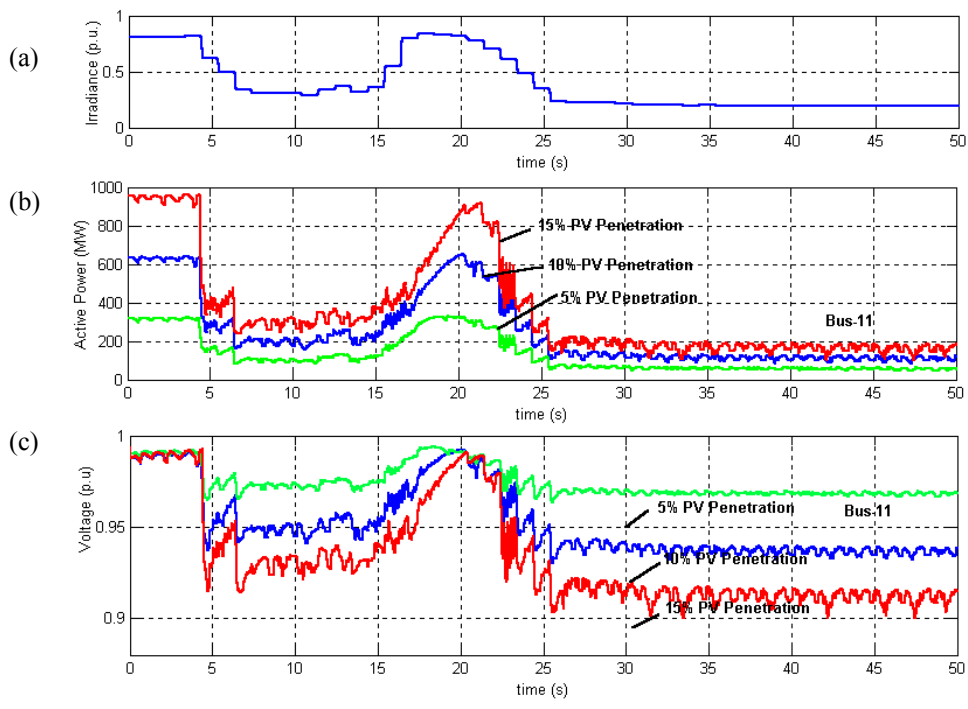
#### 4.6.1 Simulation Results

Figure 4.7 shows the simulation results for the uniform irradiance distribution and Figure 4.8 shows the comparison results of 5%, 10% and 15% PV penetration for the uniform irradiance distribution. All the PV generators are assumed to receive the same irradiance, which is shown in Figure 4.7(a) and Figure 4.8(a). A plot of the active power of PV generation versus time for 10% PV penetration is shown in Figure 4.7(b). Figure 4.7(c) shows the bus voltage as a function of time for a few selected buses. Figure 4.8(b) and Figure 4.8(c) show respectively the PV generation and bus voltages at bus-11 for three levels of PV penetration.

Figure 4.9 shows the simulation results that were carried out when a non-uniform irradiance distribution is assumed and Figure 4.10 shows the comparison results for 5%, 10% and 15% PV penetration for the non-uniform irradiance distribution [28]. The cloud is assumed to take 3 seconds time to move from the first column of the PV generating units to the second column of the PV generating units. In other words, the irradiance is shifted by 3 seconds for each column of PV generating units as shown in Figure 4.9(a) and Figure 4.10(a). Figure 4.9(b) shows the total amount of active power generated by the PV generators into bus-11. Figure 4.9(c) shows the bus voltages at bus-2, bus-3 and bus-11. The comparisons between the PV generations and the bus voltages at bus 11 for the 3 levels of PV penetration are shown in Figure 4.10(b) and Figure 4.10(c) respectively.



**Figure 4.7: Simulation results for uniform irradiance distribution. (a) Irradiance (b) Total PV active power injected at bus-11 (c) Voltage at bus-2, 3 and 11.**



**Figure 4.8: Comparison results for 5%, 10% and 15% of PV penetration with uniform irradiance distribution. (a) Irradiance, (b) Total PV active power injected at bus-11, (c) Voltage at bus-11**

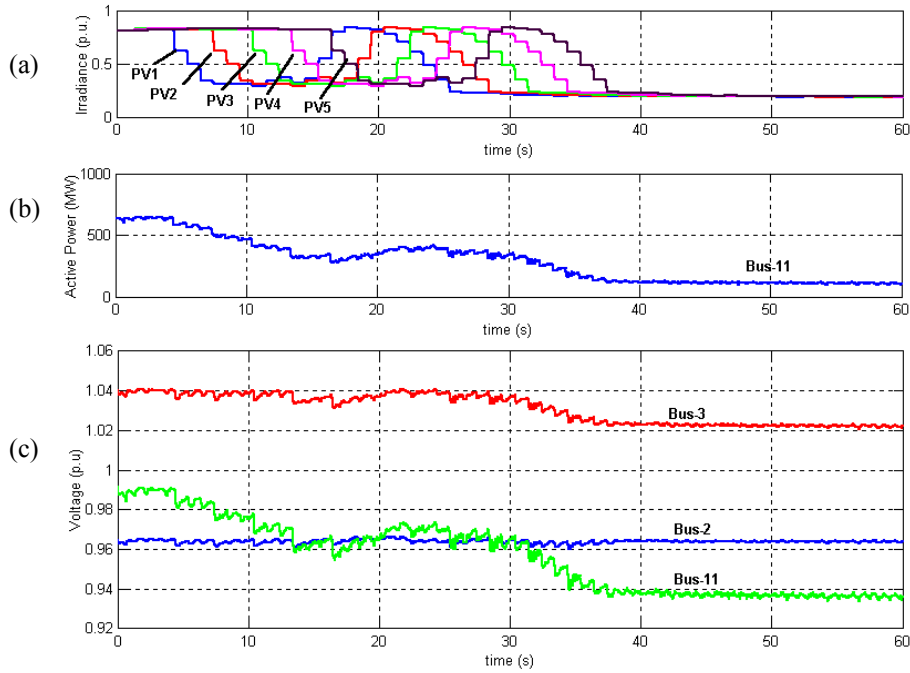


**Figure 4.9: Simulation results for non-uniform irradiance distribution. (a) Irradiance, (b) Total PV active power injected at bus-11, (c) Voltage at bus-2, 3 and 11**

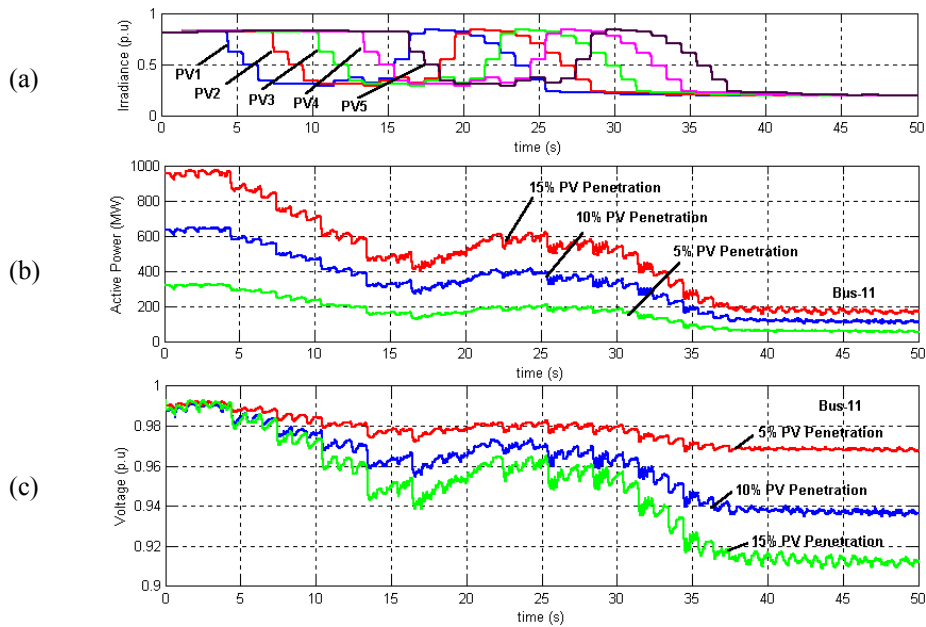


**Figure 4.10: Comparison results for 5%, 10% and 15% of PV penetration with non-uniform irradiance distribution. (a) Irradiance, (b) Total PV active power injected at bus-11, (c) Voltage at bus-11**

### 4.6.2 Analysis

Figure 4.7(b) shows that the amount of power produced by the PV generators follows the pattern of irradiance. This is because the MPPT controllers keep the PV generating units operating point at their maximum power point despite the large fluctuations in irradiance that take place over the 60 seconds time frame considered. Figure 4.7(c) and Figure 4.9(c) confirm that the voltage at the buses with conventional generator (bus-2) is not affected by the fluctuation in PV output because of the action of the automatic voltage regulators. The voltage at bus-2 at  $t = 0s$  and  $t = 60s$  remain the same, i.e. 0.962p.u. There is a slight drop in the voltage at bus-3 because the reactive power demand on the generator is higher and the field current of the generator connected to this bus exceeds its limit. The PV generator connected to bus-11 is modelled as a P injector without voltage regulator. Its bus voltage fluctuates during the large changes in irradiance level that occur between  $t = 3s$  and  $t = 25s$ . This voltage change follows the pattern of power injection at the bus.

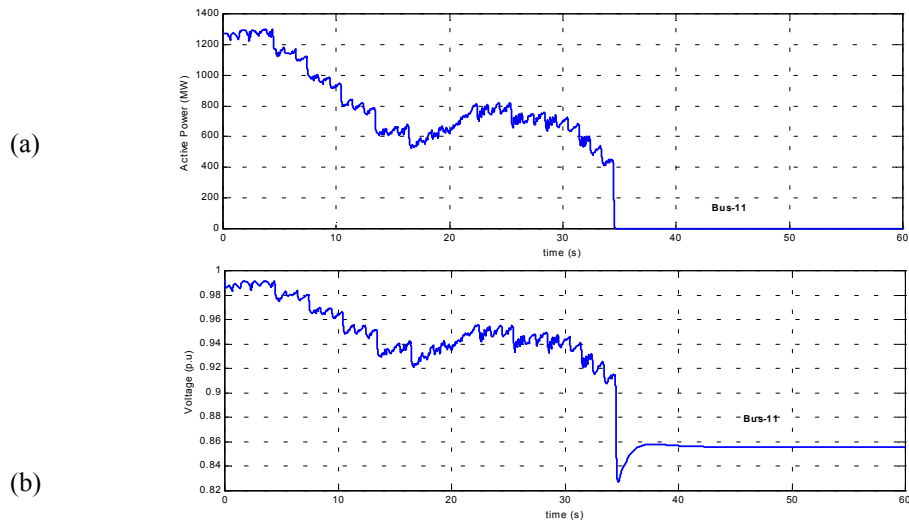
Figure 4.8 shows that when the amount of PV penetration is high, the amount of voltage fluctuation due to irradiance change becomes more significant. As shown in Figure 4.8(c) at  $t = 0s$ , all the voltages are at the same (0.992 p.u). However, at  $t = 50s$ , when the irradiance level is low, the voltage at bus-11 settles at 0.970 p.u for the 5% penetration case, 0.939 p.u for the 10% penetration case and at 0.917 p.u for the 15% case. Figure 4.10 shows that similar results are obtained when a non-uniform irradiance distribution is assumed.

### 4.6.3 Tripping of PV Generation

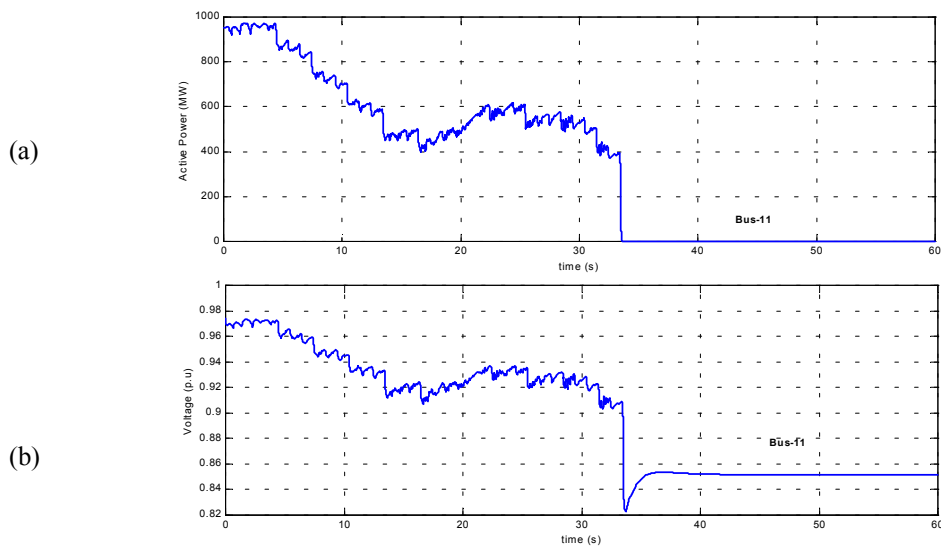
To prevent islanded operation of distributed photovoltaic generation, all photovoltaic inverters are equipped with over/under voltage relay protection. Typically the PV inverters trip when the bus voltage strays from a range of  $\pm 10\%$  of nominal voltage.

Figure 4.11 and Figure 4.12 illustrate this effect. Figure 4.11 considers the case of a non-uniform irradiance distribution and a 20% PV penetration. Figure 4.12 is for a 15% PV penetration and non-uniform irradiance distribution but a larger load (load level 3 as shown in appendix A1). These simulations are for the same irradiance variations as the

previous simulations over a 60 seconds time frame. For both the cases, at approximately  $t = 34s$ , the sudden drop in irradiance causes a sudden reduction in PV generation power. The bus voltage drops below 0.9 p.u and the PV generating units trip due to the operation of the under voltage relay. This terminates the PV generation causing a further voltage reduction but finally the bus voltage settles at the unacceptable value of 0.86 p.u and 0.85 p.u for the cases of Figure 4.11 and Figure 4.12 respectively.



**Figure 4.11: Simulation results for non-uniform irradiance distribution with 20% of PV penetration. (a) Total PV active power injected at bus-11, (b) Voltage at bus-11**



**Figure 4.12: Simulation results for non-uniform irradiance distribution with 15% of PV penetration at load level 3. (a) Total PV active power injected at bus-11, (b) Voltage at bus-11**

#### **4.7 CONCLUSION**

The methodology described in this chapter is intended to help network operators understand the changes in PV generation caused by moving cloud shadows. In practice, a system operator would need weather and insolation forecasts to make proper prediction of the variability of PV generation in the system. The operator would then be able to ensure that enough voltage control and frequency control resources are available.

# Chapter 5

## MITIGATING VOLTAGE FLUCTUATION DUE TO PHOTOVOLTAIC GENERATION

### 5.1 INTRODUCTION

Utilities in various countries are required by their respective regulations to supply power to customers at voltages where the magnitude should vary only within a very limited range. In the U.K. for example, the magnitude of voltage at the consumer site should be kept within the statutory limits of  $\pm 6\%$ . As shown in Chapter 4, the penetration of a large amount of PV generation into the power system could cause large voltage fluctuations when the irradiance incident on the PV array is not constant. Besides, the sudden reduction in PV generation due to the sudden drops in irradiance value may cause an undesirable tripping of PV generators and other generators on the system due to the mal-operation of under-voltage relays.

Currently, most of the inverters used for PV generators are designed to operate at unity power factor. Reactive power is neither absorbed nor produced. If PV generation is implemented on a large-scale, there is a need to make better use of the PV plant to help

in voltage control. Three voltage control techniques that could help overcome the voltage problems caused by the penetration of PV generation have been investigated. The techniques include constant power factor control, automatic voltage control from the PV inverter itself and Static VAR Compensators (SVC) voltage control.

## 5.2 CONSTANT POWER FACTOR CONTROL [35,36]

Figure 5.1 shows the block diagram of constant power factor controller implemented in a PV inverter. As the block diagram shows, the power factor controller includes a PI controller. The error signal driving the PI controller is derived from the difference between the reference reactive output power,  $Q_{ref}$  and the measured reactive output power  $Q_{PV}$ .  $Q_{ref}$  is obtained from the multiplication of active output power with the tangent of the inverse-cosine of the targeted power factor. In practice, the inverse-cosine function is implemented using a look-up table.  $Q_{PV}$  is measured and smoothed with a time constant  $T_v$ .

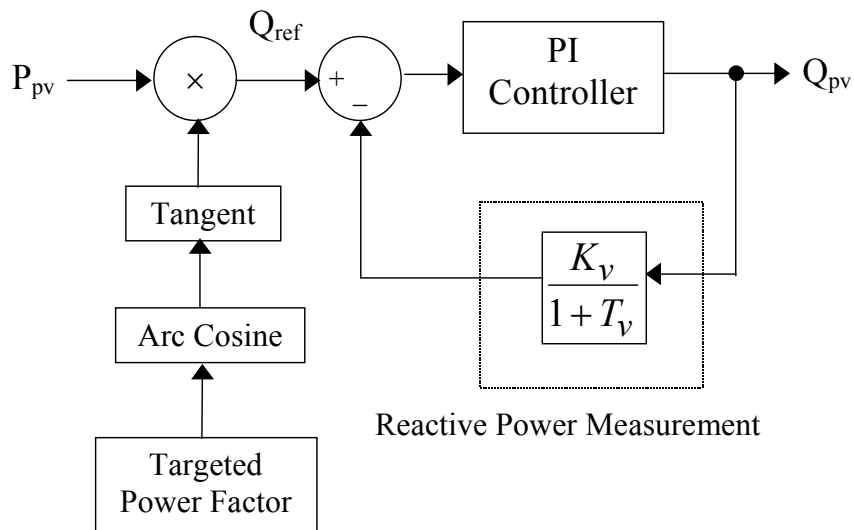


Figure 5.1: Constant power factor controller

The preset targeted power factor determines the amount of reactive power supplied or absorbed by the PV inverter. The power factors are within the range of 0.85 lagging to 0.85 leading. The lagging and leading power factor conditions corresponding to the PV generators supplying and absorbing reactive power respectively.

### 5.3 AUTOMATIC VOLTAGE CONTROL FROM PV INVERTER

Figure 5.2 shows the block diagram of the automatic voltage controller if the voltage is regulated by the PV generator itself. Again this controller includes a PI controller. The error signal driving the PI controller is equal to the differences between the reference terminal voltage,  $V_{ref}$  and the measured terminal voltage,  $V_t$ .  $V_t$  is measured and smoothed with time constant  $T_v$ . The reactive output power  $Q_{PV}$  is varied to maintain the  $V_t$ . Due to the thermal limitation, the automatic voltage control of a PV generator can only operate in the range between 0.85 lagging and 0.85 leading. During short circuit the amount of reactive power required by the controller is maximum. This situation could produce over-voltages after the fault has been cleared. Thus, this model includes a protection loop that decreases the reactive power demand (to a maximum value  $Q_{min}$ ) when the voltage passes under a threshold value.

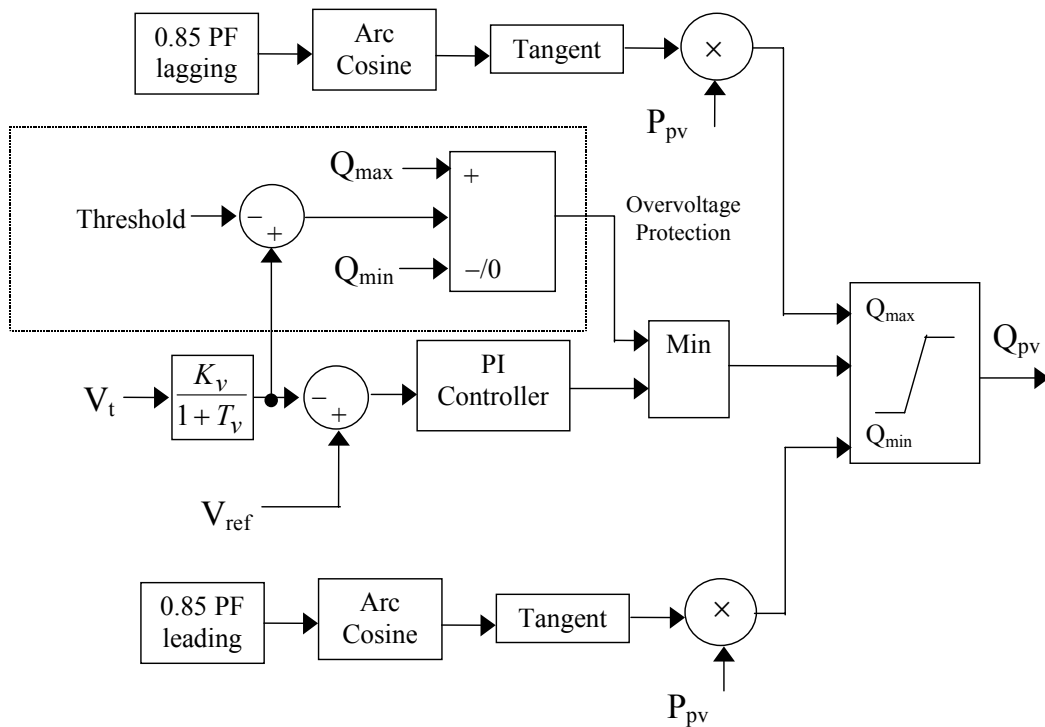


Figure 5.2: Automatic voltage control from PV generator

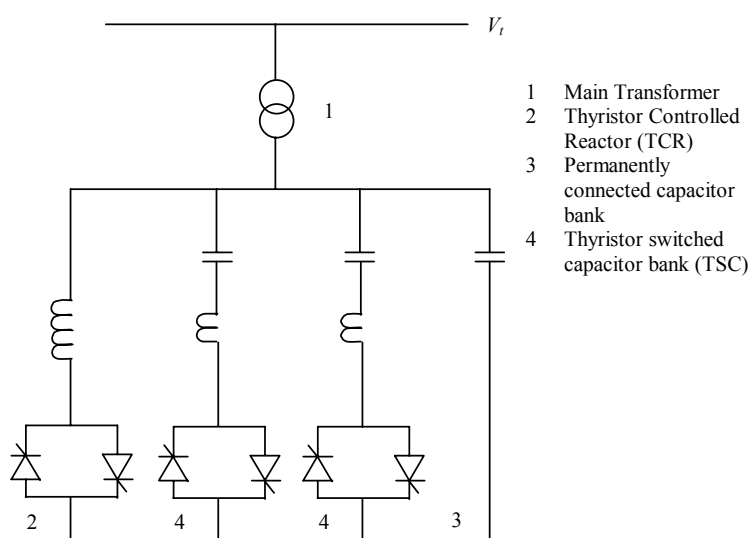
### 5.4 VOLTAGE CONTROL FROM SVC [37,38,39]

SVC forms an important part of controllable reactive power compensation in power system. A general overview on the benefits of the application of SVC is given in table 1.

**Table 5.1: Benefits of application of SVC**

Primary Benefit	Voltage control Reactive power control Over-voltage limitation at load rejection
Secondary Benefit	Improvement of AC network Stability Damping of power oscillations
Tertiary Benefit	Reactive power flow control Increase of transmission capability Preventing voltage instability Load reduction through voltage reduction Subsynchronous oscillation damping

An SVC consists of capacitive and inductive elements connected to the LV side of a transformer. This LV connection reduces the cost of the thyristor valves. With their fast acting power electronic devices (thyristor valves), it can be used for voltage control in network operation. The thyristor valves included are the TCR (Thyristor Controlled Reactor) branch and the TSC (Thyristor Switched Capacitor) branch as shown in Figure 5.3. The TCR branch allows for continuous variation of the inductive power. The TSC branch allows for stepped control of the capacitive power. Use of SVC for the duties of voltage control requires a general voltage/current characteristic as shown in Figure 5.4. The V/I curve must include a continuous operating range where any operating point is reachable as well as a certain overload characteristic at increased network voltages.

**Figure 5.3: Schematics of a static compensator**

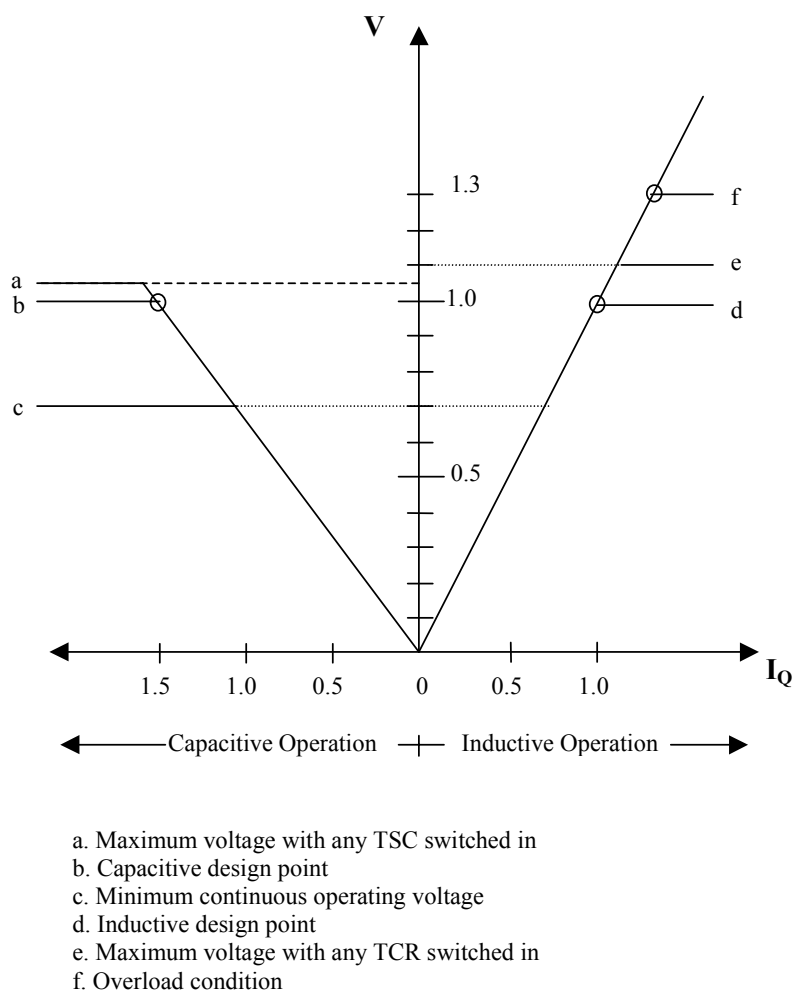


**Figure 5.4: Example of V/I characteristic of a SVC**

Figure 5.5 shows a basic closed loop controller for an SVC as described in [37]. This controller has two parts, namely a "voltage regulator block" and a "regulator droop block". In the "voltage regulator block", the output of the SVC is to be controlled to maintain or vary the voltage at the point of connection to the power system. With the basic static compensator control, it is operated as a perfect terminal voltage regulator: the amplitude  $V_t$  of the terminal voltage is measured and compared with the voltage reference  $V_{ref}$ , the error signal ( $\Delta v$ ) is processed and amplified by a PI controller to provide the VAR demand signal ( $Q_{signal}$ ) to the SVC. In many applications, the SVC is not used as a perfect terminal voltage regulator but rather the terminal voltage is allowed to vary in proportion with the compensating current. The reason for this is the linear operating range of a compensator with given maximum capacitive and inductive ratings can be extended if a regulation droop is allowed. In the "regulator droop block", an effective reference voltage ( $V_{ref}^*$ ) is calculated by introducing a regulator droop ( $k$ ) to

the reference voltage ( $V_{ref}$ ). The regulator droop allows the terminal voltage to be smaller than the nominal value at full capacitive compensation and higher at full inductive compensation as shown in Figure 5.6. The effective reference  $V_{ref}^*$  controlling the terminal voltage thus becomes

$$V_{ref}^* = V_{ref} + kI_Q \quad (5.1)$$

In Equation 5.1, the regulation droop  $k$ , (typically 1% - 5%) is defined by

$$k = \frac{\Delta V_{Cmax}}{I_{Cmax}} = \frac{\Delta V_{Lmax}}{I_{Lmax}} \quad (5.2)$$

where  $\Delta V_{Cmax}$  is the deviation (decrease) of the terminal voltage from its nominal value at maximum capacitive output current ( $I_{Qmax} = I_{Cmax}$ ),  $\Delta V_{Lmax}$  is the deviation (increase) of the terminal voltage from its nominal value at maximum inductive output current ( $I_{Qmax} = I_{Cmax}$ ),  $I_{Cmax}$  is the maximum capacitive compensating current, and  $I_{Lmax}$  is the maximum inductive compensating current.

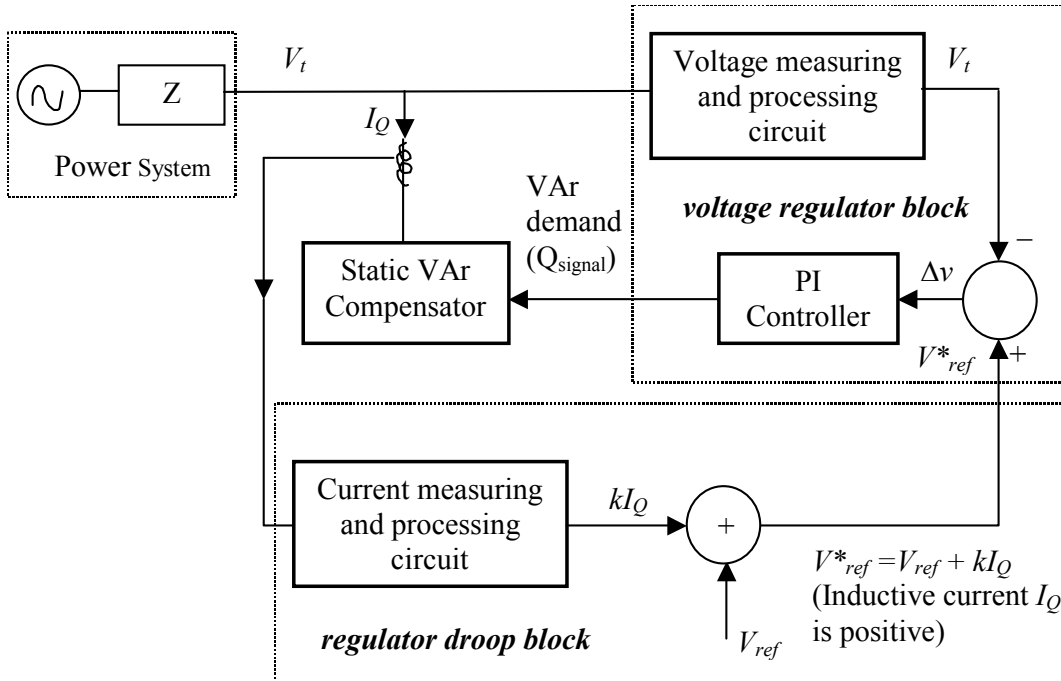
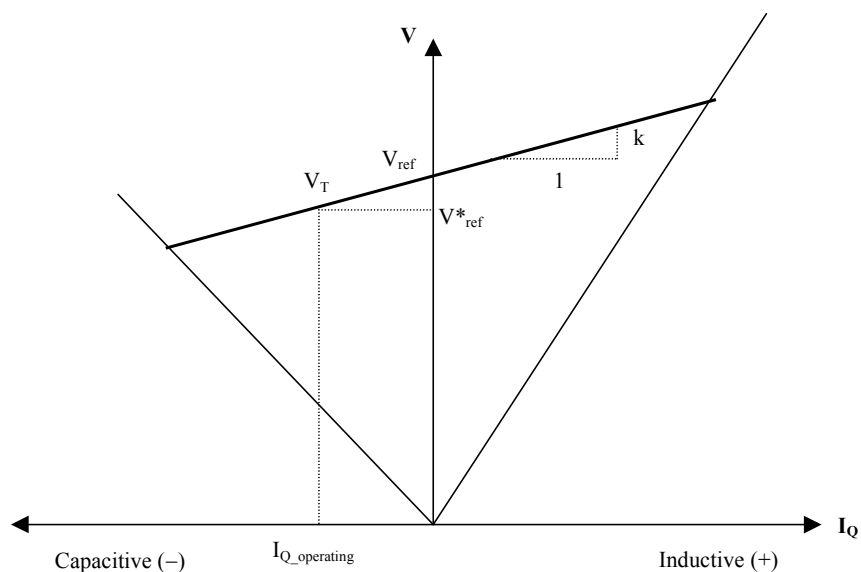


Figure 5.5: Basic closed loop control for voltage regulation



**Figure 5.6: V-I characteristic of SVC for the voltage regulation**

## 5.5 CASE STUDIES

These case studies illustrate the effectiveness of the voltage control methods described above in mitigating the voltage fluctuation problems that arise when sudden change in irradiance affect PV generation. The voltage control methods described are implemented in the test system shown in Chapter 4, Figure 4.1. The PV generators are connected at bus-11 and the simulation studies were performed for 5% and 10% PV penetration over a 60 seconds period on a typical partly cloudy day.

### 5.5.1 Simulation Results

Figure 5.7 and Figure 5.8 show the simulation result for the case of 5% and 10% PV generation respectively without voltage control. The PV generator is operating at unity power factor. The reactive power generated is zero as shown in both Figure 5.7(b) and Figure 5.8(b). The bus voltage at bus-11 fluctuates when the irradiance (shown in Figure 5.7(a) and Figure 5.8(a)) varies over a 60-seconds period. For the 5% PV penetration case, Figure 5.7(c), the bus voltage is 0.994 p.u at  $t = 18$ s when the irradiance value is at its maximum. At  $t = 25$ s, the bus voltage is 0.968 p.u. The difference in bus voltage between the maximum and minimum irradiance is thus 0.026 p.u. For the case of 10% PV penetration, the difference in bus voltage between the maximum and minimum irradiance is even larger, i.e. 0.057 p.u.

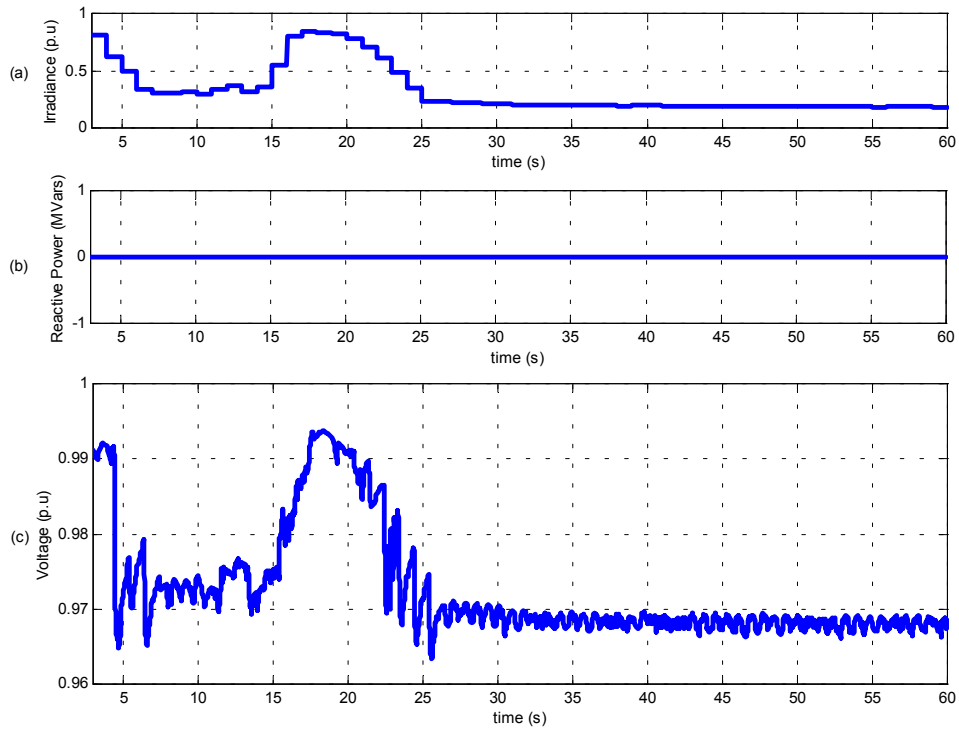


Figure 5.7: 5% PV penetration without voltage control

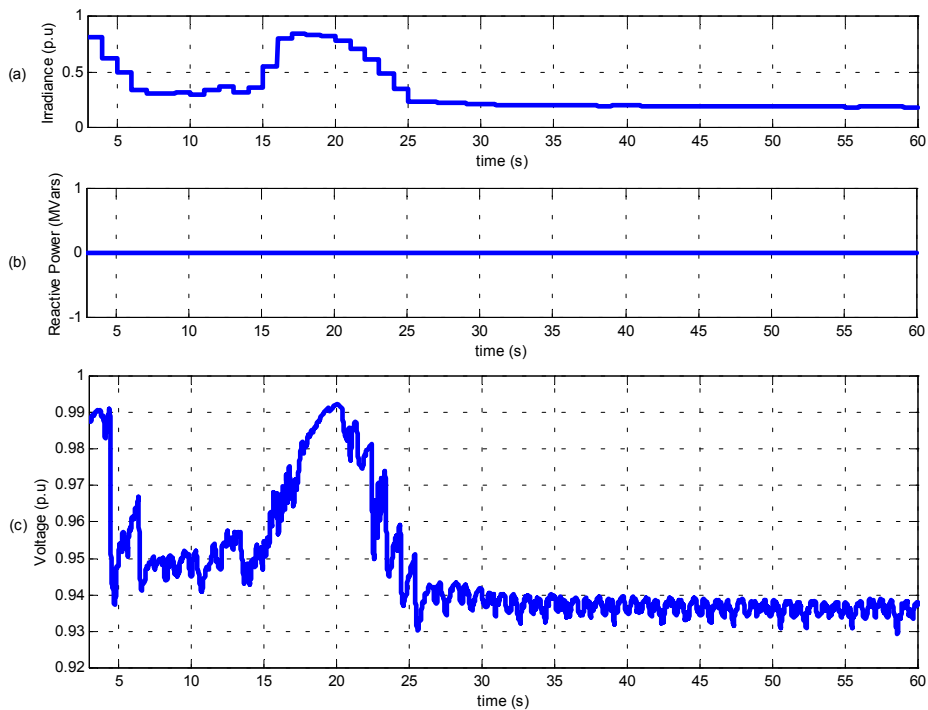


Figure 5.8: 10% PV penetration without voltage control

### 5.5.1.1 Simulation Results of Constant Power Factor Control

The effect of operating the connected PV generators with constant power factor controller on the voltage profile of bus-11 has been investigated. The power factors that have been considered are 0.95 lagging, 0.85 lagging, 0.95 leading and 0.85 leading. Figure 5.9 and Figure 5.10 show the simulation results for the case of 5% and 10% PV generation with 0.95 lagging power factor. The simulation results show that when the PV generator is operating with a lagging power factor, they generate reactive power. When the irradiance is high, the active power is high and results in large amount of reactive power being generated. When the irradiance is low, the active power is low and results in a very small amount of reactive power being produced. This approach increases the bus voltage during periods of high irradiance but doesn't change much the behaviour of the system during periods of low irradiance as compared to the case of PV generation without voltage control. The difference of bus voltage during the maximum and minimum irradiance therefore increases. For the 5% penetration case the difference is 0.033 p.u, while for the 10% penetration case, the difference is 0.075 p.u. The magnitude of the voltage fluctuations over the 60 seconds period thus increases. The situation is worse when the PV generator is operating at 0.85 lagging power factor, as shown in Figure 5.11 and Figure 5.12. In this case, the differences in bus voltages between maximum and minimum irradiance for the case of 5% and 10% PV penetration are 0.04 p.u and 0.09 p.u respectively.

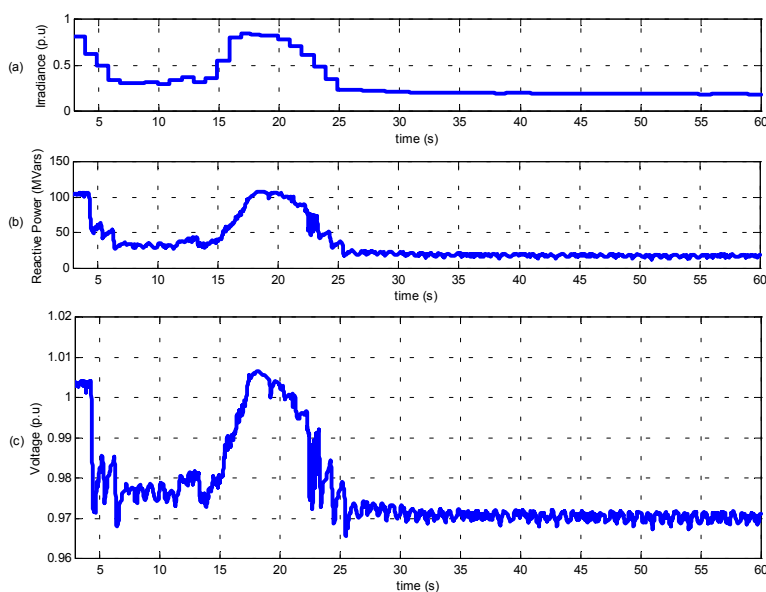


Figure 5.9: 5% PV penetration with constant power factor control, p.f = 0.95 lagging

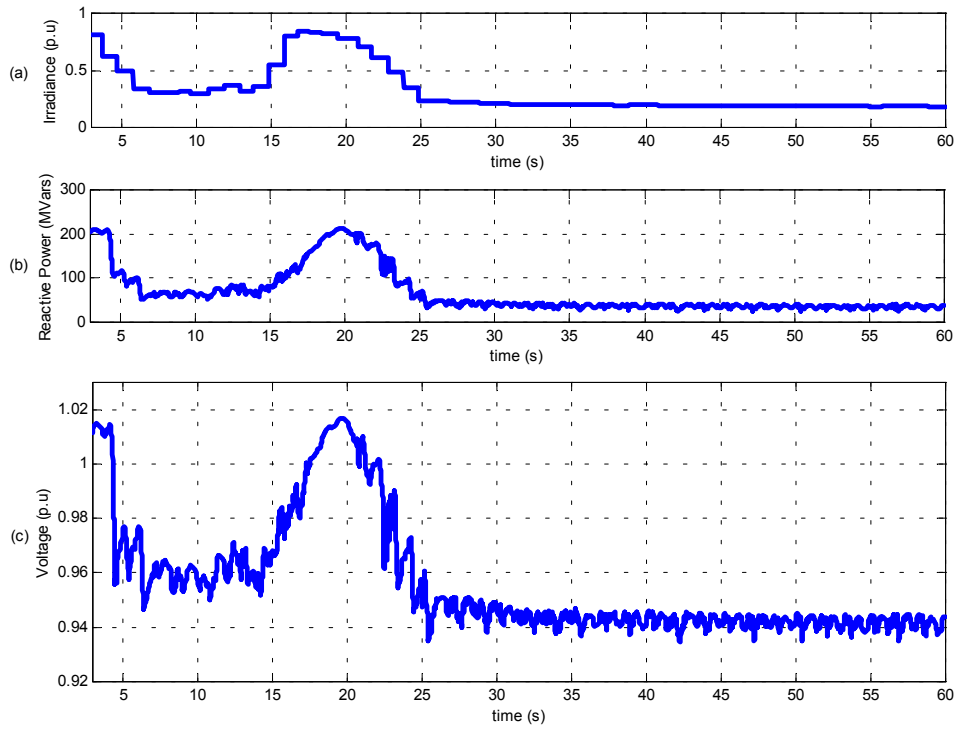


Figure 5.10: 10% PV penetration with constant power factor control, p.f = 0.95 lagging

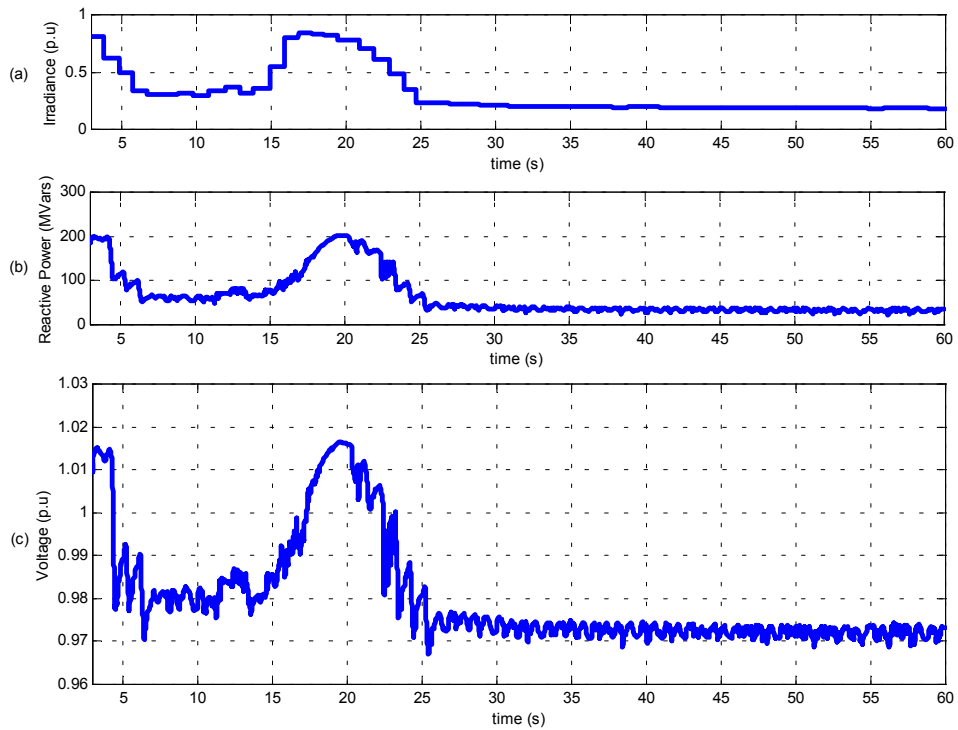
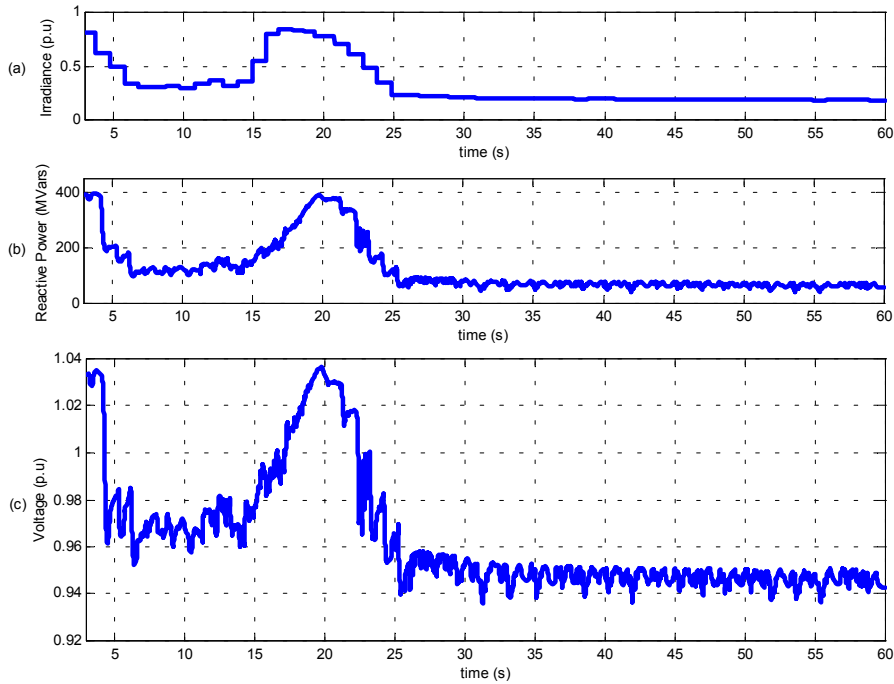


Figure 5.11: 5% PV penetration with constant power factor control, p.f = 0.85 lagging



**Figure 5.12: 10% PV penetration with constant power factor control, p.f = 0.85 lagging**

Figure 5.13 and Figure 5.14 show the simulation results for the case of 5% and 10% PV generation respectively with a 0.95 leading power factor. In this case the PV generator absorbs reactive power. When the irradiance is high, a large amount of reactive power is absorbed. When the irradiance is low, the amount of reactive power absorbed is low. This causes the bus voltage to drop for high irradiance periods but doesn't change much the voltage during periods of low irradiance value as compared to the case of PV generation without voltage control. The difference in bus voltage between high irradiance and low irradiance periods thus becomes smaller. The difference in bus voltage between maximum and minimum irradiance over the 60 seconds period of time are 0.015 p.u and 0.035 p.u for the case of 5% PV penetration and 10% PV penetration respectively. The results show that the magnitude of bus voltage fluctuation during the 60 seconds period time reduces. The situation is more significant for the case when the PV generation operates at a 0.85 constant power factor leading. The difference in bus voltage between maximum and minimum irradiance for this case is only 0.005 p.u and 0.015 p.u for 5% PV penetration and 10% PV penetration respectively, as shown in Figure 5.15 and Figure 5.16. Figure 5.17 shows the comparison results for the voltage at bus-11 for different constant power factor.

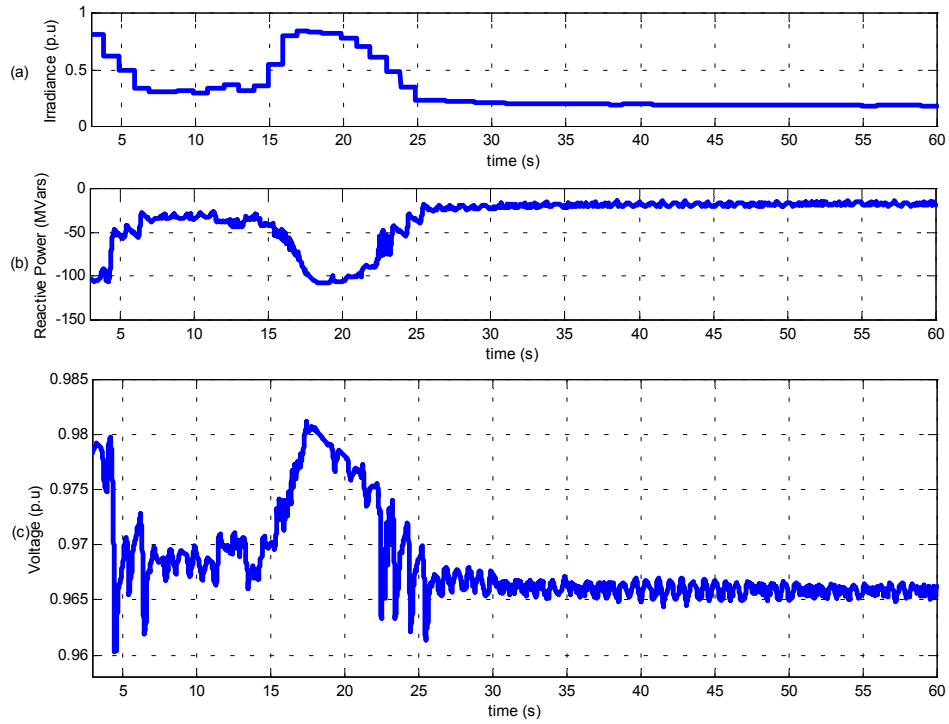


Figure 5.13: 5% PV penetration with constant power factor control, p.f = 0.95 leading.

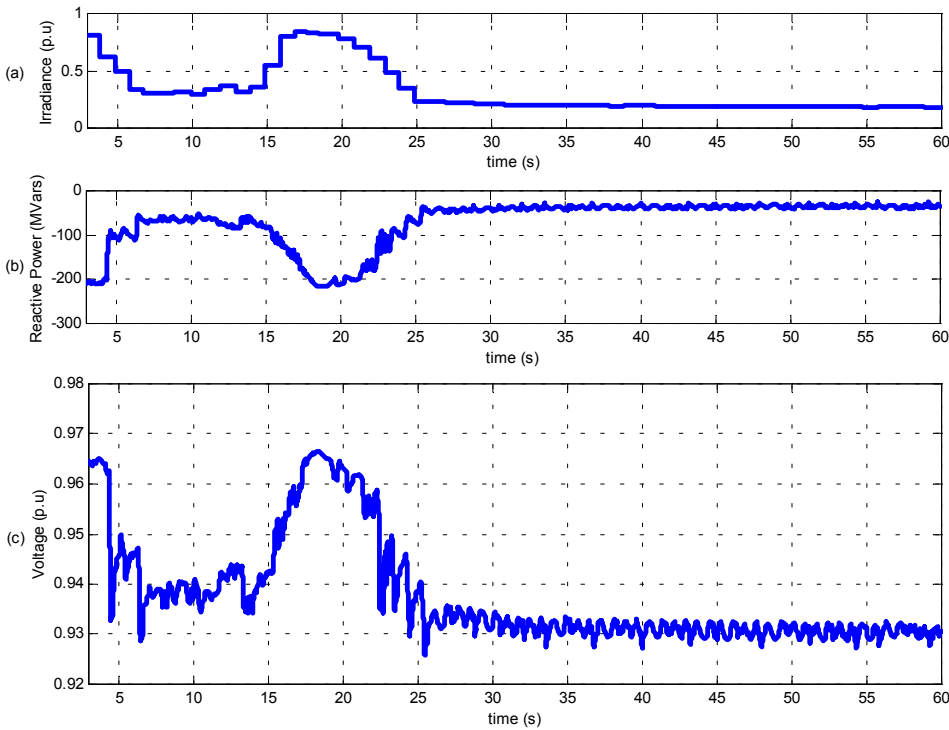


Figure 5.14: 10% PV penetration with constant power factor control, p.f = 0.95 leading

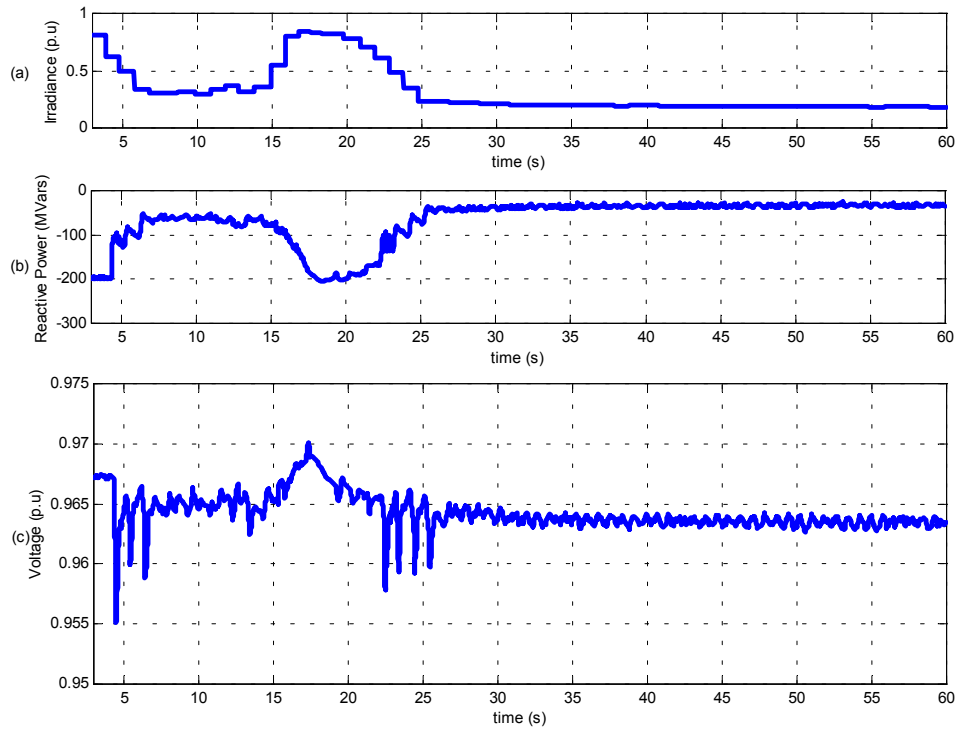


Figure 5.15: 5% PV penetration with constant power factor control,  $p.f = 0.85$  leading

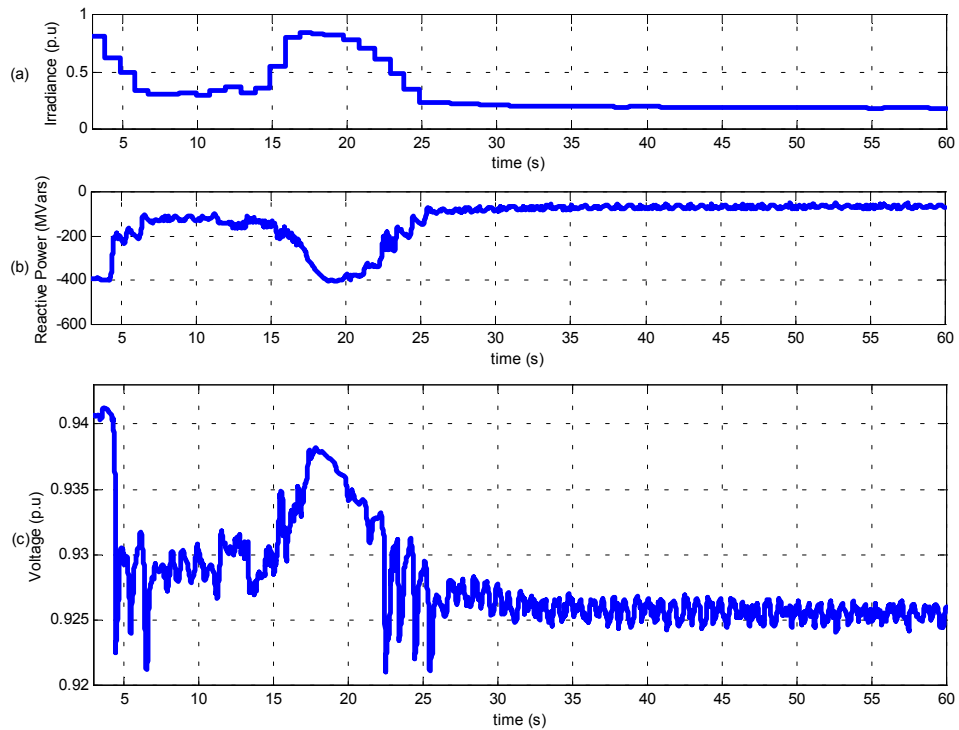
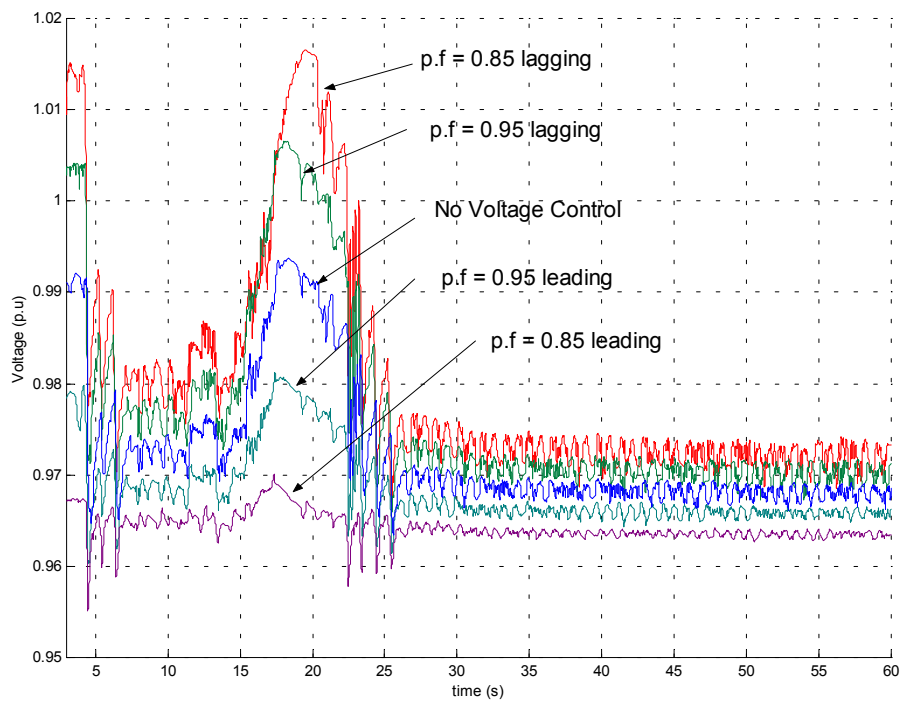
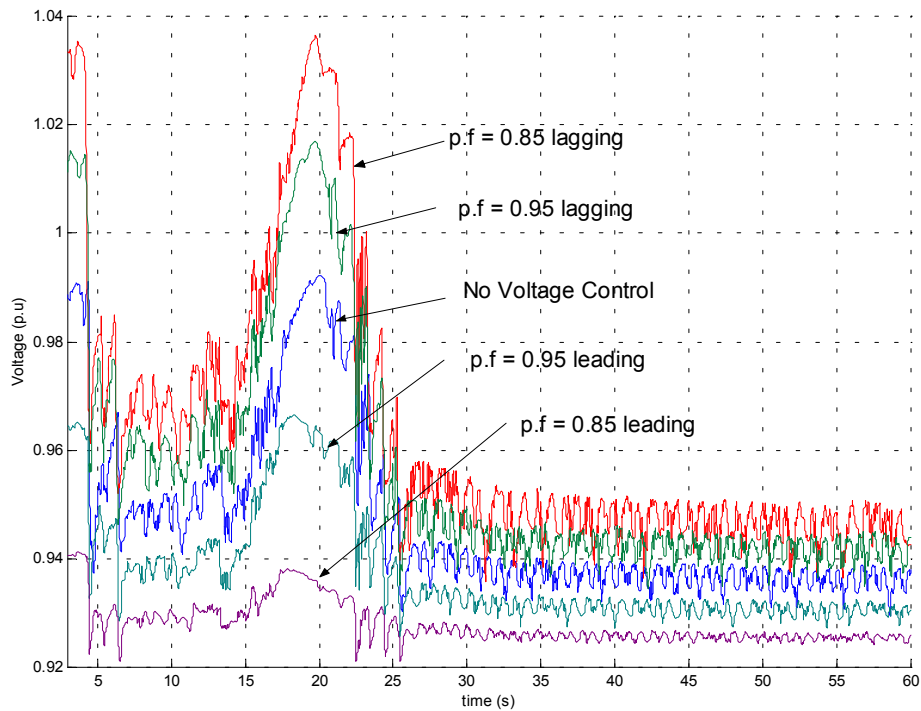


Figure 5.16: 10% PV penetration with constant power factor control,  $p.f = 0.85$  leading



**Figure 5.17: Comparison results for the voltage of bus-11 at 5% PV penetration in different constant power factor mode**



**Figure 5.18: Comparison results for the voltage of bus-11 at 10% PV penetration in different constant power factor mode**

### 5.5.1.2 Simulation Results of Voltage Control from PV Generator Itself

Figure 5.19 and Figure 5.20 shows the simulation results for the case of 5% and 10% PV generation with automatic voltage control from the PV generator itself. In this case, the targeted reference voltage,  $V_{ref}$  is set at 0.992 p.u, i.e. the voltage value when the irradiance value is at its maximum and the reactive power is zero. The simulation results show that at high irradiance values, the voltage at bus-11 is maintained at  $V_{ref}$ . At low irradiance value, the demand for reactive power increases and it reaches the upper limit of reactive power. This causes the bus voltage drops from  $V_{ref}$  and fluctuates. The differences in bus voltages between maximum and minimum irradiance over the 60 seconds period are 0.02 p.u and 0.055 p.u for 5% and 10% PV penetration respectively. Overall, this approach doesn't show a significant improvement in helping reduce the voltage fluctuation problem in the system.

However, if the  $V_{ref}$  of the PV inverter voltage controller is changed to a lower value, for example 0.975 p.u (at the condition when the irradiance is 0.5 p.u with zero reactive power demand), the voltage fluctuation problem is greatly improved as shown in Figure 5.21 and Figure 5.22. The difference in bus voltages between the maximum and minimum irradiance over the 60 seconds period are 0.004 p.u and 0.03 p.u for 5% and 10% PV penetration respectively.

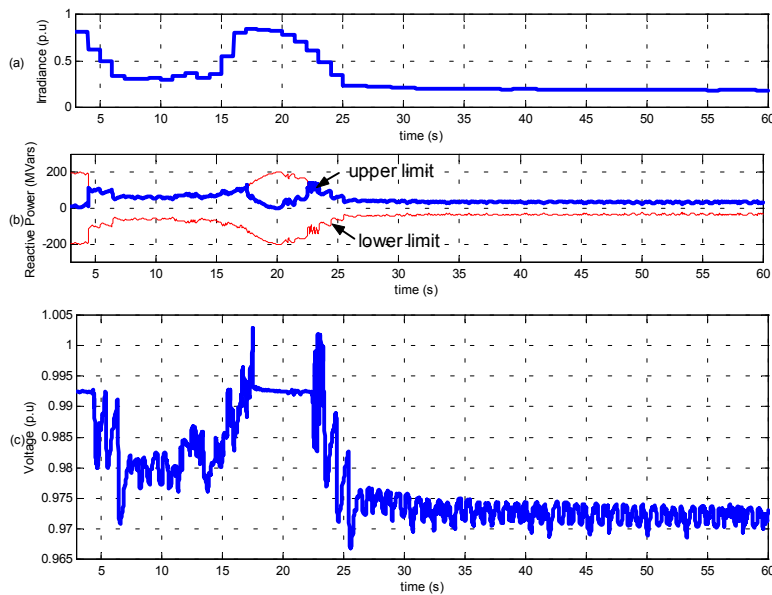


**Figure 5.19: 5% PV penetration with automatic voltage control from PV inverter itself ( $V_{ref} = 0.992$  p.u)**

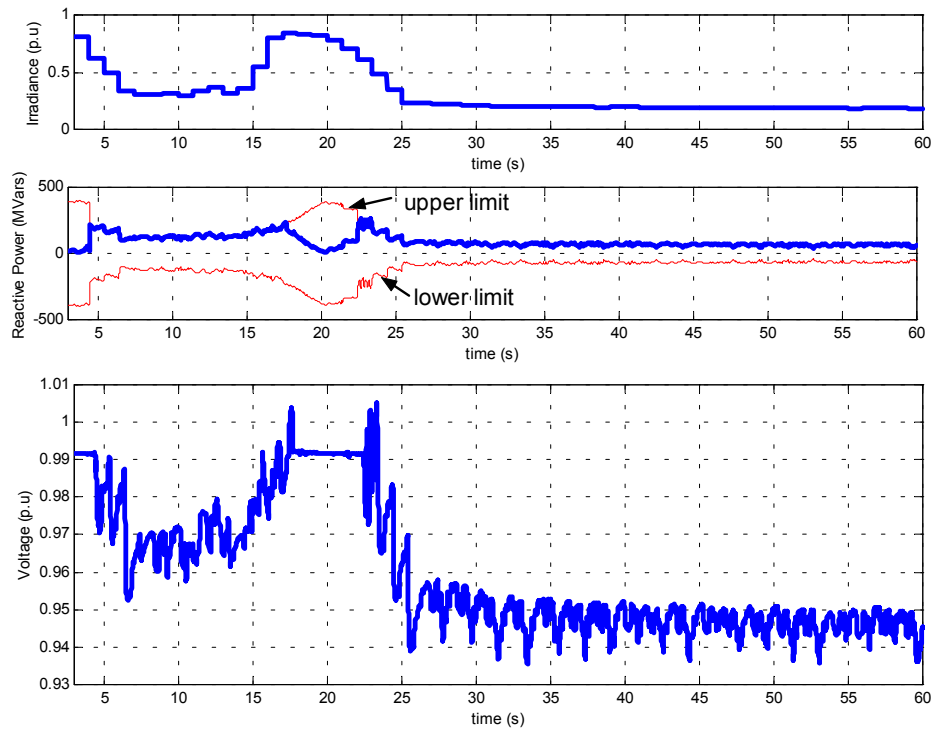


Figure 5.20: 10% PV penetration with automatic voltage control from PV inverter itself ( $V_{ref} = 0.992$  p.u)

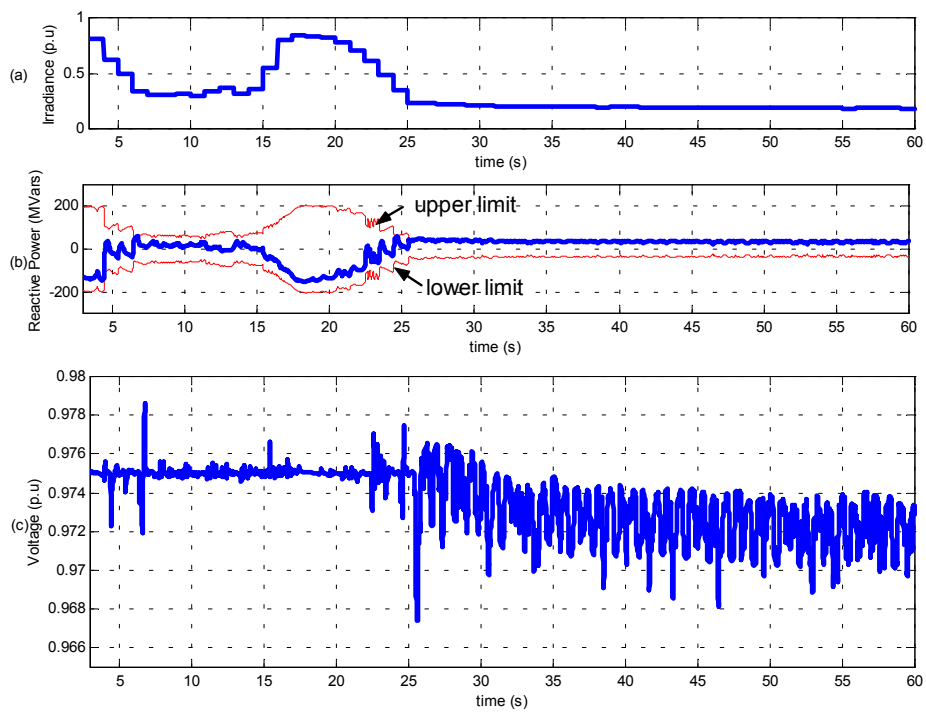


Figure 5.21: 5% PV penetration with automatic voltage control from PV inverter itself ( $V_{ref} = 0.975$  p.u)

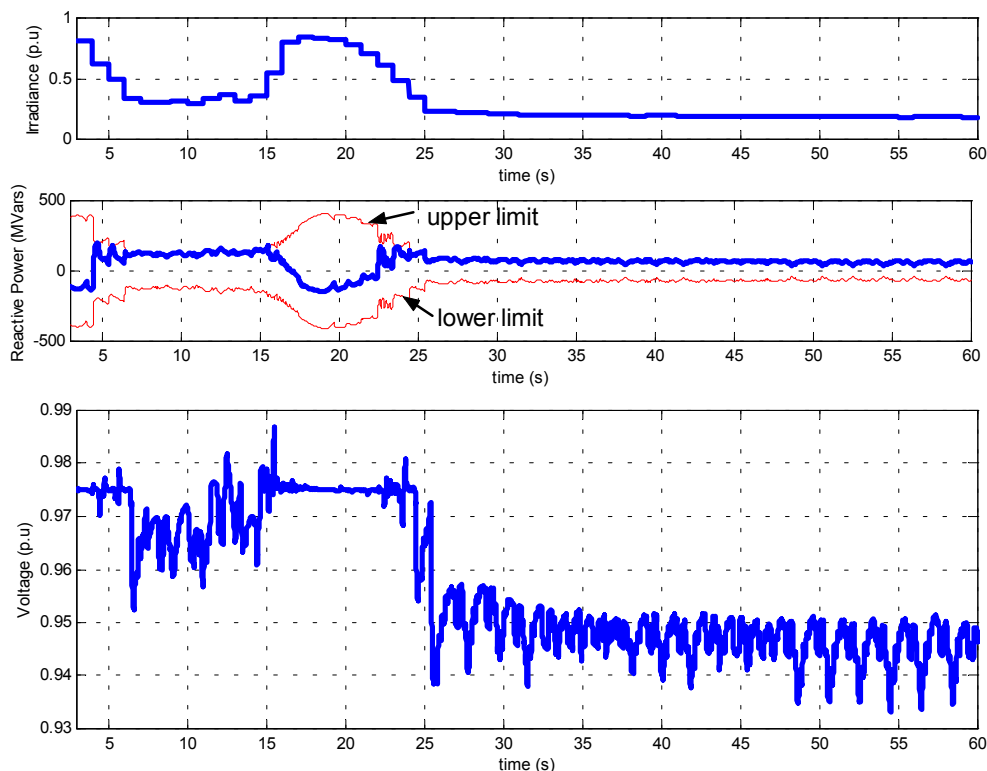


Figure 5.22: 10% PV penetration with automatic voltage control from PV inverter itself ( $V_{ref} = 0.975$  p.u)

### 5.5.1.3 Simulation Results of SVC Voltage Control

Figure 5.23 and Figure 5.24 show the simulation results for the case of 5% and 10% PV penetration with SVC voltage control. In this case, the targeted reference voltage  $V_{ref}$  is set at 0.975 p.u. The bus voltage is well regulated at the reference voltage at any irradiance value. However, this type of operation places a heavy demand on the SVC to supply or absorb reactive power from the network especially when the irradiance value is low. Therefore, the rating of the SVC used is very dependant on the amount of PV generation at the connected bus. The higher the PV generation is, the higher the rating of SVC is required and thus its associated cost will increase as well.

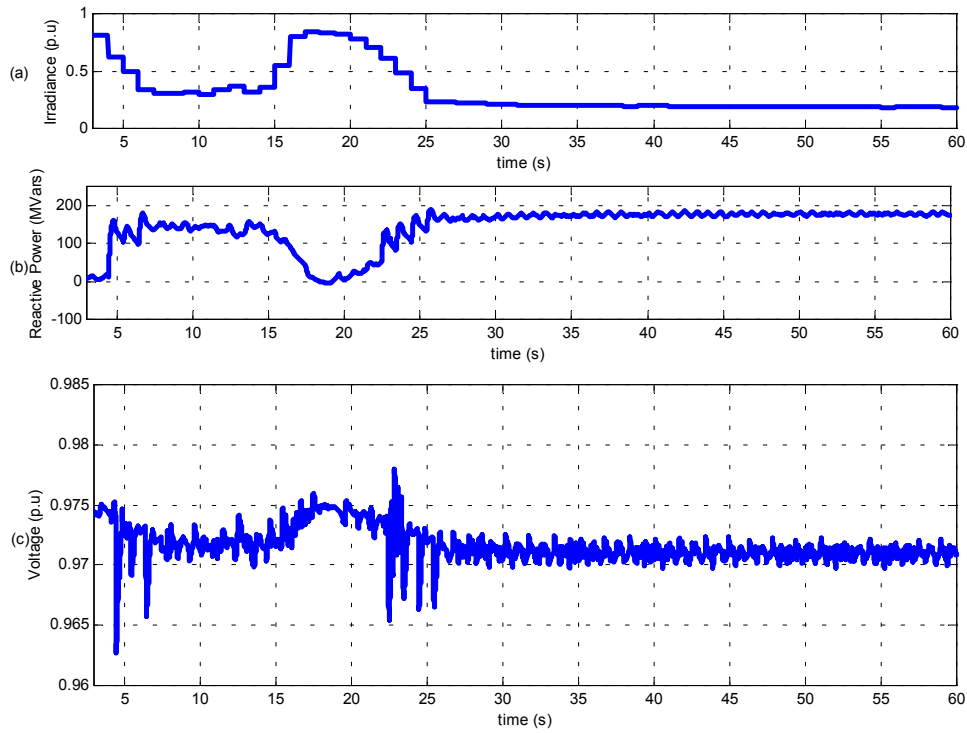


Figure 5.23: 5% PV Penetration with SVC voltage control

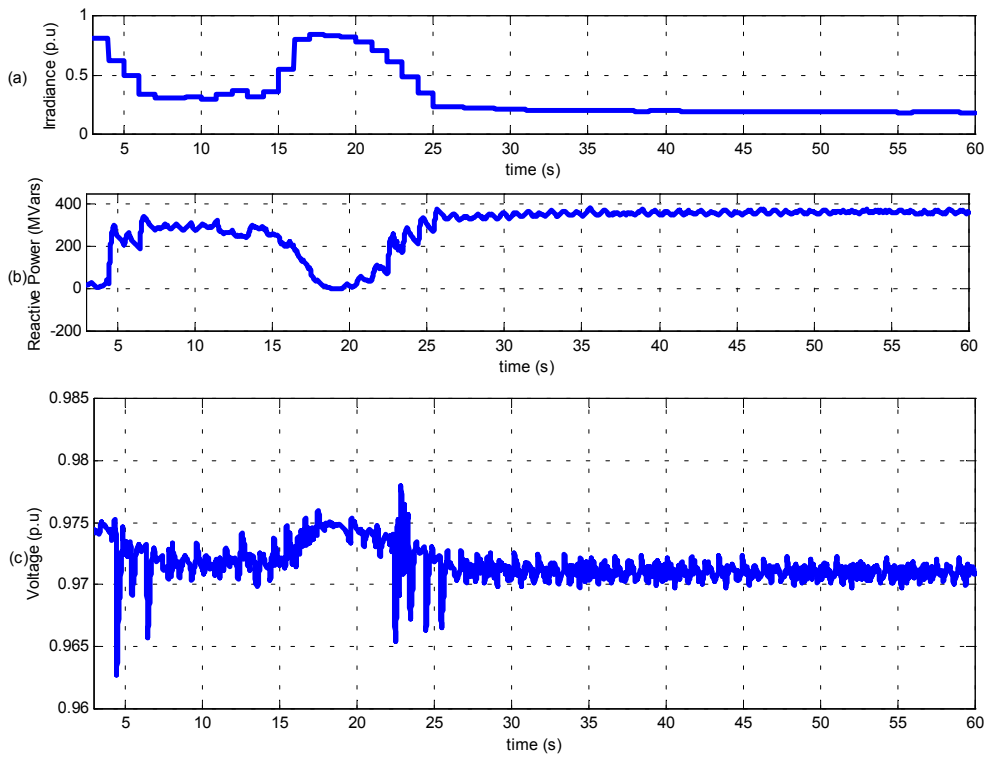


Figure 5.24: 10% PV penetration with SVC voltage control

Figure 5.25 shows a comparison of the results for the cases of 20% PV penetration both with and without SVC voltage control. For the case of PV penetration without voltage control, the PV generator trips at  $t = 4$ s when the bus voltage drops below 0.9 p.u due to the sudden drops in irradiance. By implementing the SVC voltage control, the bus voltage is kept above 0.9 p.u and this prevents the trigger of the protection relays.

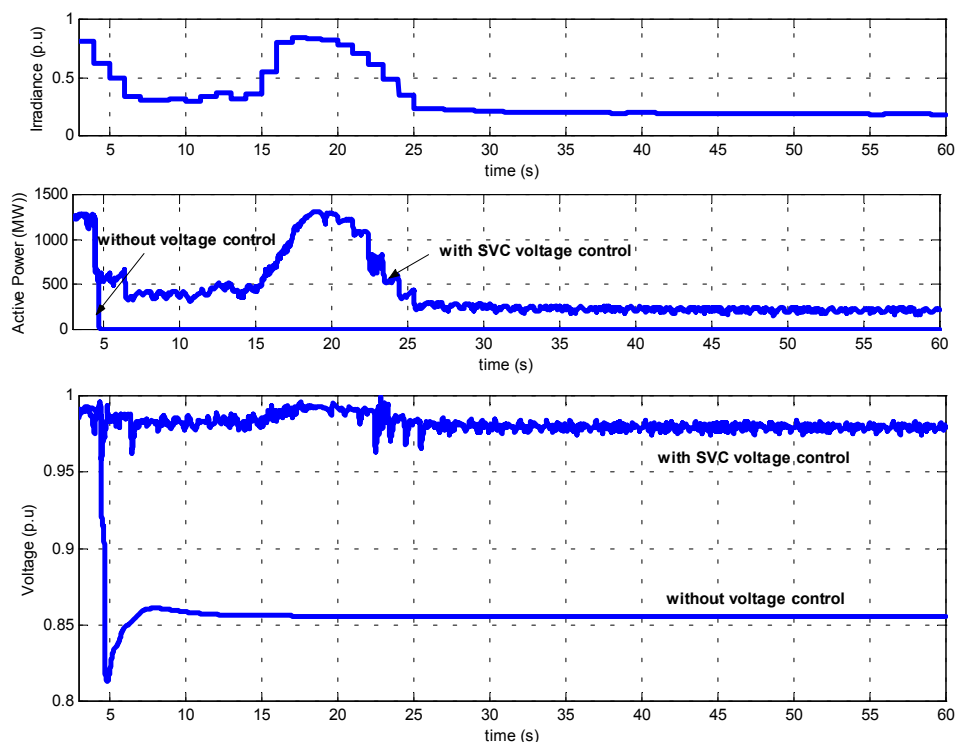


Figure 5.25: Effect of SVC control in avoiding the tripping of PV generator

## 5.6 CONCLUSION

Voltage control techniques that might help overcome the voltage fluctuation problems caused by changes in irradiance due to moving clouds have been studied. Simulation results obtained from these voltage control methods show that when the PV generator is operating at a constant lagging power factor, it cannot mitigate the voltage fluctuation problem effectively. However, when the PV generator is operating in constant leading power factor, it helps to reduce the voltage fluctuation but the bus voltage will be kept at lower value. Voltage control from the PV inverter itself has better performance in helping mitigate the voltage fluctuation problem. However, its ability to provide large amounts of reactive power for low irradiance values is limited by the thermal limit of the

inverter. Injecting reactive at low voltage is not an effective way of controlling voltage. The bus voltage is best controlled using an SVC, which is able to maintain the bus voltage at a constant value. However, this type of operating system would be much more costly than the other voltage control methods and it may place heavy demand on the SVC to supply or absorb reactive power from the network especially when the irradiance value is very low.

# Chapter 6

## IMPACT OF PHOTOVOLTAIC GENERATION ON TRANSIENT STABILITY

### 6.1 INTRODUCTION

The development of a model of PV generation implemented with P&O MPPT technique is described in Chapter 3. Chapter 4 described the aggregated models of PV generation. In this chapter, these models are incorporated with a model of a power system to investigate the impact of PV generation on transient stability. The concept of transient stability is described in the first part of this chapter. In the second part of this chapter, the responses of the PV generation to faults that occur in the power system are analysed using a time-domain simulation of a widely used dynamics test system. The effects of the level of PV penetration, fault impedance, protection parameters and fault clearing time on the fault response are investigated.

### 6.2 TRANSIENT STABILITY [34,45]

Transient stability is defined as the ability of the power system to maintain synchronism when subjected to a severe transient disturbance such as a fault on

transmission facilities, loss of generation or loss of a large load. The system response to such disturbances involves large excursions of generator rotor angles, power flows, bus voltages, and other system variables. Stability is influenced by the nonlinear characteristics of the power system. If the resulting angular differences between the machines in the system remains within certain bounds, the system maintains synchronism. Loss of synchronism because of transient instability, if it occurs, is usually evident within 2 to 3 seconds of the initial disturbance.

In most cases, system instability is prevented by the action of protective devices. The goal of these protective devices is to prevent damage to components in the power system, e.g. due to fault currents, over-voltage or over-speed. Protective devices detect the existence of abnormal system conditions by monitoring appropriate system quantities and disconnecting appropriate generators, loads or lines. In order to perform their functions satisfactorily, the protective devices should satisfy three basic requirements: selectivity, speed, and reliability. In many cases, the change in the system's topology restores the stability of the power system, because the faulted component, threatening the stability is removed from the system.

The stable operating point that is reached after a disturbance can be different from the initial state. This is the case if either the disturbance itself or the actions of protection devices occurring during the transient phenomenon cause a permanent change in the topology of the power system. Examples of such topology changes are a generator or line trip and a load change. A fault that is cleared without tripping any components, however, does not lead to a permanent change in the topology of the power system. In this case, the steady state after the event is normally identical to that before its occurrence.

### **6.3 RESPONSE OF PV GENERATION TO DISTURBANCES**

The transient behaviour of the PV generator is related to their working principles. A thorough understanding of the transient behaviour of PV generator is essential for evaluating the transient stability of the PV generator and for investigating the causes of any instability that may be observed.

As mentioned in the previous chapter, most PV generators are currently designed to operate at unity power factor. This implies that PV generators do not contribute to voltage control. Controlling voltages when using PV generators operating at unity power factor therefore requires further modification to the design of PV generator or additional technology for controllable reactive power generation, such as switched capacitors, STATCOMs or SVCs.

### 6.3.1 Mechanism Causing Instability

When a fault occurs in the network, the generator terminal voltage drops. If the fault is not cleared fast enough, the under-voltage protection relay is triggered and disconnects the PV generator. On the other hand, if the fault is cleared before the terminal voltage drops below the “trigger threshold” value, the PV generator remains connected. However, as shown in figure 3.9 in Chapter 3, a sudden drop in terminal voltage will cause a sudden drop in PV generation. Consequently, there is a further drop in terminal voltage due to the sudden reduction in PV generation. Eventually this may trigger the under-voltage protection relay and disconnect the PV generator. The PV generator can only be reconnected after the restoration of the grid voltage in the affected parts of the network, which may take several seconds to several minutes, depending on the amount of penetration of PV generation and the number of PV generator that were disconnected from the system. In this case, the power system with the PV generators connected is not transiently stable: it does not return to a stable operating point after the disturbance. The exact quantitative behaviour of the terminal voltage and required restoration time depend on the actual irradiance amount, PV generator characteristic, network topology and protection system setting.

Wherever possible, it should be ensured that a fault is removed from the system to avoid the mechanism pointed out above, which leads to instability of the PV generators. A fault should therefore be cleared quickly to limit the voltage drops. The time available to clear the fault before it leads to instability is called the critical clearing time.

Note that the above sequence of events may also be initiated by a drop in terminal voltage resulting, for example, from the tripping of a nearby synchronous generator. When the PV generator delivers its nominal power and the terminal voltage drops, the active power drops. This leads to a further lowering of the terminal voltage. This mechanism can lead to a voltage collapse that is not preceded by a short circuit. This is an example of voltage instability.

## 6.4 CASE STUDIES

### 6.4.1 Test System Preparation [45,46]

The test system used in these case studies is the well-known IEEE-39 bus dynamic test system. This system does not exist in reality, but is an artificial test system that is used in many publications on various aspects of power system dynamics. The reasons for using a test system rather than a model of a practical system are the following:

- Models of practical power system are not very well documented and the data is partly confidential. This easily leads to a shift in focus from using the model to investigating certain phenomena towards improving the model itself. Most parameters of test systems are, however, given in the literature, which make them convenient to use.
- Models of practical power systems tend to be very large, which makes the development and calculation of numerous scenarios cumbersome and time consuming and complicates the identification of general trends.
- The results obtained with models of practical systems are less generic than those obtained with a general-purpose test systems and can be validated more easily with results of other investigations given the availability of the system data.

Table 6.1 gives the system characteristic of the IEEE 39 bus test system. The diagram of the system is shown in Figure 6.2. The system was first modelled in the steady state

using the Power World simulation software. The data for this system is shown in appendix B1.

Table 6.1 Characteristic of the IEEE 39 bus test system

System Characteristic	Value
Number of buses	39
Number of generators	10
Number of loads	19
Number of transmission lines	34
Number of transformers	12
Total generation	6200.6 MW / 1326.4 MVars
Total loads	6150.1 MW / 1283.9 MVar

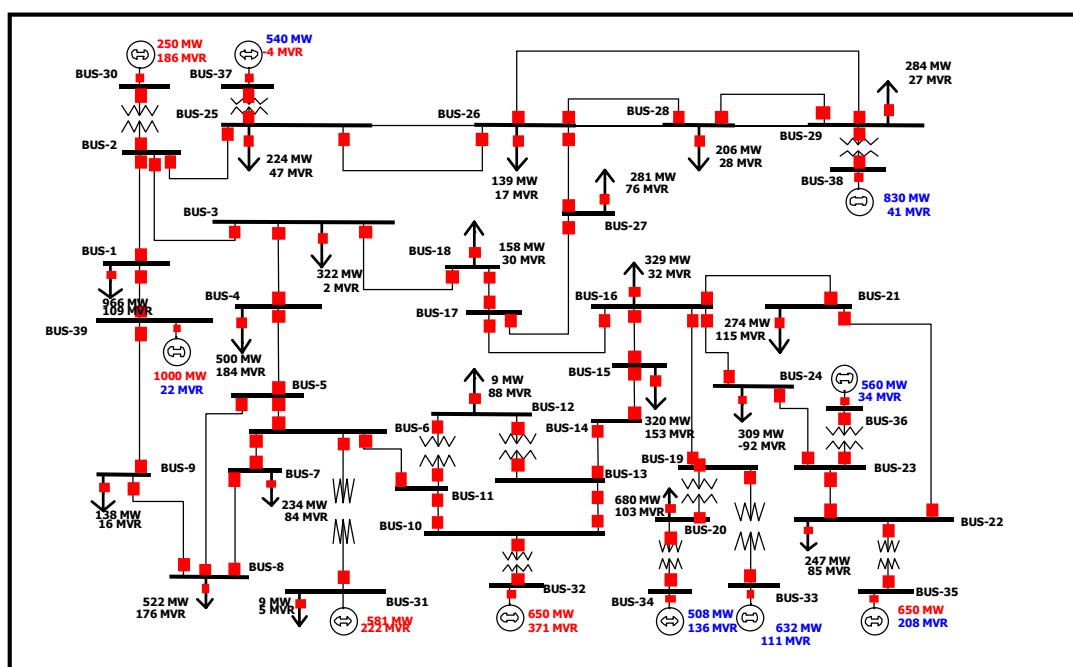


Figure 6.1: One line diagram of the IEEE 39 bus test system

### 6.4.1.1 Steady State Load Flow

In order to create a realistic steady state operating point, this system was modeled in the steady state using the Power World Simulation software. A number of load flows were run and the load flow results are given in appendix B2. The results show that the bus voltages for every node are within the acceptable range, i.e. between 0.95 p.u. and

1.05 p.u. Figure 6.2 shows the contouring of the bus voltages of the system. It can be seen that the busses at the upper part of the one line diagram have higher bus voltage than the others. The 5 buses in the middle bottom of the one line diagram, i.e. bus-32, 10, 11, 13 and 12 also have higher bus voltage in the initial load flow. Therefore special care should be taken for these particular busses in the system.

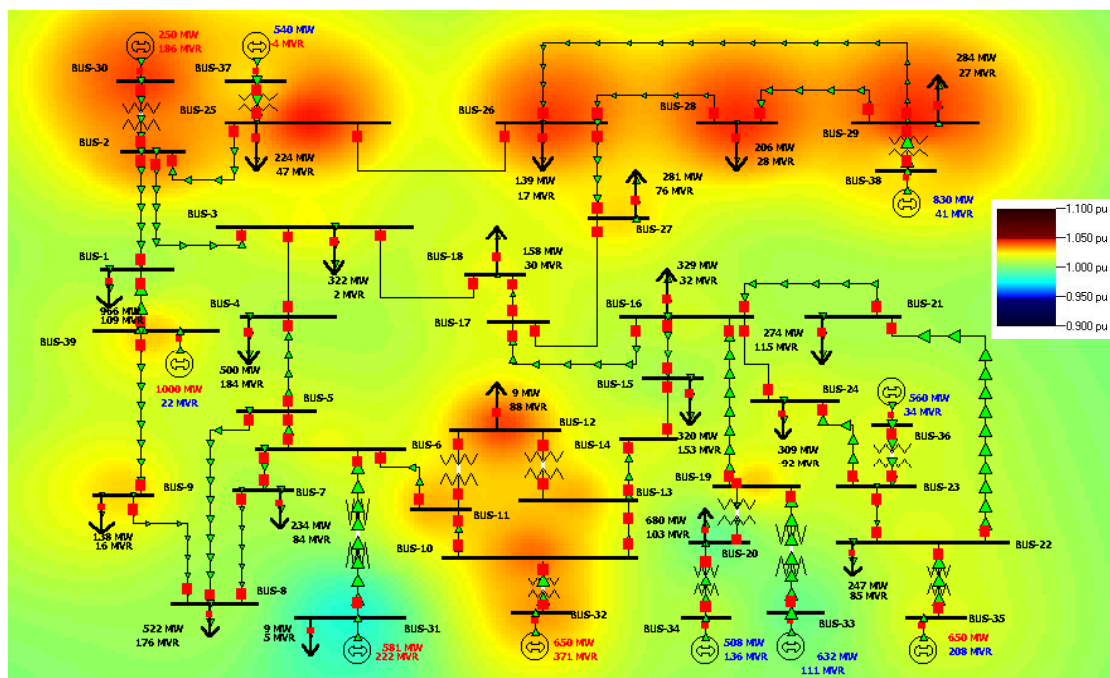


Figure 6.2: Contouring of the bus voltage of the system

#### 6.4.1.2 Dynamic Modelling

For dynamic simulations, a dynamic model of a power system is necessary and load flow data are not sufficient. In order to obtain a dynamic model of the test system from Figure 6.1, the dynamic models of generators, governors and automatic voltage regulators are included in the overall system model. The system is modeled in EUROSTAG<sup>TM</sup> for dynamic simulation. The block diagrams of these models, including the values of the parameters for the IEEE 39 bus test system are shown in appendix B3. To represent the PV generators in the dynamic simulations, the PV generator and the aggregated models explained in chapters 3 and 4 were used.

## 6.4.2 Simulation Results

The focus here is to investigate the impact of various variables on the fault response, namely: -

- Level of PV penetrations
- Fault impedances
- Protection parameters
- Fault clearing time

Some of the synchronous generators in this test system are replaced by an aggregated model of PV generator. Simulation results are given and if applicable, the results of the base case as shown in Figure 6.3 and the modified system are compared.

### 6.4.2.1 Level of PV Penetrations

The impact of the amount of PV penetration was investigated first. The generator at bus-32 of the IEEE-39 bus test system depicted in Figure 6.1 was replaced by an aggregated model of PV generator. At  $t = 2\text{s}$ , a fault was applied at bus-32. The fault was cleared after 150 ms. The active power produced by the PV generator, the terminal voltage and the rotor angle of generator at bus-39 are plotted on Figure 6.4. The simulations were repeated by increasing the amount of PV penetration by replacing generators at buses-35, 34, 37 and 30 with PV generation. The simulation results are plotted on Figure 6.5, Figure 6.6, Figure 6.7 and Figure 6.8 respectively. Amount of power injected by the PV generation at each bus is shown in appendix B4. A comparison of the voltage at bus-32 and the rotor angle of generator at bus-39 are plotted on Figure 6.9 and Figure 6.10 respectively.

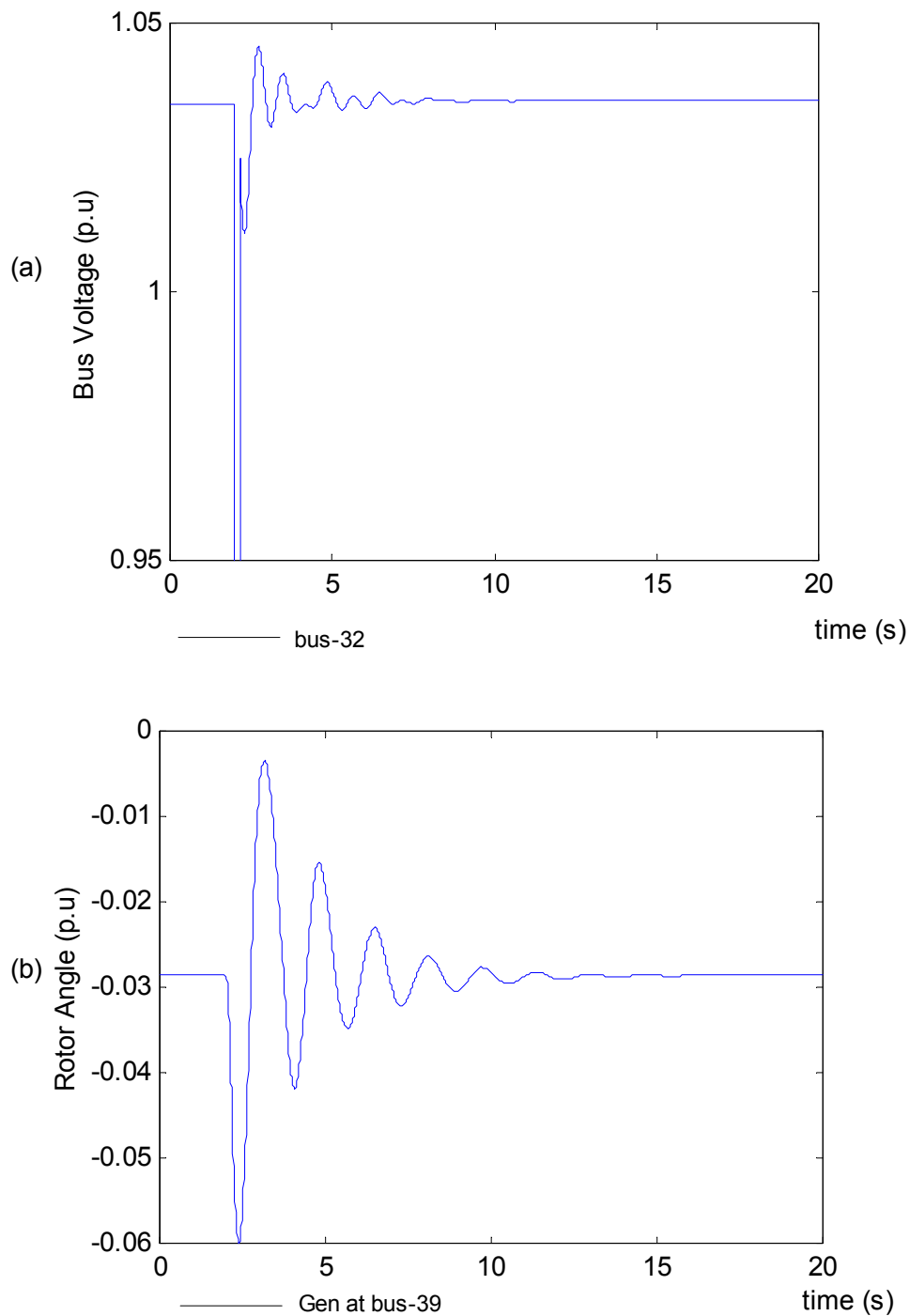
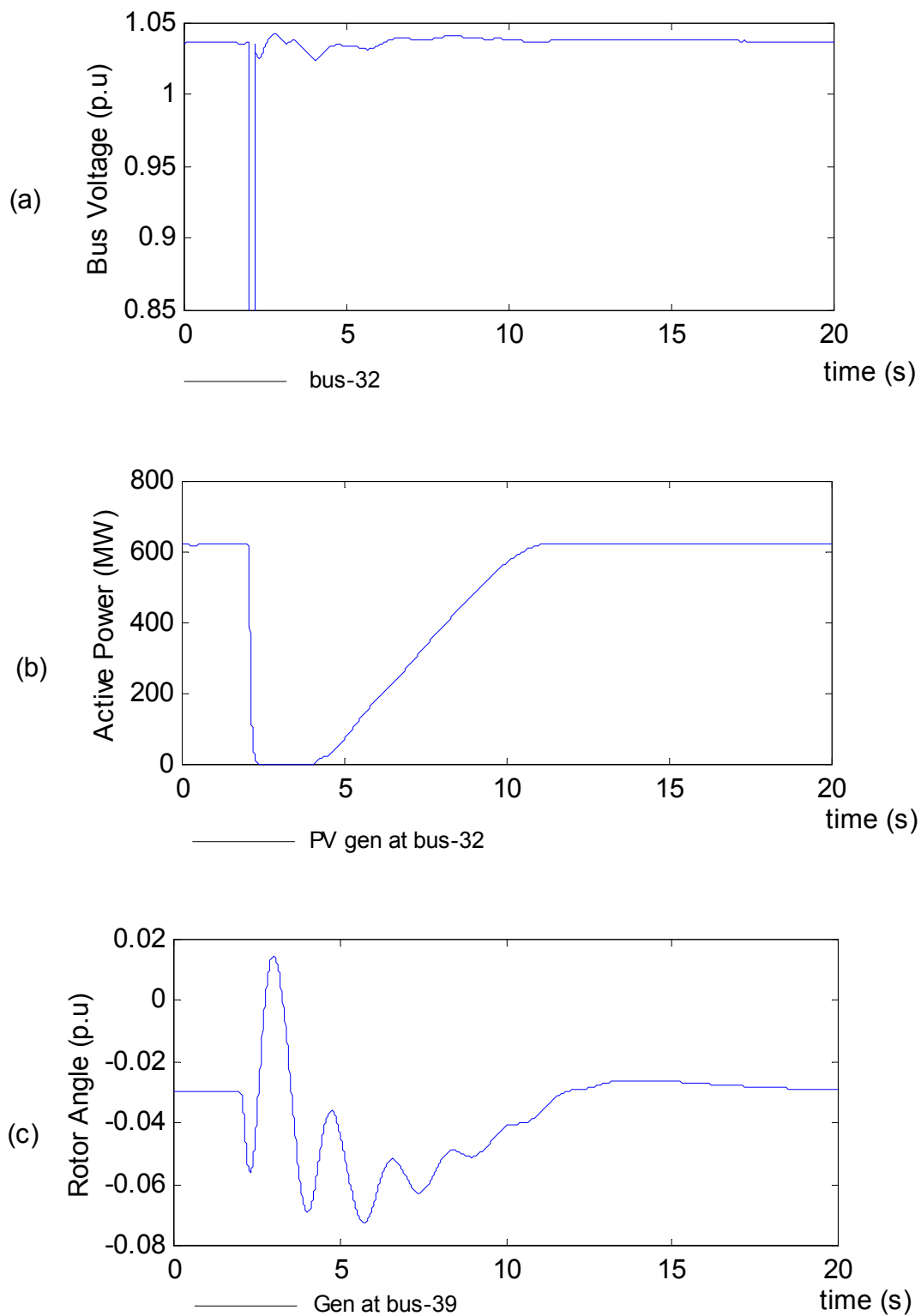
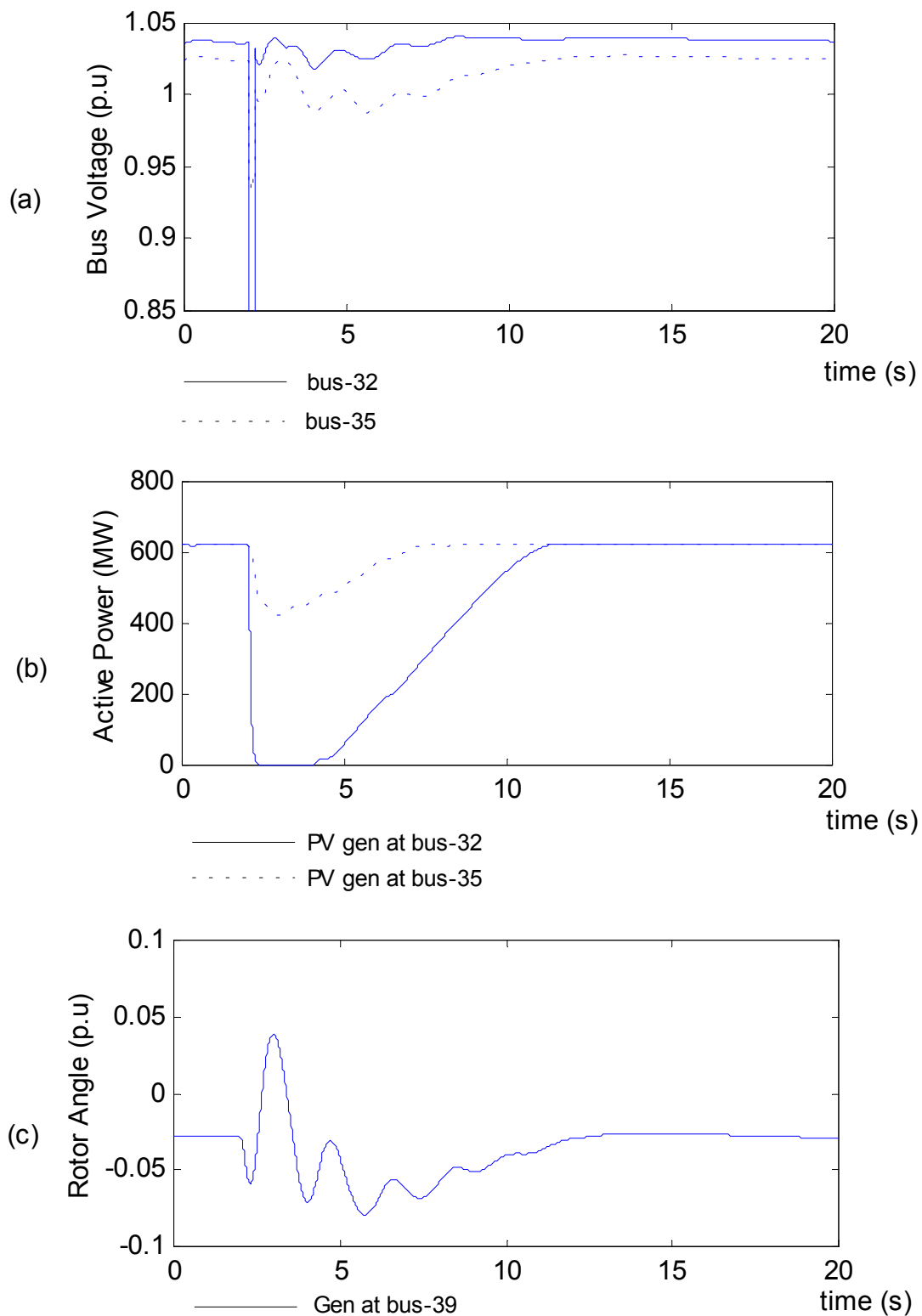


Figure 6.3: Simulation of fault response on the IEEE-39 bus test system without PV generators. (a) terminal voltage (b) rotor angle of conventional generator



**Figure 6.4: Simulation of fault response on the IEEE-39 bus test system with PV generators integrated at bus-32. (a) terminal voltage (b) active power from PV generators (c) rotor angle of conventional generator**



**Figure 6.5: Simulation of fault response on the IEEE-39 bus test system with PV generators integrated at buses-32 and 35. (a) terminal voltage (b) active power from PV generators (c) rotor angle of conventional generator**

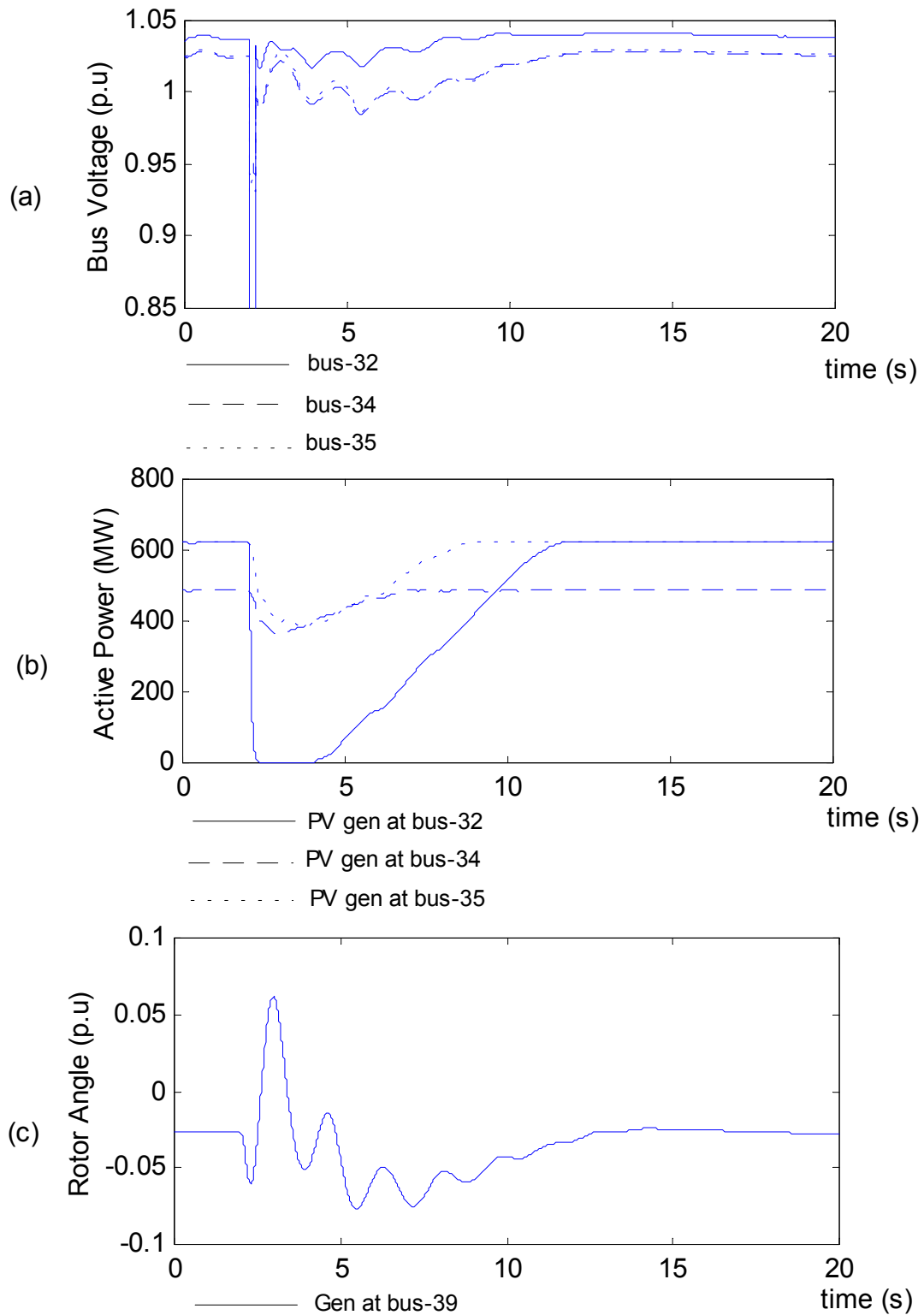


**Figure 6.6: Simulation of fault response on the IEEE-39 bus test system with PV generators integrated at bus-32, 34 and 35. (a) terminal voltage (b) active power from PV generators (c) rotor angle of conventional generator**

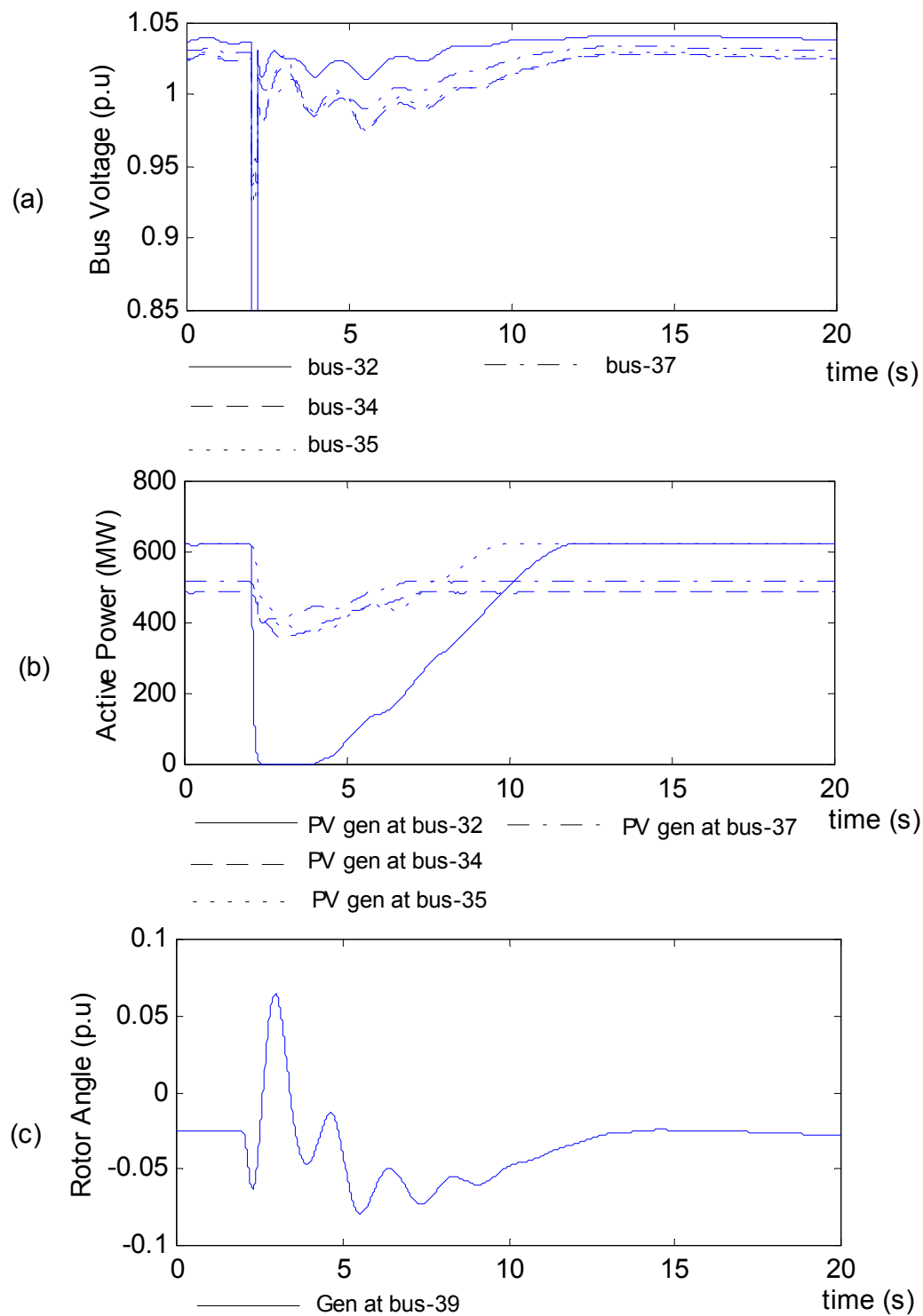


**Figure 6.7: Simulation of fault response on the IEEE-39 bus test system with PV generators integrated at bus-32, 34, 35, and 37. (a) terminal voltage (b) active power from PV generators (c) rotor angle of conventional generator**

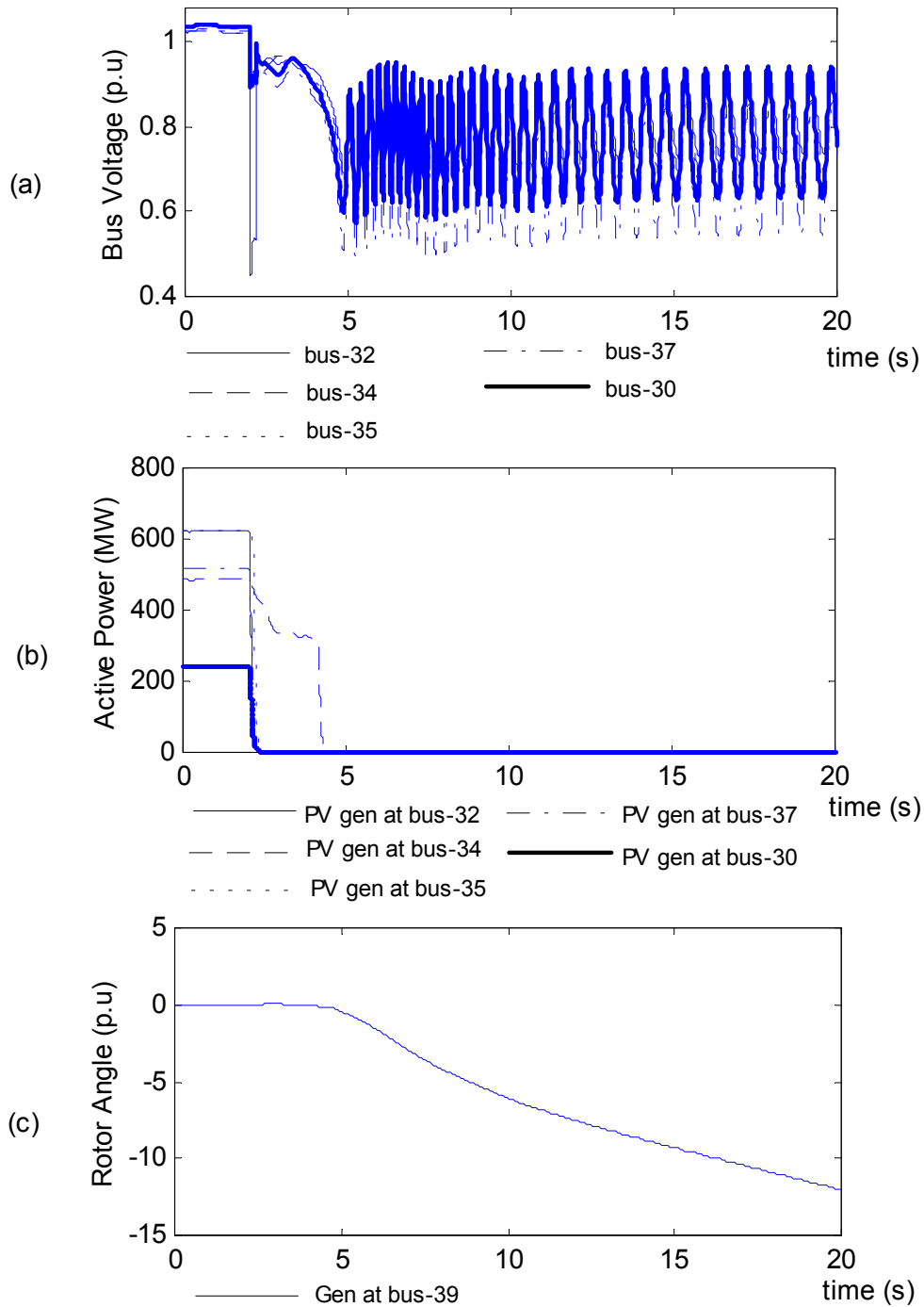


**Figure 6.8: Simulation of fault response on the IEEE-39 bus test system with PV generators integrated at bus-32 bus-34 bus-35, bus-37 and bus-30. (a) terminal voltage (b) active power from PV generators (c) rotor angle of conventional generator**

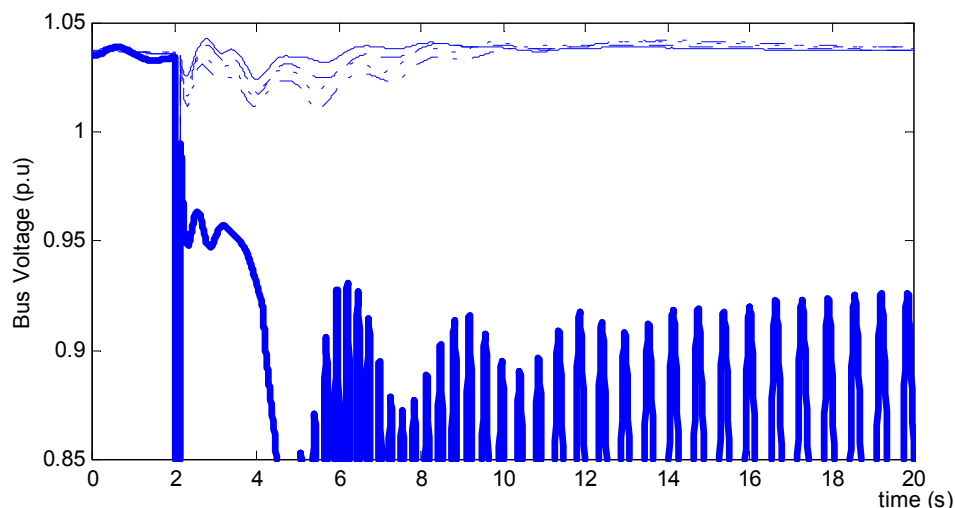


**Figure 6.9: Comparison of fault response of terminal voltage at bus-32 on the IEEE-39 bus test system with different level of PV penetration. The solid line, dashed line, dotted line, dashed-dotted line, and bold solid line correspond to increasing penetration of PV generation.**

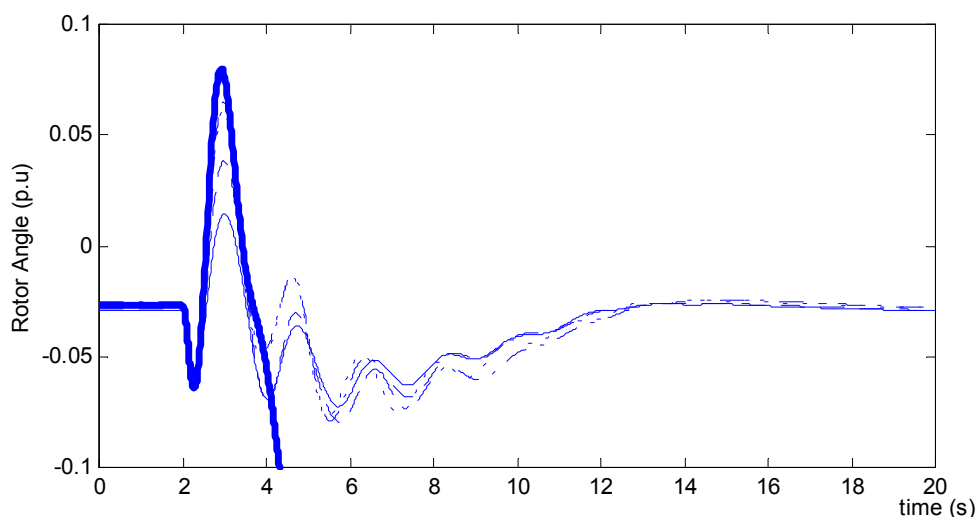


**Figure 6.10: Comparison of fault response of rotor angle for generator at bus-39 on the IEEE-39 bus test system with different level of PV penetration. The solid line, dashed line, dotted line, dashed-dotted line, and bold solid line correspond to increasing penetration of PV generation.**

#### 6.4.2.2 Fault Impedance

The impact of the fault impedance was investigated. The generator at buses-32, 35, 34, 37 and 30 of the IEEE 39 bus test system were replaced by an aggregated model of PV generation. Amount of power injected by the PV generation at each bus is same as the case shown in Figure 6.8. The fault impedance was set at 0.1 p.u. At  $t = 2s$ , a fault was applied at bus-32. The fault was cleared after 150 ms. The resulting PV generator

active power, terminal voltage and the rotor angle of generator at bus-39 are plotted on Figure 6.11. The simulations were repeated with fault impedances equal to 0.09 p.u, 0.08 p.u, 0.07 p.u, 0.06 p.u and 0.05 p.u. The simulation results are plotted on Figure 6.12, Figure 6.13, Figure 6.14 and Figure 6.15 respectively. The comparison of the voltage at bus-32 and the rotor angle of generator at bus-39 are plotted on Figure 6.16 and Figure 6.17 respectively.

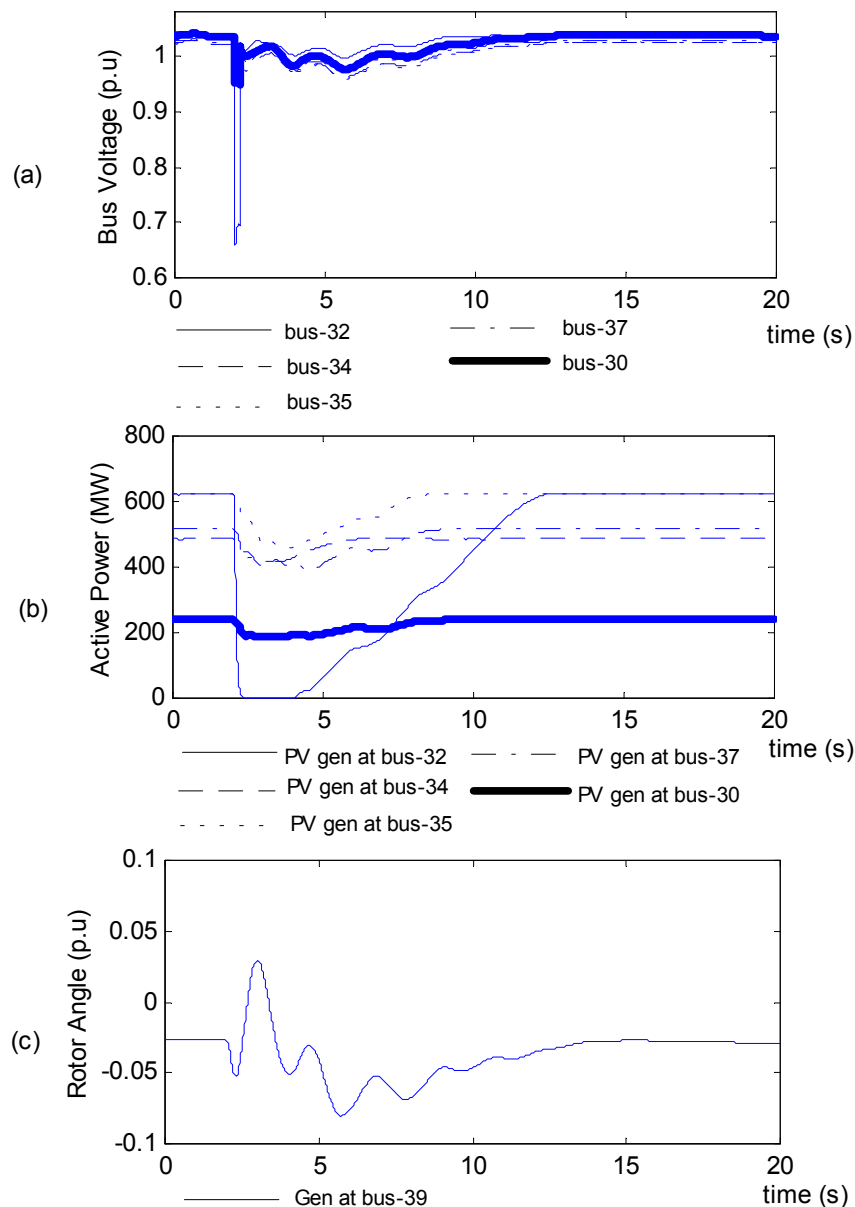


**Figure 6.11: Simulation of fault response on the IEEE-39 bus test system with PV generators integrated at bus-32, 34, 35, 37 and 30. Fault impedance is 0.1 p.u. (a) terminal voltage (b) active power from PV generators (c) rotor angle of conventional generator**

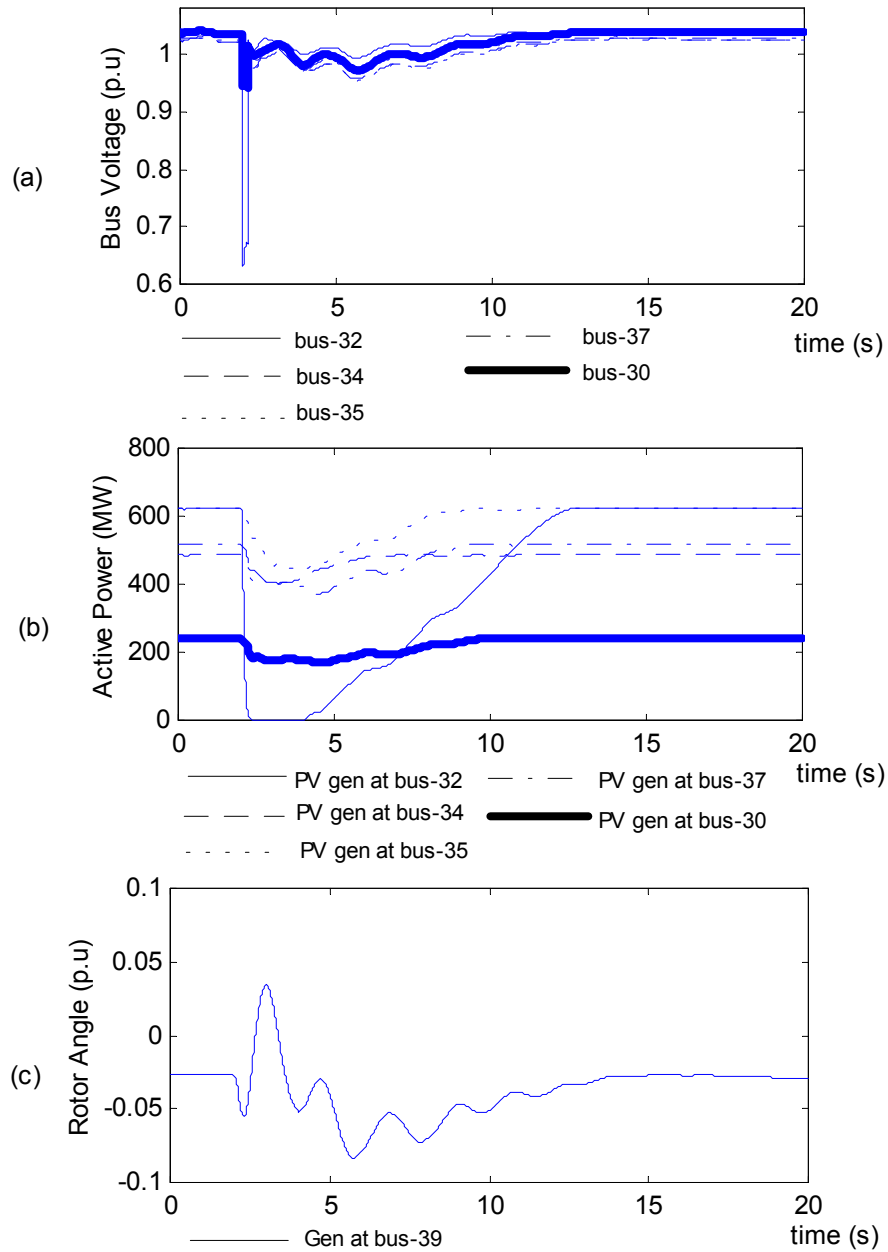


**Figure 6.12: Simulation of fault response on the IEEE-39 bus test system with PV generators integrated at bus-32, 34, 35, 37 and 30. Fault impedance is 0.09 p.u. (a) terminal voltage (b) active power from PV generators (c) rotor angle of conventional generator**

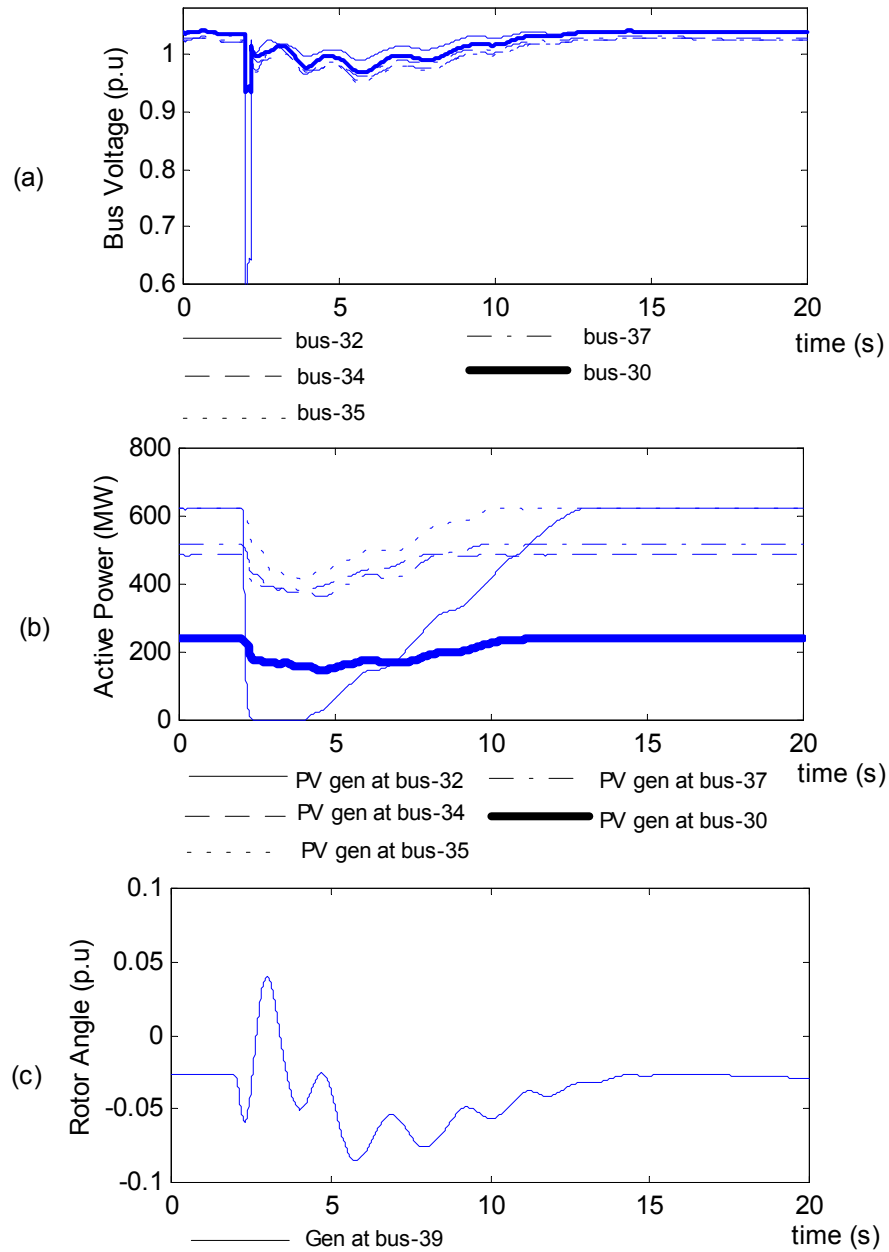


**Figure 6.13: Simulation of fault response on the IEEE-39 bus test system with PV generators integrated at bus-32, 34, 35, 37 and 30. Fault impedance is 0.08 p.u. (a) terminal voltage (b) active power from PV generators (c) rotor angle of conventional generator**

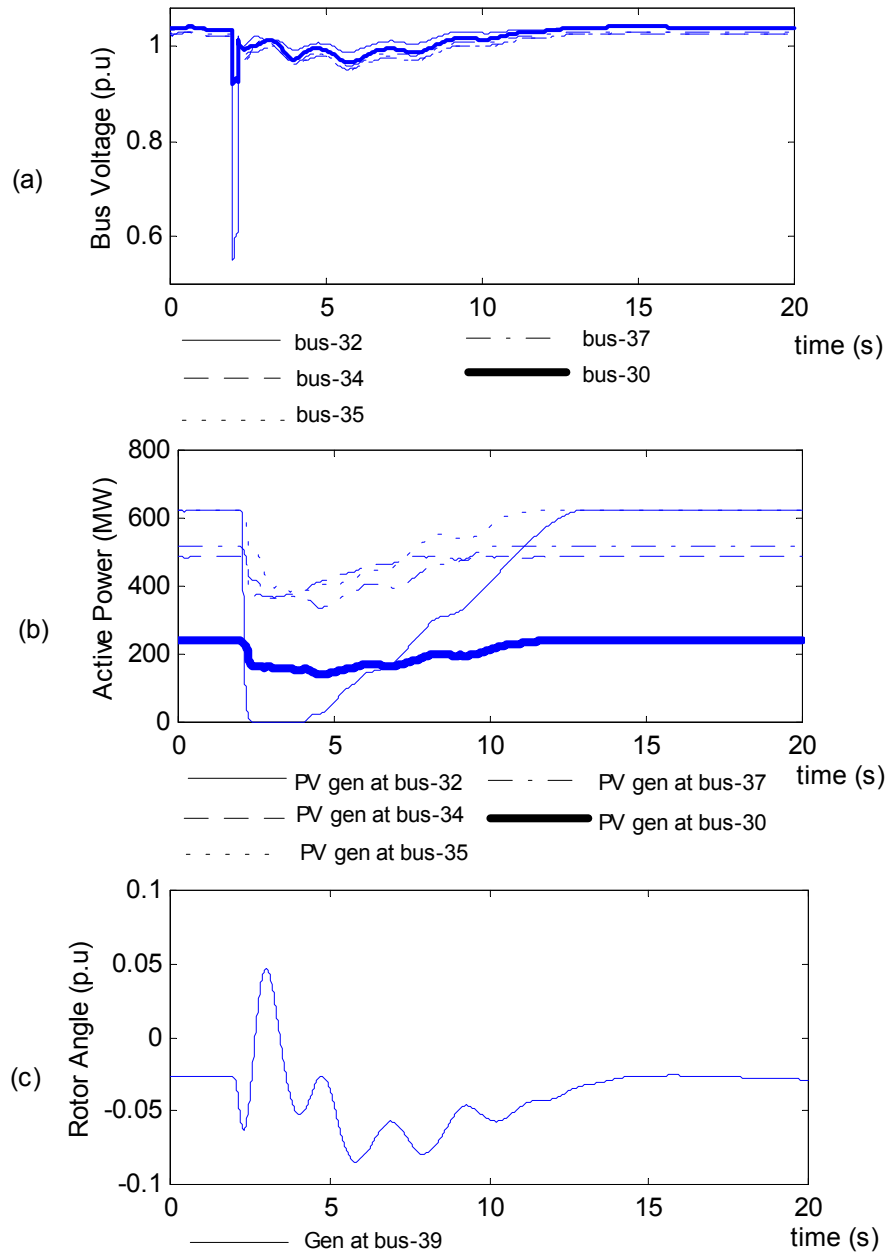


**Figure 6.14: Simulation of fault response on the IEEE-39 bus test system with PV generators integrated at bus-32, 34, 35, 37 and 30. Fault impedance is 0.07 p.u. (a) terminal voltage (b) active power from PV generators (c) rotor angle of conventional generator**

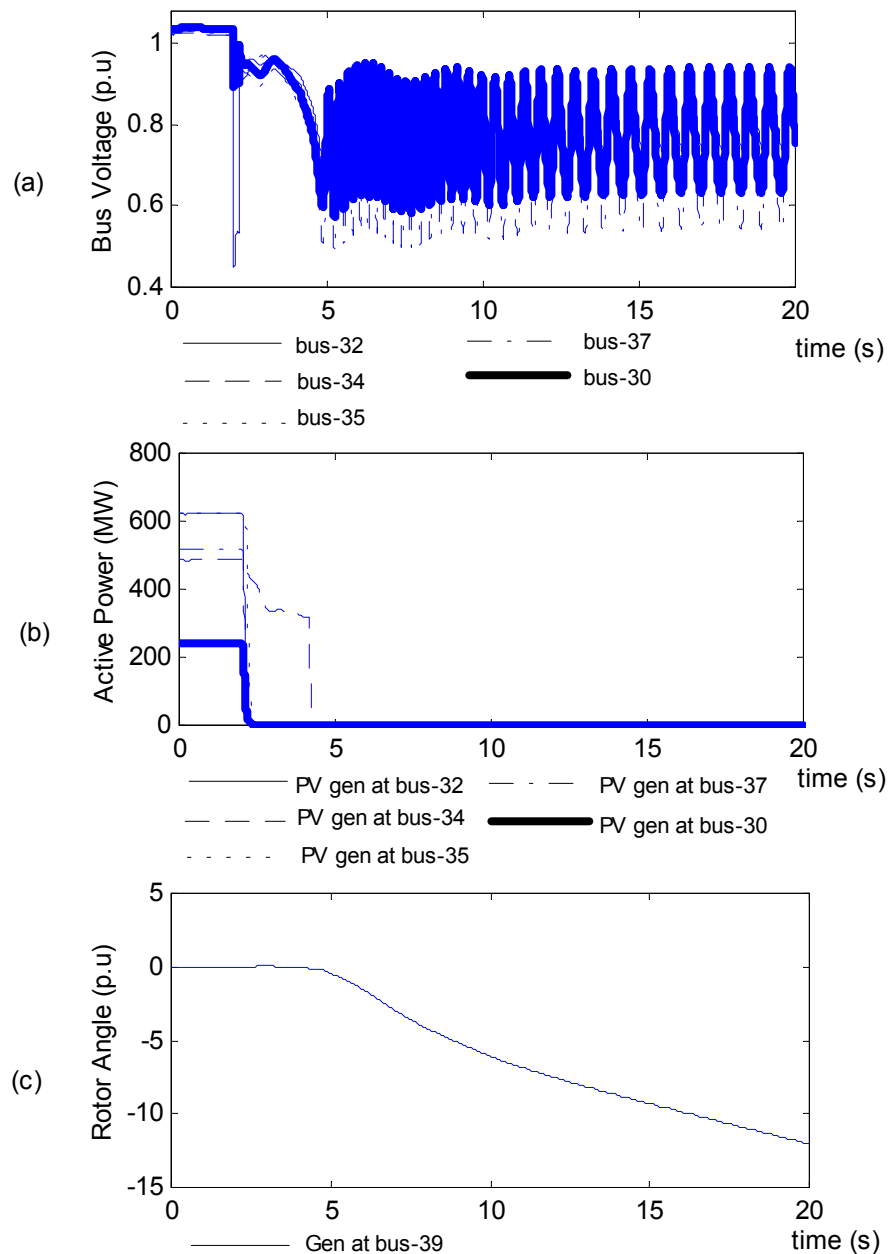


**Figure 6.15: Simulation of fault response on the IEEE-39 bus test system with PV generators integrated at bus-32, 34, 35, 37 and 30. Fault impedance is 0.06 p.u. (a) terminal voltage (b) active power from PV generators (c) rotor angle of conventional generator**

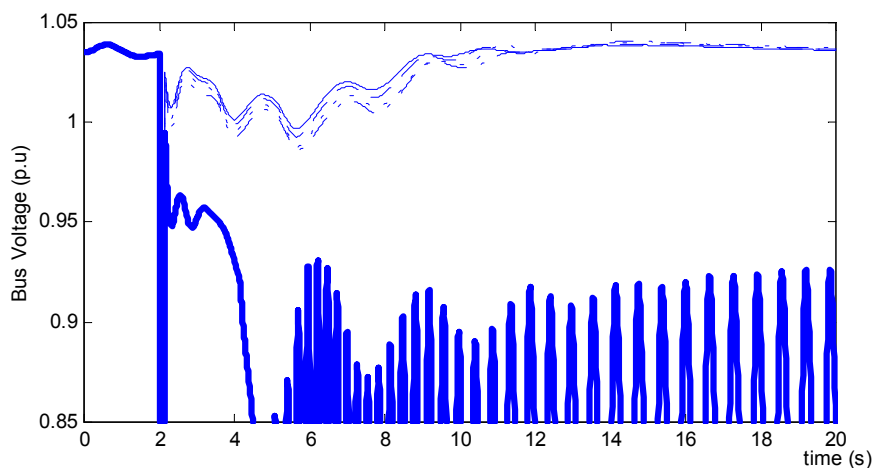


**Figure 6.16: Comparison of fault response of terminal voltage at bus-32 on the IEEE-39 bus test system with different fault impedance. The solid line, dashed line, dotted line, dashed-dotted line, and bold solid line correspond to decreasing value of fault impedance.**

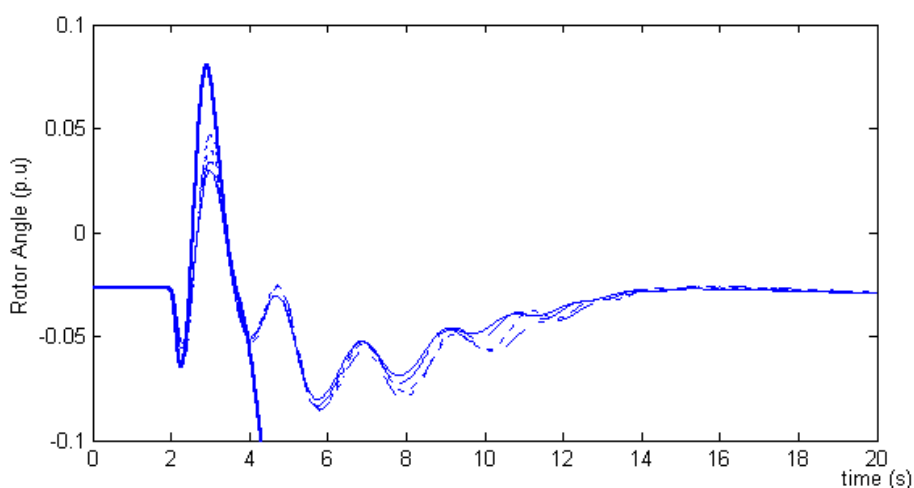


**Figure 6.17: Comparison of fault response of rotor angle for generator at bus-39 on the IEEE-39 bus test system with different fault impedance. The solid line, dashed line, dotted line, dashed-dotted line, and bold solid line correspond to decreasing value of fault impedance.**

### 6.4.2.3 Protection Parameters

Next, the impact of the protection parameters of the PV generators is illustrated. As in the previous studies, the generators at buses-32, 35, 34, 37 and 30 were replaced by an aggregated model of PV generator. Amount of power injected by the PV generation at each bus is same as the case shown in Figure 6.8. The under-voltage relay of the PV generator is set to trip at a voltage of less than 0.9 p.u. At  $t = 2$ s, a fault is applied at bus-32. The fault is cleared after 150 ms. The resulting PV generator active power,

terminal voltage and the rotor angle of the generator at bus-39 are plotted in Figure 6.18. The simulations are repeated with the value of the parameter of the under-voltage relay equal to 0.8 p.u and 0.4 p.u and the simulation results are plotted on Figure 6.19 and Figure 6.20 respectively. A comparison of the voltage at bus-32 and the rotor angle of the generator at bus-39 is plotted on Figure 6.21 and Figure 6.22 respectively.

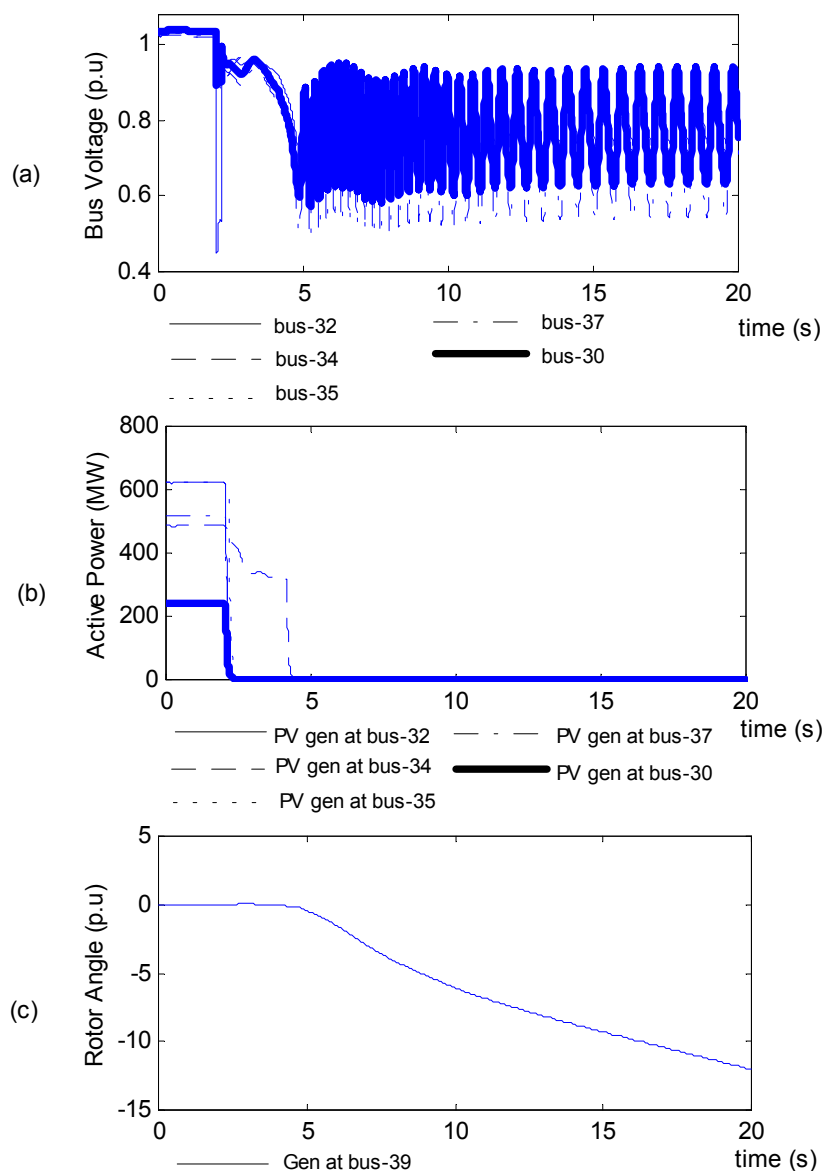


**Figure 6.18: Simulation of fault response on the IEEE-39 bus test system with PV generators integrated at bus-32, 34, 35, 37 and 30. The PV generator will trip when the terminal voltage is less than 0.9 p.u. (a) terminal voltage (b) active power from PV generators (c) rotor angle of conventional generator**

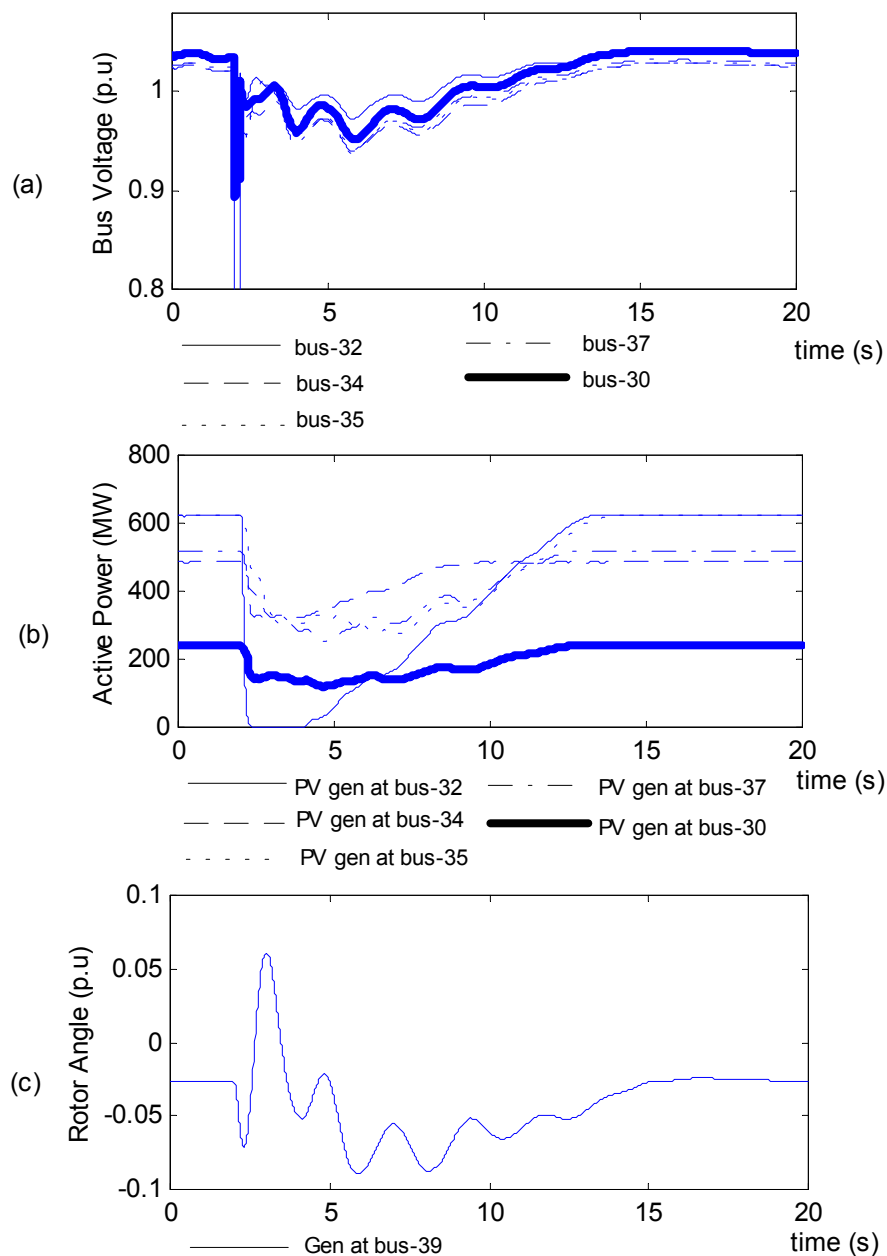


**Figure 6.19: Simulation of fault response on the IEEE-39 bus test system with PV generators integrated at bus-32, 34, 35, 37 and bus-30. The PV generator will trip when the terminal voltage is less than 0.8 p.u. (a) terminal voltage (b) active power from PV generators (c) rotor angle of conventional generator**

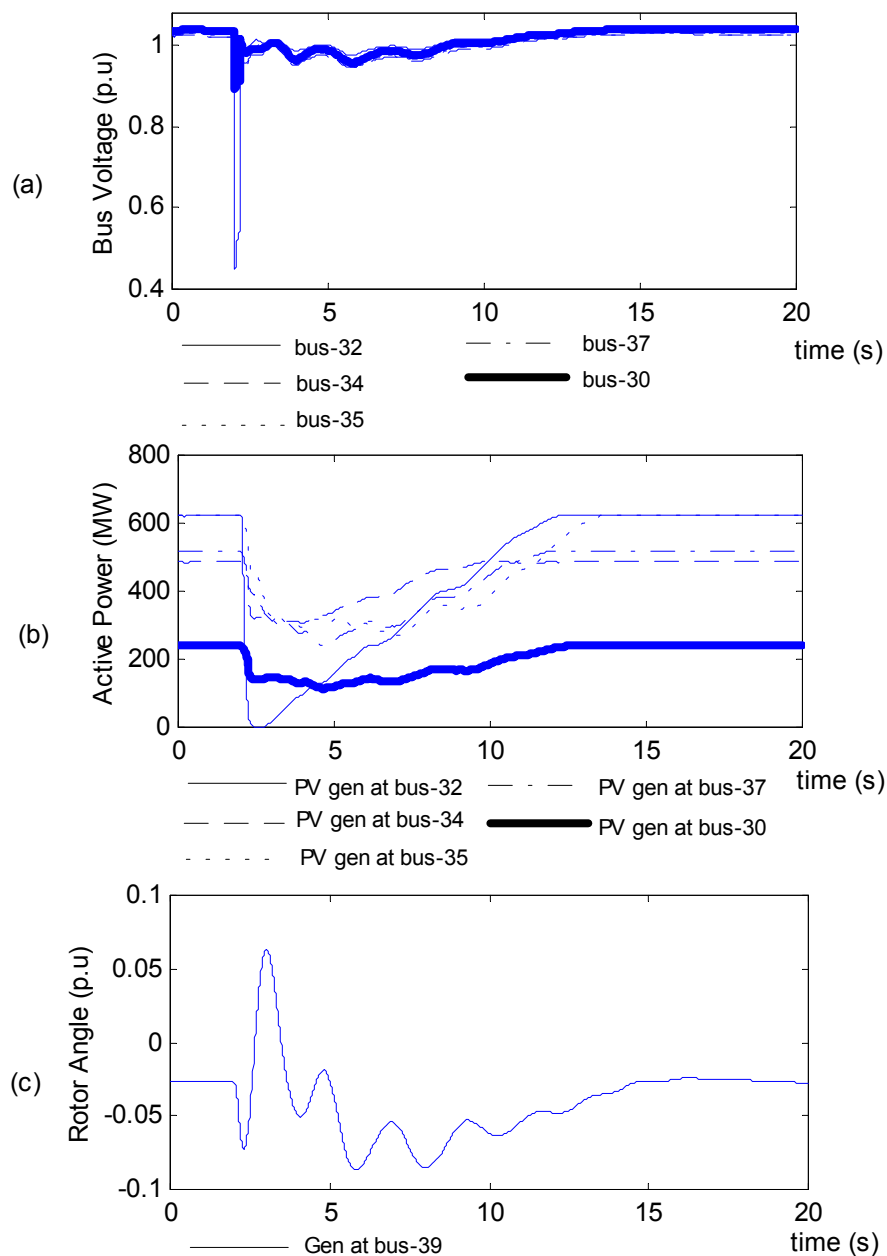


**Figure 6.20: Simulation of fault response on the IEEE-39 bus test system with PV generators integrated at bus-32, 34, 35, 37 and 30. The PV generator will trip when the terminal voltage is less than 0.4 p.u. (a) terminal voltage (b) active power from PV generators (c) rotor angle of conventional generator**

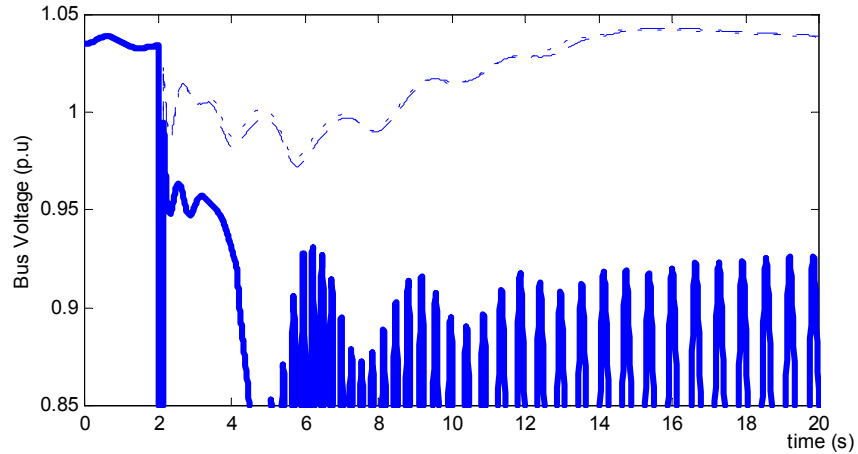


**Figure 6.21: Comparison of fault response of terminal voltage at bus-32 on the IEEE-39 bus test system with different fault impedance. The solid line, dashed line and dotted line correspond to tripping parameter of 0.9 p.u, 0.8 p.u and 0.4 p.u respectively**

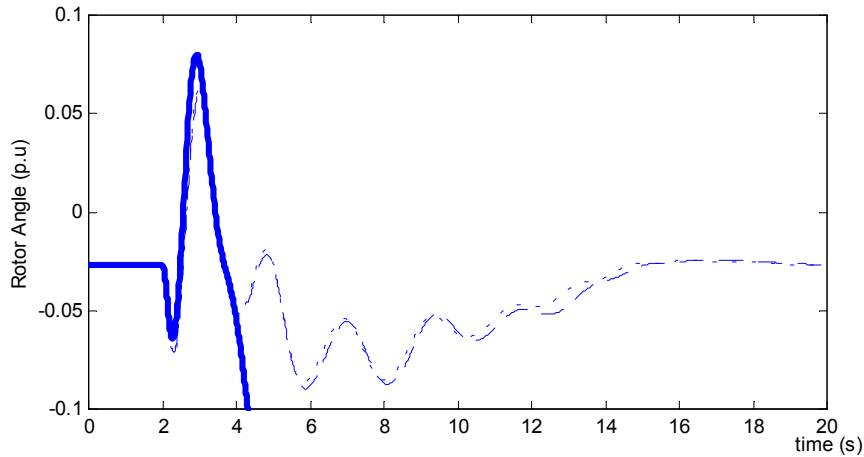


**Figure 6.22: Comparison of fault response of rotor angle for generator at bus-39 on the IEEE-39 bus test system with different fault impedance. The solid line, dashed line and dotted line correspond to tripping parameter of 0.9 p.u, 0.8 p.u and 0.4 p.u respectively.**

#### 6.4.2.4 Fault Clearing Time

Finally, the impact of the fault clearing time is investigated. To illustrate clearly the effect of the fault clearing time without the influence of PV generator tripping, the PV generator model is adjusted in such a way that the voltage has to drop below 0.8 p.u for more than 500 ms before the PV generators trip. The protection relay is set at 0 p.u. The generator at buses-32, 35, 34, 37 and 30 were replaced by an aggregated model of PV generation. Amount of power injected by the PV generation at each bus is same as the case shown in Figure 6.8. At  $t = 2s$ , a fault is applied at bus-32. This fault is cleared

after 100 ms. The resulting PV generator active power, terminal voltage and the rotor angle of the generator at bus-39 are plotted on Figure 6.23. These simulation results are repeated for fault clearing times of 200ms, 300ms and 350ms. The simulation results are plotted on Figure 6.24, Figure 6.25 and Figure 6.26. A comparison of the voltage at bus-32 and the rotor angle of generator at bus-39 is plotted on Figure 6.27 and Figure 6.28 respectively.

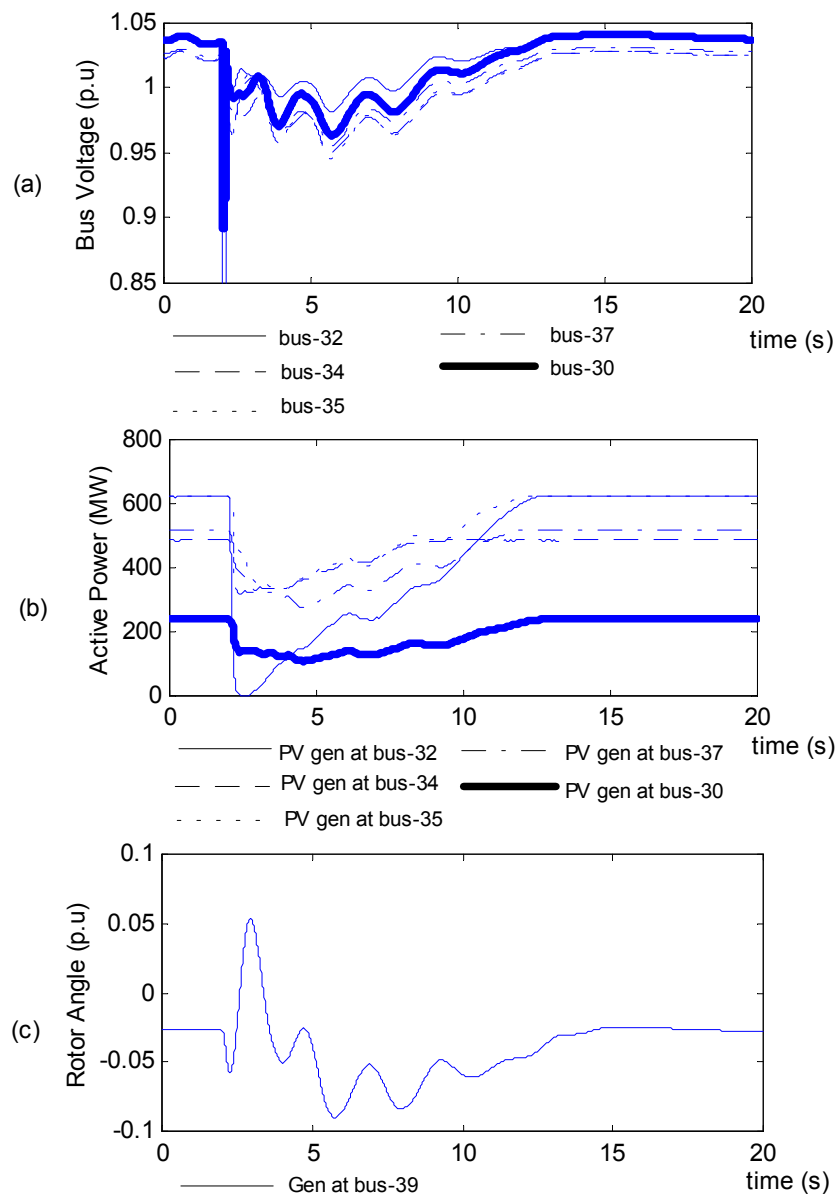


**Figure 6.23: Simulation of fault response on the IEEE-39 bus test system with PV generators integrated at bus-32, 34, 35, 37 and 30. The fault clearing time is 100ms. (a) terminal voltage (b) active power from PV generators (c) rotor angle of conventional generator**

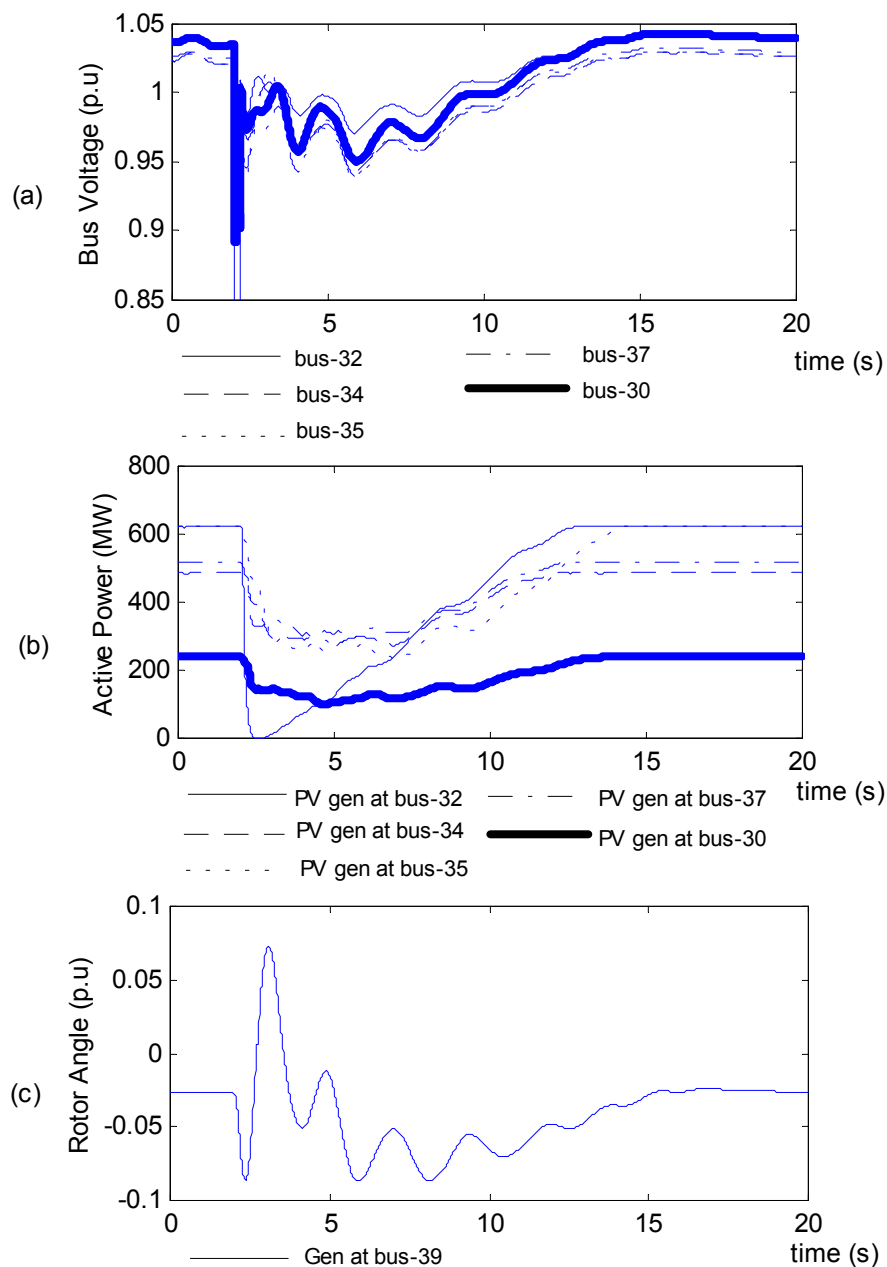


**Figure 6.24: Simulation of fault response on the IEEE-39 bus test system with PV generators integrated at bus-32, 34, 35, 37 and 30. The fault clearing time is 200ms. (a) terminal voltage (b) active power from PV generators (c) rotor angle of conventional generator**

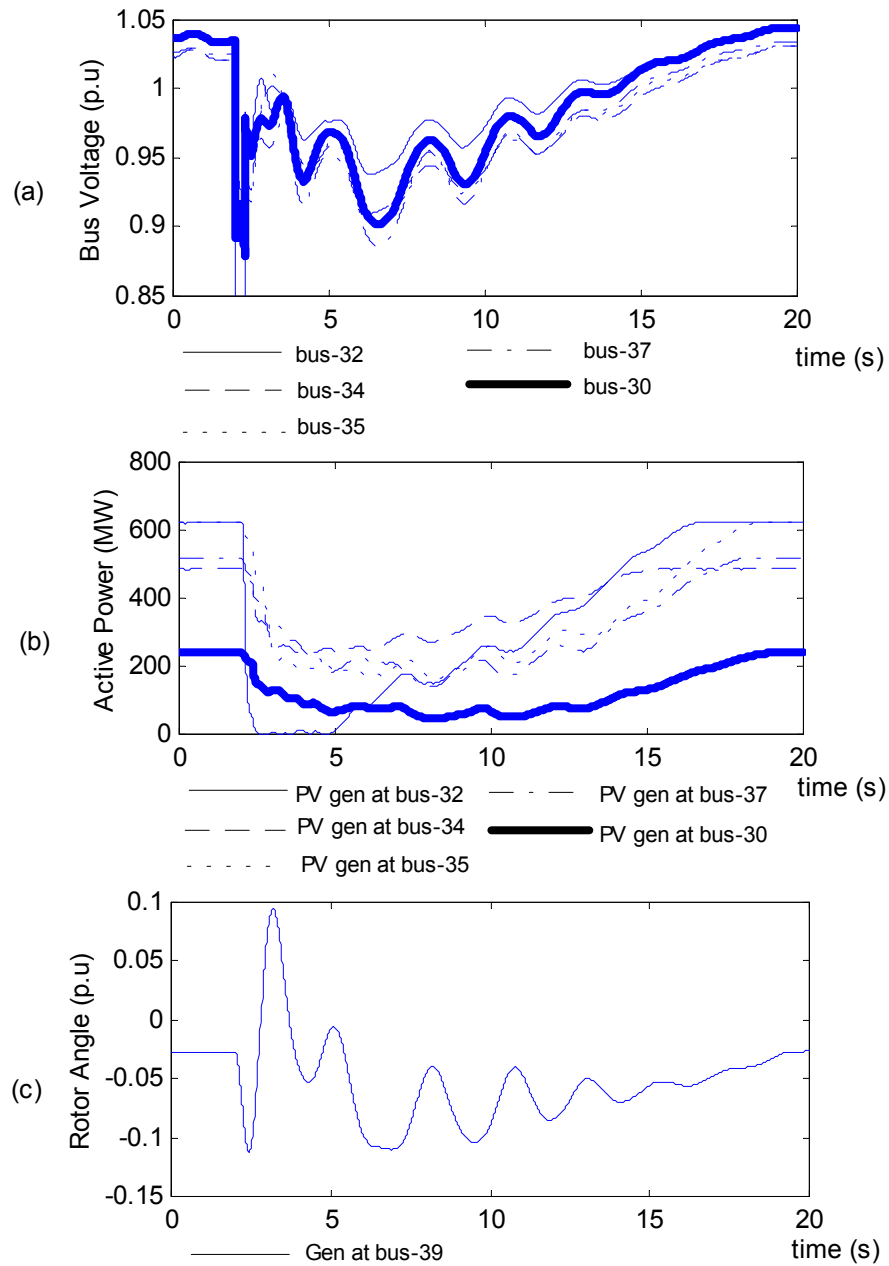


**Figure 6.25: Simulation of fault response on the IEEE-39 bus test system with PV generators integrated at bus-32, 34, 35, 37 and 30. The fault clearing time is 300ms. (a) terminal voltage (b) active power from PV generators (c) rotor angle of conventional generator**

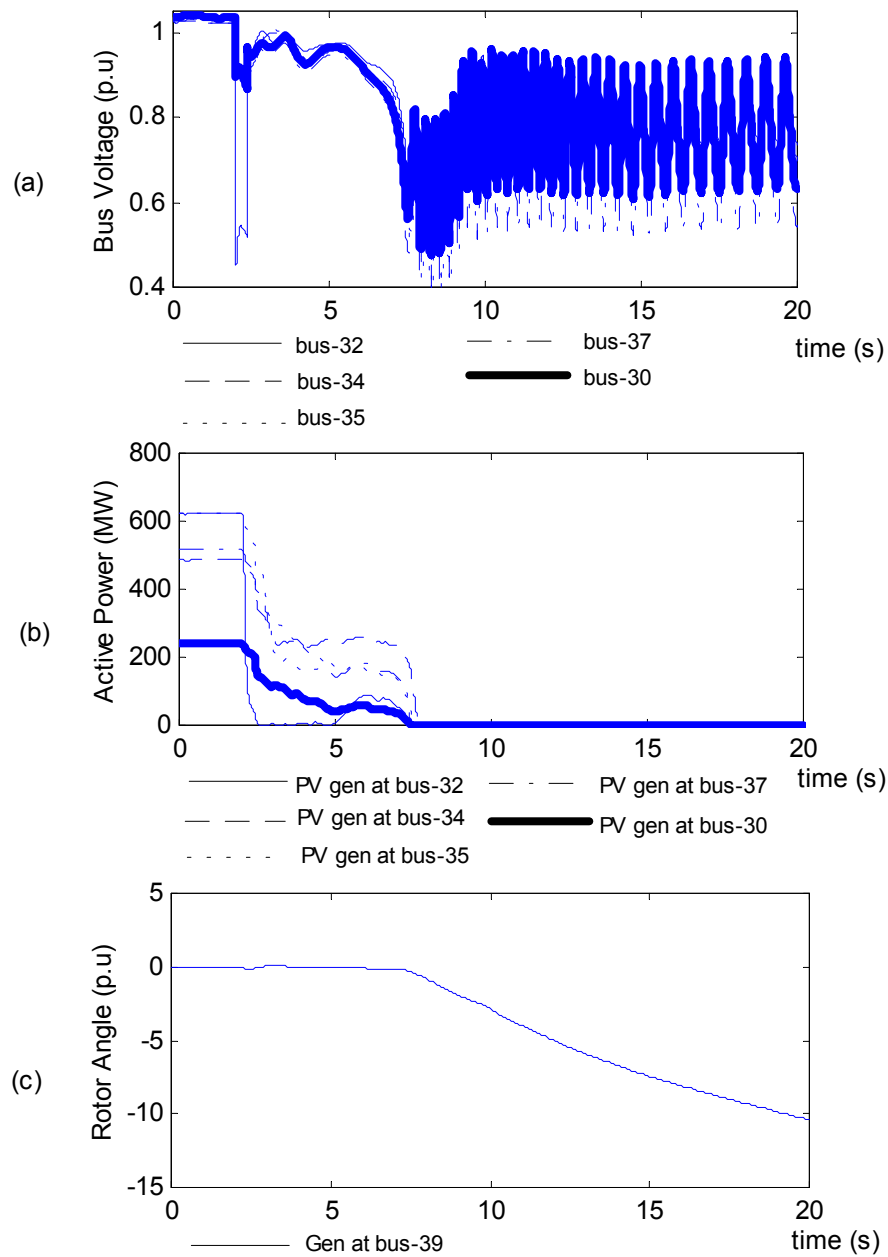


**Figure 6.26: Simulation of fault response on the IEEE-39 bus test system with PV generators integrated at bus-32, 34, 35, 37 and 30. The fault clearing time is 350ms. (a) terminal voltage (b) active power from PV generators (c) rotor angle of conventional generator**

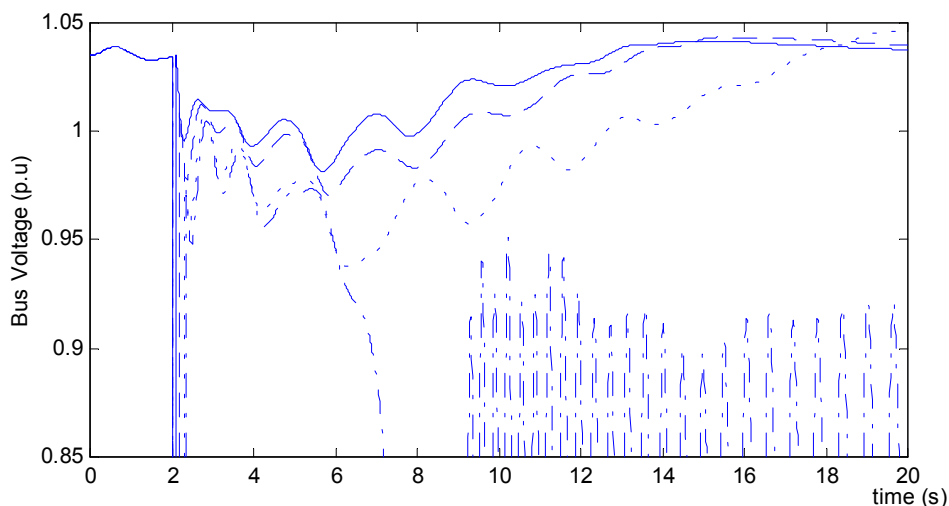


**Figure 6.27:** Comparison of fault response of terminal voltage at bus-32 on the IEEE-39 bus test system with different fault clearing time. The solid line, dashed line, dotted line and dashed-dotted line correspond to fault clearing times of 100ms, 200ms, 300ms and 350ms respectively.

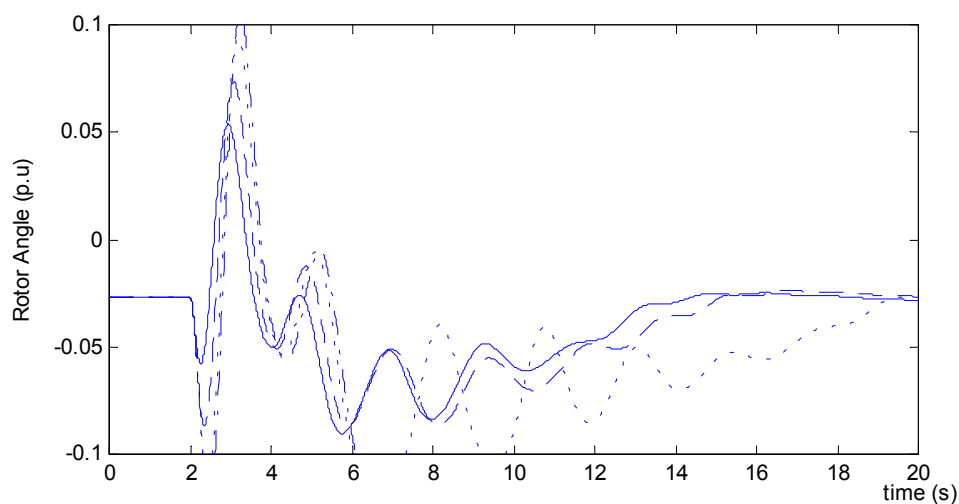


**Figure 6.28:** Comparison of fault response of rotor angle for generator at bus-39 on the IEEE-39 bus test system with different fault clearing time. The solid line, dashed line, dotted line and dashed-dotted line correspond to fault clearing times of 100ms, 200ms, 300ms and 350ms respectively.

The reactive power of the PV generators is not plotted for all the simulation mentioned because the PV generator is operating at unity power factor and therefore the reactive power consumed or produced by the PV generator is equal to zero. For all the simulation described above, shunt capacitors were connected to the buses with PV

generation in order to make sure that the bus voltage of the initial load flow remained approximately the same before and after PV generation was integrated

### 6.4.3 Analysis of the Simulation Results

The first conclusion that can be drawn from the simulations is that there is a strong relation between the terminal voltage, the active power produced by the PV generators, and the rotor angle of the conventional generators. A fault in the network affects the terminal voltage, whereas mechanical oscillations of the rotor angle of conventional generator after the fault reflect the transient stability of the system. The disturbance in the bus terminal voltage directly affects the performance of the PV generator.

As shown for example in Figure 6.5, active power was lost from the PV generators directly after the fault. This is because some of the PV generators were disconnected due to the operation of under-voltage relay, e.g. the PV generator at bus-32. Some of the PV generators have a sudden decrease in active power due to the sudden drop in terminal voltage, e.g. PV generator of bus-35. The bus voltage therefore oscillates below the steady state voltage value due to the loss of some PV generation. The scenario becomes worse as the PV penetration increase (see Figure 6.4 to Figure 6.8). It can be concluded from Figure 6.10 that a higher PV penetration results in a higher magnitude of oscillation in generator rotor angle and causes the system to be less transiently stable. Figure 6.8 shows that a fault on the system with a very high penetration of PV generation could eventually lead to a bus voltage collapse.

As shown from Figure 6.11 to Figure 6.15, as the fault impedance decrease, the magnitude of the voltage drop during the fault increases. This causes the magnitude of the PV generator active power drop after the fault to increase. As can be seen from Figure 6.11, the active power of PV generator at bus-35 drops to 470 MW for a fault impedance of 0.1 p.u. The active power of the PV generator at bus-35 drops to below 400 MW when the value of fault impedance is 0.07 p.u (see Figure 6.14). When the fault impedance is below 0.07 p.u, the amount of active power that the PV generator drops during the fault was so high that the voltage was not able to recover back to its original value and collapsed. It can be concluded from Figure 6.17 that the lower the

value of fault impedance the higher the magnitude of the oscillation in generator rotor angle. This cause the system less transiently stable.

The behaviour of the PV generator is governed by the protection system parameters and reconnection time. The reconnection time is the time that the PV generators need before reconnecting after a disconnection induced by a terminal voltage or frequency deviation. In this study the reconnection time was set at 2 seconds. The simulation results shown in Figure 6.18 to Figure 6.20 illustrate the impact of different protection parameter value on the PV generator after fault to system transient stability. When the protection parameter is set as 0.9 p.u, the system collapse after the fault was cleared. All the PV generators in the system were disconnected. When the protection parameters is set as 0.8 p.u, only the PV generator at bus-32 is disconnected and at  $t = 2$  seconds, it is reconnected at  $t = 4$  seconds and the system remains stable. Figure 6.20 shows that when the protection parameter is set below 0.4 p.u, none of the PV generators is disconnected after the fault is cleared. However, the voltage drops at bus-32 was so high that the active power drops to zero (but the generator remains connected) during the fault and slowly increases back to its original value after the fault is cleared. Figure 6.21 and Figure 6.22 show that the PV generators which are equipped with lower protection parameter value tends to have lower voltage drops after the fault and lower magnitude of rotor angle oscillation.

Figure 6.23 to Figure 6.26 illustrate the effect of the fault clearing time to the transient stability of the system with PV generators. The simulations results show that the longer the fault clearing time, the more likely the system will become unstable.

Apart from the factors listed above, other factors such as the presence of voltage control and the presence of a source of reactive power, e.g. SVC as explained in Chapter 5 also affect the fault response of the PV generation. A quantitative investigation of modifications to the design of PV generation and the power system's topology in order to improve the transient stability of PV generation is not presented in this thesis. The principles on which these issues can be approached can, however, be understood intuitively when considering the fault response of the PV generator as described in section 6.3.1 and the above simulation results. The post-fault behaviour is governed by the reactive power consumption, and the terminal voltage restoration,

which are interdependent. If a source of reactive power is added to the PV generation, it will improve the terminal voltage restoration. This will reduce the drop in PV generator active power at the same time result in less PV generators being disconnected from the system. This will further improve voltage restoration.

### **6.5 CONCLUSION**

In this chapter, the transient response of PV generators to faults was discussed. The mechanism which causes the instability of the PV generation system after faults was described. The impacts of the penetration of PV generation, the impedance of faults, the protection parameters of the PV generation and the fault clearing time to the fault response were illustrated using simulation results on a realistic test system. The simulations demonstrate that with higher penetration of PV generation the system becomes less transiently stable with: -

- A lower value of fault-impedance
- A higher value of under voltage relay settings
- A larger fault clearing time

# Chapter 7

## FREQUENCY RESPONSE FROM PHOTOVOLTAIC GENERATION

### 7.1 INTRODUCTION [47,48]

The generation of electrical power from renewable energy sources is developing rapidly after the announcement of government targets for reduction of greenhouse gases by 2010. The government targeted to supply 10% of the total UK electricity demand from renewable sources by 2010. This means that a capacity of up to 8-10GW will be supplied by renewable generating plant. Looking further ahead, if the UK is to achieve the ambitious target of achieving a 60% reduction in carbon emissions by 2050 this will required that renewable source to be contributed at least 30% to 40% of the energy used for electricity generation [49]. Such a change in the mix of generating sources could have a dramatic effect on the way the system is controlled.

To date, it has not been necessary for small PV generators to provide frequency regulation services to the power system. The current practice is that they are disconnected from the power system in the event of network disturbances. In the future, with an increasing penetration of PV generation, their impact upon the overall

control of the power system will become significant. This will lead to a situation where the PV generators will be required to share some of the duties, such as frequency control. Various transmission system operators might need to revise their grid codes to ensure that large PV generation contribute to the operation of the power system. In this chapter, the capability of the PV generator to provide frequency response for the power system using electronic control is studied.

### **7.2 FREQUENCY CONTROL [47, 48, 50, 51]**

National Grid Company (NGC) as the grid operator manages the quality of system frequency control on the British Grid System through instructions to individual generating units for energy commitment, frequency response and reserves, and through a partnership role with Scottish Power and Scottish Hydro Electric. In any power system, all the larger generators connected to the England and Wales network must have the technical capability to contribute to frequency control under the grid code. The frequency delivered to the consumer must not vary from the declared value by more than  $\pm 1\%$  [50] in accordance with the Electricity Supply Regulation 1989 and hence the NGC Transmission License. These requirements are summarized in [51].

The frequency service must be automatic. It can be divided into two categories; there are continuous services and occasional services as shown in Figure 7.1. For continuous services, the generator output is continuously adjusted as the demand varies to control the system frequency. The balancing of the generation of power against load is achieved on a second by second basis. It also requires an ability to respond to occasional larger mismatches in generation and load caused, for example, by the tripping of a larger generation or load.

The system frequency of England and Wales network is maintained within the range of 49.8 Hz – 50.2 Hz under normal condition in order to meet the statutory requirements specified by the grid code. A number of the generators operate to provide continuous response to frequency changes within this range. The generators

are operating at normally around 4% governor droop. However, the system frequency is allowed to deviate to up to  $\pm 0.5\text{Hz}$  if there is a sudden change in generation or load.

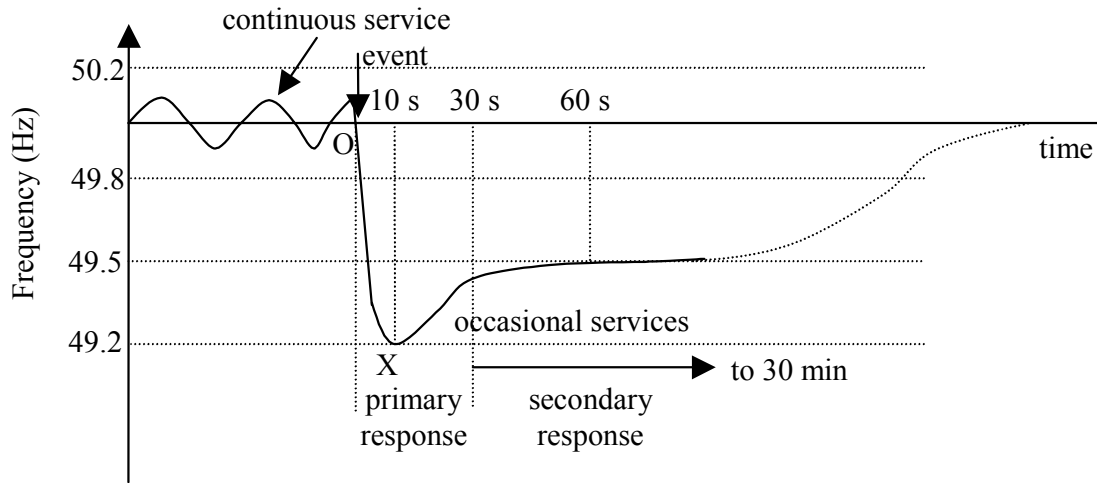


**Figure 7.1: Frequency Control in England and Wales [50]**

Occasionally the system frequency may drop below its continuously control limit when there is a connection of a large load or sudden failure in generation as shown in Figure 7.1. The rate of frequency drops is mainly determined by the total angular momentum of the system. In those cases, response from generating plants and load reduction is then used. These generators that have agreed to provide frequency response increase their output through the governor action and the load of certain customers may be shed by low frequency relays. These occasional response services can be divided into primary and secondary responses. Following a loss of generation, the initial short-term automatic power output increase to the negative frequency change is termed primary response. It is important that the primary response from synchronised generation is released increasingly with time, through automatic governor action, in the period 0-10 seconds after the incident and sustained for a further 20 seconds. The automatic positive power response in the subsequent frequency stabilisation phase beyond 30 seconds to 30 minutes after the incident is termed secondary response.

With a steam turbine, primary response is normally achieved by de-loading its maximum power. It can be done by partially closing the steam valve, then that plant can provide primary response proportional to its de-load. In a manner similar to steam turbine, the continuous service events and primary response of occasional frequency

control can be achieved by de-loading PV generator and regulating the output according to the frequency variations.

If there is a sudden loss of system load causing the frequency to rise above its target value, the automatic reduction in power output is termed high frequency response and it will be available at 10 seconds after an event and can be sustained indefinitely. The provision of high frequency response can be achieved in the PV generation by regulating the degree of de-loading.

### 7.3 DE-LOADING OF PV GENERATOR

In order to provide frequency response, PV generators must be able to increase or decrease their output with system frequency changes. To respond to a low frequency, PV generators must be de-loaded to leave a margin for power increase. If the operating point of the PV generators can be changed so as to operate it off the maximum power point, then de-loading can be achieved using electronic control.

In chapter 2, the characteristic of a photovoltaic array has been discussed. The relation between  $V_{pv}$  and  $I_{pv}$  of a photovoltaic array is highly non-linear and dependent on the solar irradiance ( $I_r$ ) incident on the PV array (see Chapter 2, Section 2.3). The combination of  $V_{pv}$  and  $I_{pv}$  that maximizes the output of the inverter depends on the irradiance and is also affected by the temperature of the cells. The maximum power point tracking (MPPT) controller optimizes the efficiency of the photovoltaic energy conversion.

Figure 7.2 shows the set of 100% maximum power points for the PV system. It shows how a 10% de-loading can be achieved on the  $V_{pv} - P_{pv}$  curve. However, as the PV generator controller is based on  $I_{pv}$ , the same set of maximum power points is transformed to the  $I_{pv} - P_{pv}$  plane as shown in Figure 7.3. The set of 100% maximum power points (OA of Figure 7.3) for the PV generator can be replaced by the set of 90% maximum power points (PQ of Figure 7.3) to obtain frequency response from the PV generator. When the PV generator is de-loaded this way for any irradiance level, the  $I_{pv}$  will be less than the  $I_{pv}$  corresponding to the 100% case.

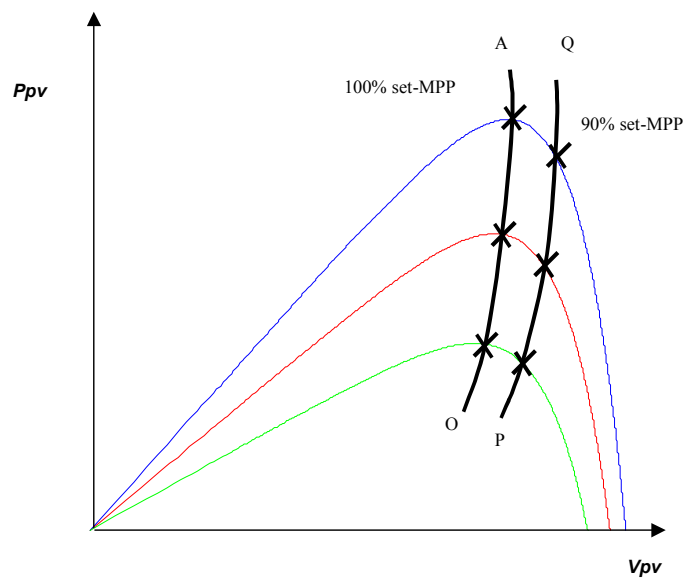


Figure 7.2: 10% de-loading on power in  $V_{pv} - P_{pv}$  plane

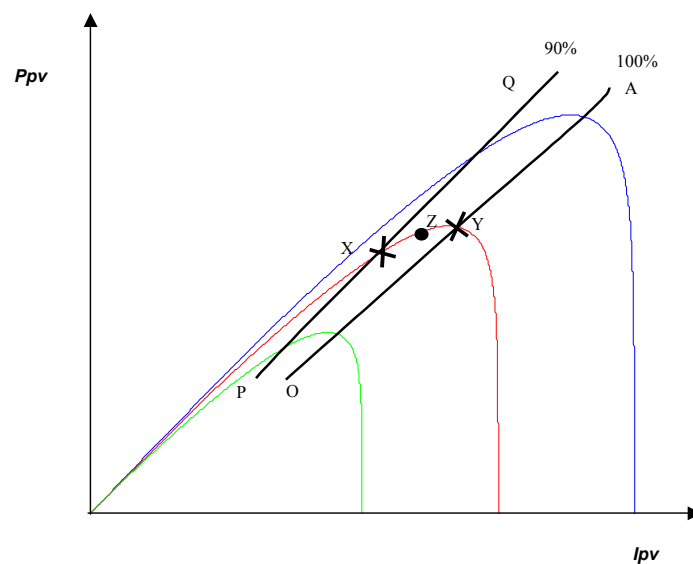


Figure 7.3: 10% de-loading on power in  $I_{pv} - P_{pv}$  plane

## 7.4 METHODOLOGY

De-loading of PV generator with P&O MPPT technique is difficult. P&O MPPT searches the maximum power point by perturbing the operating point and comparing the current value of the output power with the one at the previous cycle (see Chapter 3, section 3.6). Therefore, the value of maximum power point is not known before

hand. This makes the de-loading of the PV generator as a fraction of the maximum power a difficult task.

To overcome this problem, the controller of the PV generator is designed to have two separate control modes: - the MPPT mode and the Frequency Response (FR) mode. The PV generator will alternate between the two modes to be able to track changes in operating condition. In MPPT mode, the PV generator searches for the maximum power point using P&O MPPT technique. The period during which the PV generator remains in MPPT mode is long enough for the operating point to move from zero power to maximum power. Once the maximum power point is known, it is then possible for the PV generator to be de-loaded in the FR mode. The PV generator stores the information of maximum power value in MPPT mode and de-loads it to the required value in the FR mode.

In order to achieve this control algorithm, a number of additional control components have been added to the basic dynamic PV generator model as described in Chapter 3. These include the  $P_{pv}^{freq}$  control block, the  $\Delta I_{pv}^{frequency}$  control block and the *relay with timer* block as shown in Figure 7.4. This figure shows how these electronic might be used for frequency response in PV generator. When the PV generator is in MPPT mode, the relay switch is located at point A. The PV generator searches for the maximum power point using the MPPT technique that is implemented in the inverter controller. After a period of time, the PV generator switches to FR mode by changing the position of the relay from location A to location B. At the same time, the Sample and Hold (S&H) block in the  $P_{pv}^{freq}$  control block will read and sample the  $P_{pv}$  value as  $P_{pv}^{ref}$ . The PV generator is de-loaded by modifying the 100% maximum power point to the point on PQ of Figure 7.3 at a given irradiance. This can be achieved by adding a droop on the set point power,  $P_{pv}^{ref}$  at nominal frequency. The droop characteristic from the *Power-Frequency Curve* is used to control the output of the PV generator. The droop characteristic allows the PV generator to increase its output power when the system frequency is low and to decrease its output power when the system frequency is high. The details of the implementation of each control block are described in the sections below.

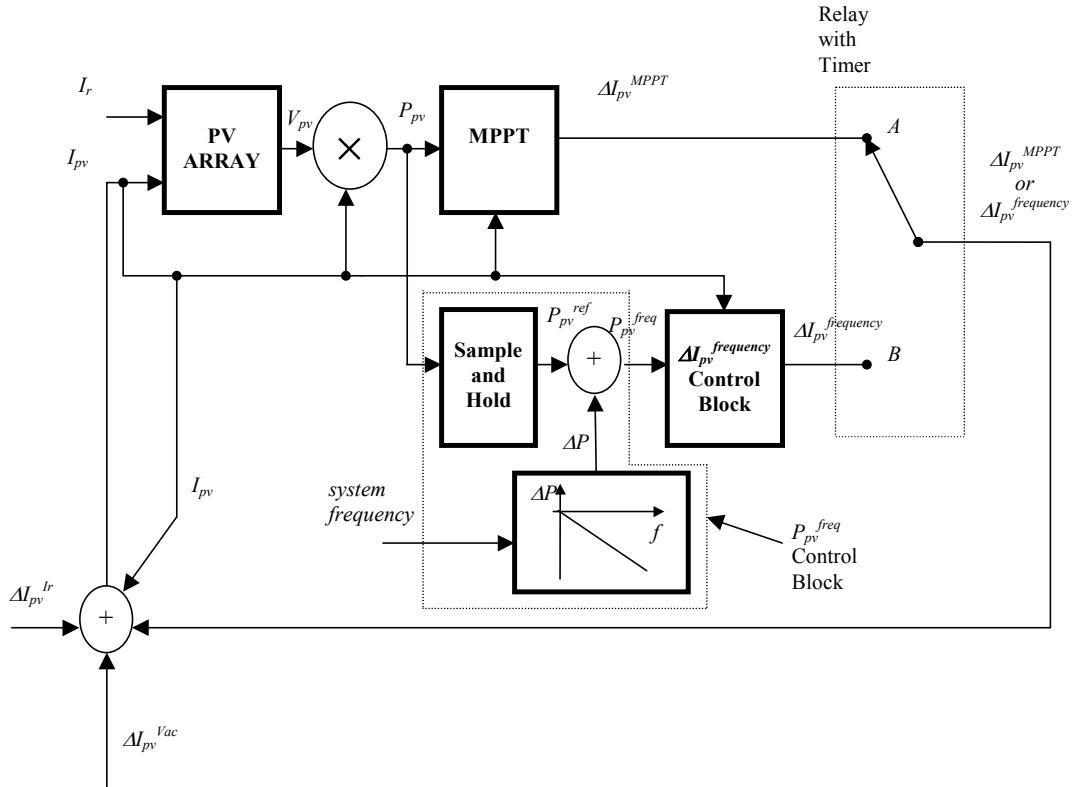


Figure 7.4: Block diagram of PV generator with frequency response controller

## 7.5 IMPLEMENTATION OF ELECTRONIC CONTROL CIRCUIT OF FREQUENCY RESPONSE

### 7.5.1 $P_{pv}^{freq}$ Control Block

Figure 7.5 shows the block diagram of the  $P_{pv}^{freq}$  control block.  $P_{pv}^{freq}$  is the reference de-loaded output power of the PV generator in FR mode. It consists of two sub-control blocks which are the *S&H* block and the *Power-Frequency Curve* block.  $P_{pv}$  is one of the inputs to the  $P_{pv}^{freq}$  control block which is fed into the *S&H* block. The other input of the  $P_{pv}^{freq}$  control block is the system frequency which is fed into the *Power-Frequency Curve* block. The main function of the  $P_{pv}^{freq}$  control block is to generate the required reference de-loaded output power,  $P_{pv}^{freq}$  in FR mode.

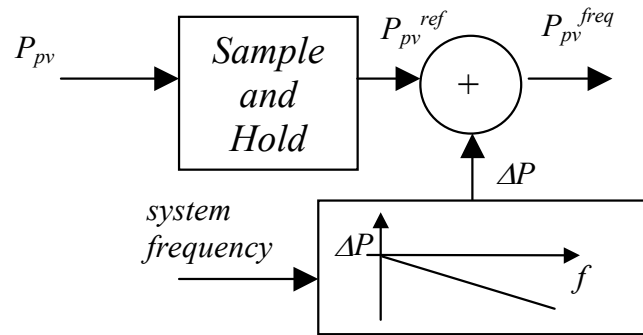


Figure 7.5:  $P_{pv}^{freq}$  Control Block

### 7.5.1.1 S&H Block

The main function of the *S&H* block is to sample the input  $P_{pv}$  value at the time the PV generator is changing from MPPT mode to FR mode and hold the value at the output. This process is repeated at each cycle. In Simulink™, the *S&H* block will sample the new  $P_{pv}$  value and hold it at the output when the input signal A as shown in Figure 7.6 is a falling edge trigger signal. The digital clock used is synchronized with the digital clock in the *relay with timer* block which will be explained later. To avoid every PV generators having the same starting time, a random number is used to spread the starting time. The pattern of signal A is shown in Figure 7.7.

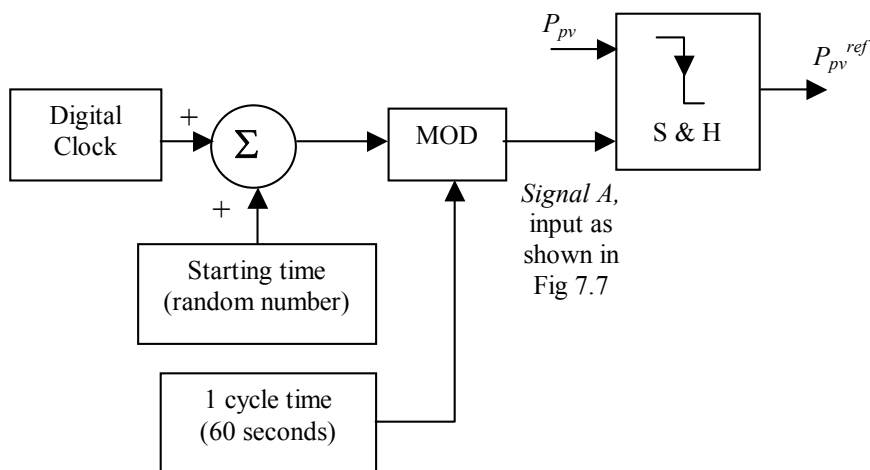


Figure 7.6: Implementation of *S&H* block

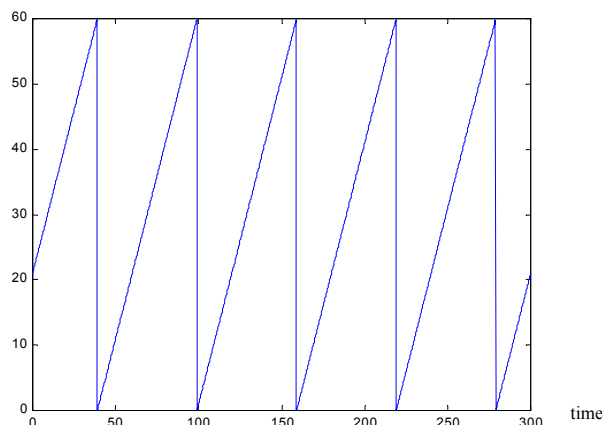


Figure 7.7: Pattern of signal A

### 7.5.1.2 Power-Frequency Curve Block

Figure 7.8 shows how a droop on the power can be added to the to the set point  $P_{pv}^{ref}$  through the *Power-Frequency Curve* to control the output of the PV generator. For example, say the PV generator operates at system frequency 50 Hz, the value of  $-\Delta P_I$  will be added to the set point  $P_{pv}^{ref}$  to produce a reference de-loaded power of  $P_{pv}^{freq}$ . This leaves to a margin of  $\Delta P_I$  for power increase. If the frequency drops,  $\Delta P$  decreases. It causes the required output power  $P_{pv}^{freq}$  to increase in FR mode. In the other way, if the frequency increases,  $\Delta P$  increases. This causes  $P_{pv}^{freq}$  to decreases.

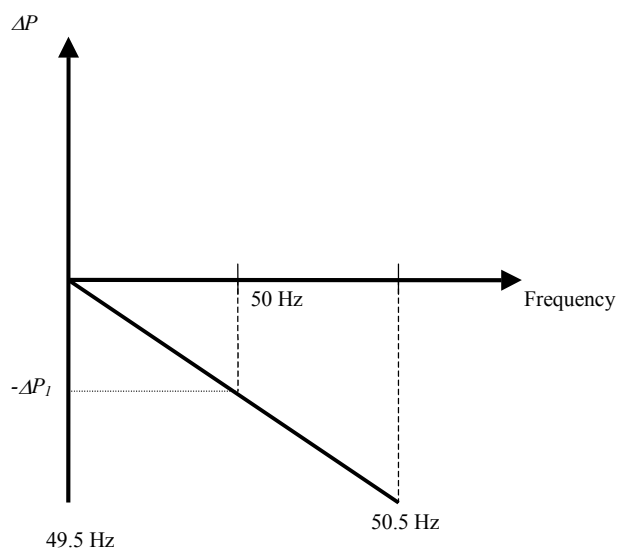


Figure 7.8: Power Frequency Curve

### 7.5.2 $\Delta I_{pv}^{frequency}$ Control Block

Figure 7.9 is the flow chart that shows how the  $\Delta I_{pv}^{frequency}$  control block controls the incremental current,  $\Delta I_{pv}^{frequency}$  to obtain the required output power  $P_{pv}^{freq}$  in FR mode. The operation of this control is explained using Figure 7.10.

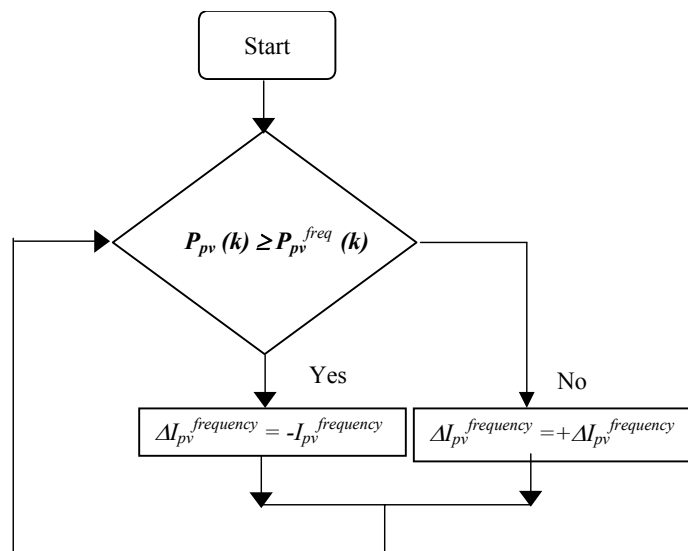


Figure 7.9: Flow chart of  $\Delta I_{pv}^{frequency}$

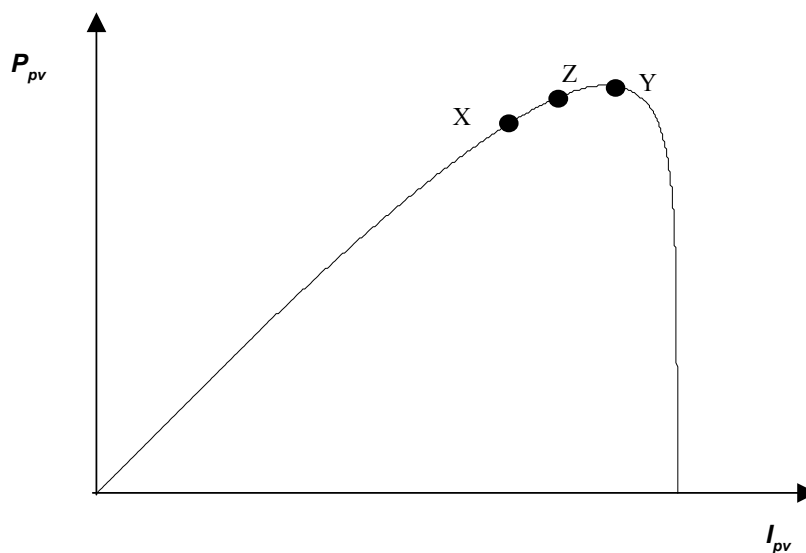


Figure 7.10:  $I_{pv} - P_{pv}$  plane

For example, say the PV generator operates at the point Z with 5% de-loaded power at a given irradiance value. If the frequency drops, the value of  $P_{pv}^{freq}$  initially increases to the new value of  $P_{pv}^{freq}$  at Y. The control system compares the output power  $P_{pv}$  at the current operating point at Z with the new value of  $P_{pv}^{freq}$  at Y. In this case, the  $P_{pv}$

at the current operating point at Z is smaller than the new value of  $P_{pv}^{freq}$  at Y. The control increases the  $I_{pv}$  with a incremental step of  $+\Delta I_{pv}^{frequency}$  to reach the new value of  $P_{pv}^{freq}$ . On the other hand, if the frequency increases, the value of  $P_{pv}^{freq}$  initially decreases to the new value of  $P_{pv}^{freq}$  at point X. The control system again compares the value of  $P_{pv}$  at the current operating point Z with the new value  $P_{pv}^{freq}$  at X. The value of  $P_{pv}$  at the current operating power point at Z is larger than the new value of  $P_{pv}^{freq}$  at X. The control system then decreases the value of  $I_{pv}$  with an incremental step of  $-\Delta I_{pv}^{frequency}$  moving the operating point from point Z towards point X.

### 7.5.3 Implementation of Relay with Timer

Figure 7.11 shows the *relay with timer* block diagram. The relay has 3 main inputs. Two of them are  $\Delta I_{pv}^{MPPT}$  and  $\Delta I_{pv}^{frequency}$ . When the input X is greater or equal than the threshold parameter K, the output Y is equal to  $\Delta I_{pv}^{MPPT}$ . On the other hand, if the input X is smaller than the threshold parameter K, the output Y is equal to  $\Delta I_{pv}^{frequency}$ . The digital clock and starting time used is synchronised with the one used in the S&H block. This allows the S&H block to sample the value of  $P_{pv}$  at the time the relay is switched from position  $X_1$  to position  $X_2$ .

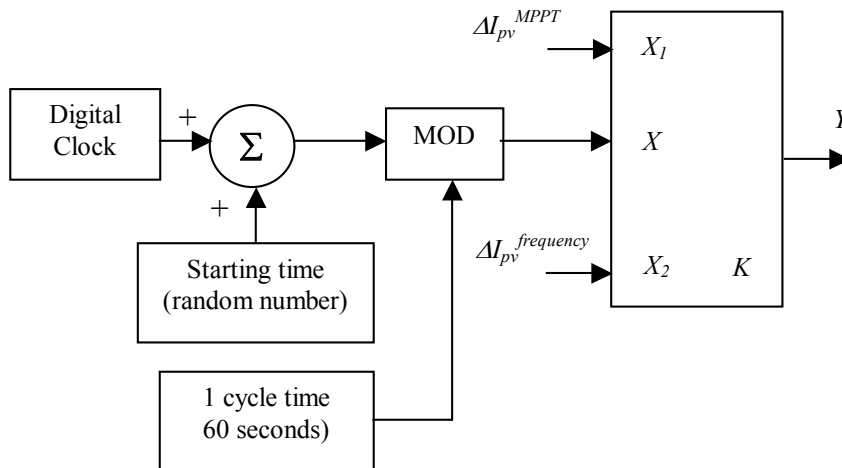
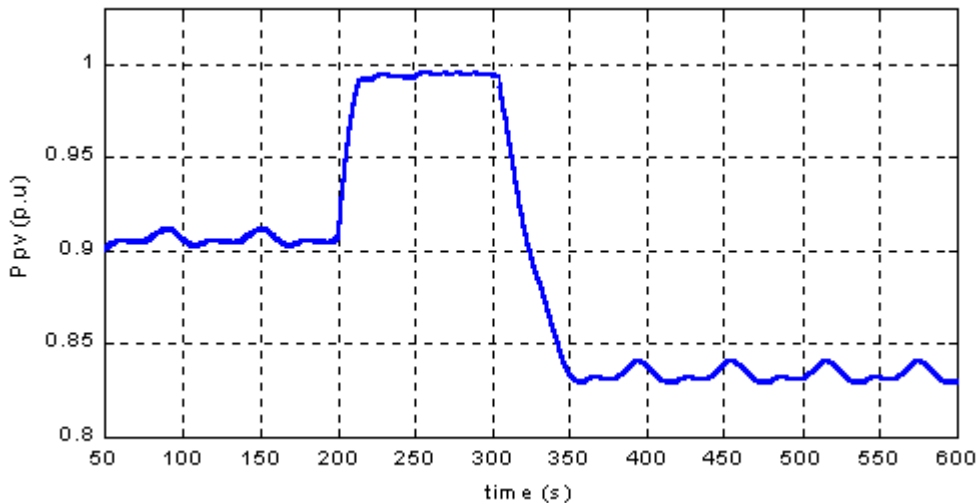


Figure 7.11: Implementation of Timer with Relay

## 7.6 SIMULATION RESULTS

The operation of the frequency response of the PV generators is illustrated at a constant irradiance in Figure 7.12. In this study, it consists of 100 individual PV generating units with a total output power of 0.7 MW. All the PV generators operate independently and are not synchronised with each other. The total PV generators output is de-loaded to 0.9 p.u at 50 Hz and a step change in frequency of  $\Delta f = -0.5\text{Hz}$  is applied at  $t = 200\text{s}$  and  $\Delta f = +0.5\text{Hz}$  at  $t = 300\text{s}$ . The results show that the proposed controller provides a frequency response to the step changes in frequency by increasing or decreasing the output power from the PV generators.



**Figure 7.12: Frequency response of the PV generator with constant irradiance**

Figure 7.13 shows the simulation results of frequency response of the PV generator with sudden change in irradiance. A step decrease of irradiance is applied at  $t = 200\text{s}$  and a step change in frequency of  $\Delta f = -0.5\text{Hz}$  is applied at  $t = 400\text{s}$ . The results show that at  $t = 200\text{s}$ , the output power of PV generators drops due to the sudden decrease in irradiance. At  $t = 400\text{s}$ , the proposed controller provides a frequency response to the step decrease in frequency by increasing the output power from the PV generator. This shows that the proposed controller of frequency response works well under changing frequency.

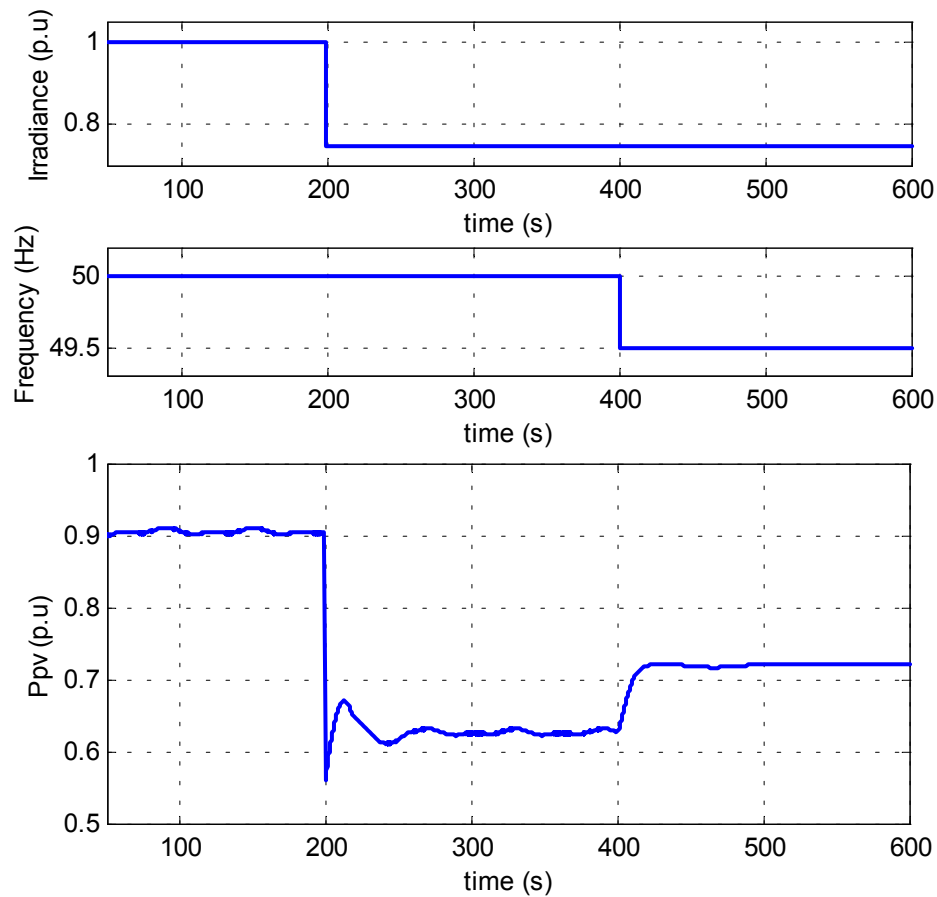


Figure 7.13: Frequency Response of the PV generator with sudden change in irradiance

## 7.7 CASE STUDY

In order to investigate the proposed frequency response controller for frequency response it is required to integrate the model together with a power system model. To demonstrate the impact of photovoltaic generators output power on frequency deviations resulting from load changes, a power system model was developed. The power system model was represented by a transfer function with system angular momentum ( $M$ ) and damping ( $D$ ) [34]. In this case,  $M = 10\text{s}$  and  $D = 0.75\%$ . This model is shown in Figure 7.14.

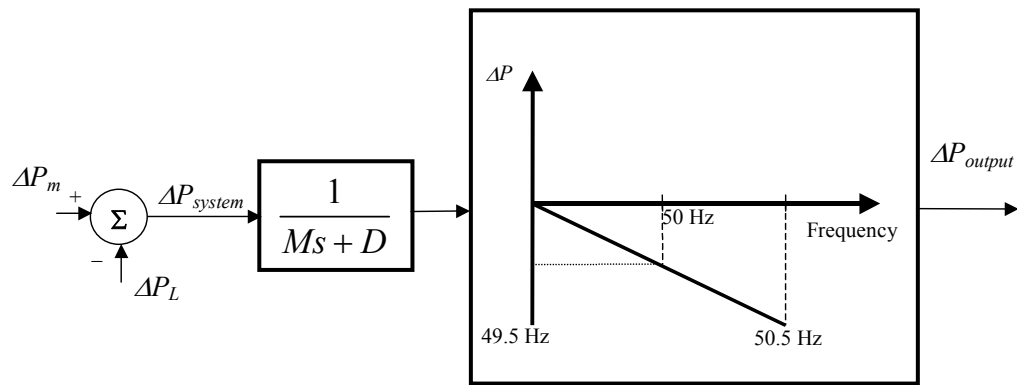


Figure 7.14: Power system model transfer function and slope characteristic

The PV generator model was initialised to operate at 10% de-loaded power with nominal frequency (50Hz). At  $t = 200s$ , a step change in load was applied which results in a decreasing system frequency as defined by the power system model. The PV generators frequency response controller responds to the frequency deviation by increasing the output power. Similarly, a step decrease in load was applied at  $t = 400s$ . The PV generator frequency response controller responds to the increase in frequency by decreasing the output power. The results are shown in Figure 7.15.

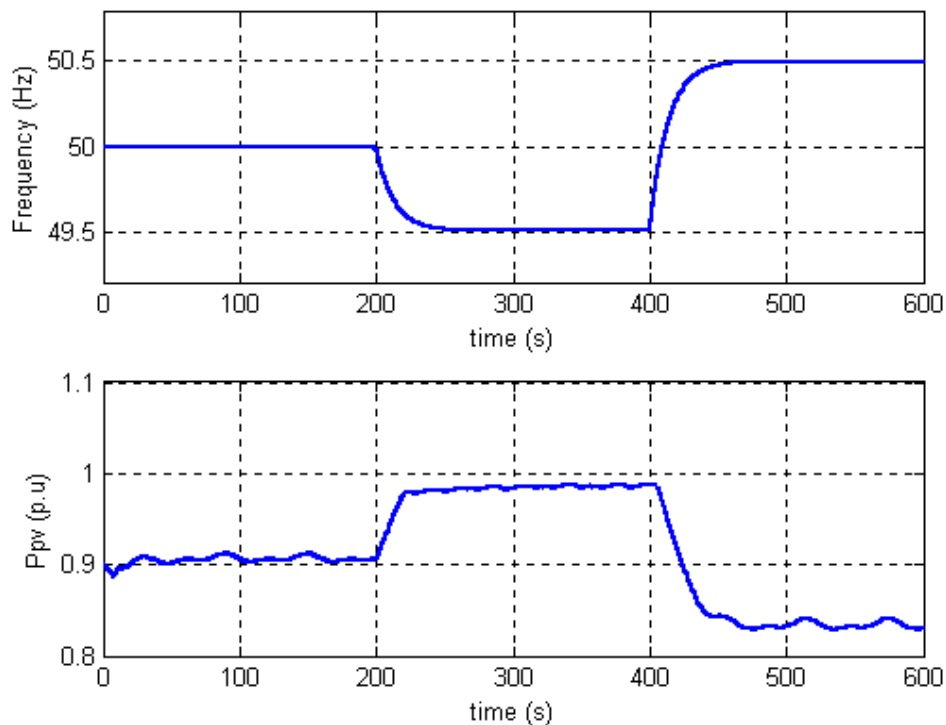


Figure 7.15: PV generator response to frequency deviation at constant irradiance

## **7.8 CONCLUSION**

The installed capacity of PV generators will continue to increase in the future in many countries. If they become significant fractions of the connected generation, it is no longer appropriate for the PV generators to be considered as a "negative load". They must take part in the operation of the power system.

The requirement of power system frequency control and the classification of the continuous and occasional services have been discussed. A control strategy to provide frequency response from the PV generators using electronic control is developed.

The simulation results illustrate that a PV generator can have the ability to assist in frequency control as specified by the transmission system operator grid codes. A case study was carried out by connecting the PV generators to a power system model having an angular momentum (M) and damping (D). It shows that the PV generators give a good response to frequency control.

# Chapter 8

## CONCLUSIONS

### 8.1 SUMMARY

The development of dynamic models of PV generation has been the object of only a few scientific publications. A review of these papers shows that the voltage reference signal of the inverter is assumed to be equal at all times to the point corresponding to maximum power for the current irradiance level. The operation of the MPPT controller is thus not represented in these models. Simulation results obtained with these models suggest that PV generating units should respond to disturbances in irradiance and line voltage within milliseconds. Experiments carried out with commercial inverters contradict these simulations. The experimental results indicate that the response time of PV generating units is considerably longer. It was therefore decided to develop an empirical model based on experimental results rather than on analytical manipulations. This model should reflect accurately the dynamic behaviour of the PV generating unit following small or slow changes in irradiance, sudden large increases and decreases in irradiance, as well as sudden changes in ac grid voltage. This approach is also well suited to the modelling of commercial systems for which no information regarding the control algorithms is available. A PV system was thus subjected to a number of such disturbances in a laboratory environment. An analysis

of the response of the PV system to these disturbances led to the identification of various response modes and the development of a model capable of representing this complex dynamic and non-linear behaviour. We have implemented this model using both the Simulink<sup>TM</sup> and Eurostag 4.1<sup>TM</sup> software packages. The experimental results were compared with simulation runs performed by both tools. Results shows that the proposed model accurately represents the dynamic behaviour of the PV generating unit.

The PV generation model that has been built was incorporated within a power system model to analyse the impact on the power system of incorporating a significant amount of PV generation. The analysis was carried out on a 10-bus test system to predict the effects of sudden irradiance changes on a utility interactive PV system. These results should be generally applicable to a power system of any size. These results illustrate the slow transient responses in bus voltages corresponding to fluctuation in photovoltaic generation resulting from the passage of clouds. Analysis of these results shows that the amount of power produced by the PV generator follow the pattern of irradiance. This is because the MPPT controller implemented in the PV generator keeps the PV system operating at their maximum power point despite the large fluctuations in irradiance. The busses where conventional generation is connected are not affected by the fluctuation in PV output because of the action of the automatic voltage regulators unless the reactive power demand on the generator is higher and causes the field current of the generator to exceed its limit. On the other hand, the photovoltaic generators are modeled as power injectors without voltage regulators. The voltage at buses where PV generators are connected fluctuate during the large change in irradiance level. The voltage fluctuations due to changes in irradiance become more significant when the amount of PV penetration is higher.

Three voltage control techniques have been investigated to overcome these voltage fluctuation problems. The techniques include power factor control, automatic voltage control from the PV inverter itself and voltage control using an SVC. Simulations and comparisons between these three methods have been performed. It was found that although operating the PV generator at lagging power factor tends to raise local voltage magnitude, it could not mitigate the voltage fluctuation problem effectively. Voltage control from the PV inverter itself has better performance in helping mitigate

the voltage fluctuation problem, but it has a limitation when the reactive power demand is high because of the thermal limit of the inverter. The bus voltage can best be controlled using SVC voltage regulation which keeps the bus voltage at constant voltage. However, this mode of operation may place a heavy demand on the SVC to supply or absorb reactive power from the network especially when the irradiance is low.

The PV generator model has been integrated into the IEEE 39-bus test system to investigate the impact of faults on the power system. Faults obviously cause voltage drops. If the fault is not cleared fast enough, e.g. for the case where the bus voltage drops below 0.9 p.u, the PV generator may trip and this may lead to a further drop in bus voltage due to the loss of PV generation. This is because all the grid interactive PV inverters are equipped with over/under voltage protection to prevent islanding operation of grid-connected inverters. Typically, PV inverters trip when the grid bus voltage exceeds the range of  $\pm 10\%$  of nominal voltage. The impacts of the penetration of PV generation, the impedance of faults, the protection parameters of the PV generation and the fault clearing time to the fault response were illustrated. The simulation results show that a higher penetration of PV generation, a lower value of fault impedance, a higher value of under-voltage relay setting and longer fault clearing time make the system less transiently stable.

A frequency response controller has been developed and incorporated in the PV generator model. This controller de-loads the PV generator, leaving a margin for power increase. This enables the PV generator to increase as well as decrease the power output when the system frequency changes. This controller was tested using a simple power system model. Simulation results demonstrate that PV generation has the ability to assist in frequency control as specified by proposed new grid codes.

## **8.2 FURTHER WORK**

### **8.2.1 PV Generators with Different MPPT Controllers**

The PV generators analysed in this research rely mostly on a P&O MPPT controller. Due to the "perturb and observe" algorithm, the response time of the PV generator to

disturbances is longer when compared to PV generator with other types of MPPT controllers. If there is a large penetration of PV generation in the future, there will be a mix of PV generations with different types of MPPT controller. In order to obtain a more precise analysis of the impact of PV generations on the power system, different types of PV generator with different types of MPPT controller should be modelled.

### **8.2.2 Simulation Studies on a Model of the UK System**

It was originally planned that a dynamic model of the NGC network would be developed using data provided by National Grid Company. Unfortunately, it was not possible to obtain the data. In the future if the relevant data becomes available, it will be interesting to incorporate the PV generators models into a model of the UK system to investigate the impact of large penetration of PV generation on the system. Besides, the details of the correlation irradiance data of two different cities in the UK, e.g. London and Manchester should be obtained for more details simulation studies of the effect of irradiance change on the UK system.

### **8.2.3 Incorporation of the Frequency Response Controller to Power System Model**

Due to the time constraints, the frequency response controller described in chapter 7 could not be modelled using Eurostag 4.1<sup>TM</sup>. It would be desirable if case studies could be performed on the interaction of the power system with PV generators that are equipped with frequency response controller. Simulations and analysis should be carried out to investigate the effects of frequency response from PV generators on the operation of a realistic power system.

## **8.3 RESEARCH IMPACT AND BENEFITS TO SOCIETY**

The consultation documents issued by the DTI "New and renewable energy, prospects for the 21<sup>st</sup> century" suggest the idea that PV generation has a huge potential for further cost reduction and could be a major contributor to energy needs in the longer term. However the integration of a large number of embedded PV generators will have far reaching consequence not only on the distribution sector but also on the

national transmission and generation system. The effects of this integration on system stability and security should therefore be considered carefully. This research approach helps the generation and distribution company foresee the possible impact of PV generation on system stability. We provide possible methods and solutions to mitigate the negative impact that PV generation might have. This should help PV be one of the technologies that have longer term potential in the UK. If the integration of large PV generation becomes realistic, it will greatly benefit society, as the energy is clean and environmental friendly.

## References

1. R. J. V. Overstraeten and R. P. Mertens, "Physics, technology and use of photovoltaic", Adam Hilger, 1986.
2. C. Prapanavarat, "Investigation of photovoltaic inverters", PhD Thesis submitted to The University of Manchester Institute of Science and Technology, 2000.
3. C. Riordan and R. Hulstrom, "What is an air mass 1.5 spectrum", Solar Energy Research Institute, pp. 1085-1088
4. J. H. R. Enslin, M. S. Wolf, D. B. Snyman, W. Swiegrs, "Integrated photovoltaic maximum power point tracking converter", IEEE Transaction on Industrial Electronics, Vol. 44, No. 6, December 1997, pp. 769-773.
5. N. Mohan, T. M. Undeland and W. P. Robbins, "Power electronic converters, application and design", John Wiley, 1995.
6. C. C. Hua, J. R. Lin and C. M. Shen, "Photovoltaic system characteristics of solar cells and control of battery charger", Proceedings of national science council ROC, Vol. 21, No. 5, pp. 476-484.
7. K. H. Hussein, I. Muta, T. Hoshino, M. Osakada, "Maximum photovoltaic power tracking: an algorithm for rapidly changing atmospheric conditions", IEE

## References

---

- Proceedings on Generation Transmission and Distribution, Vol. 142, No. 1, January 1995, pp. 59-64.
8. W. Bower, M. Ropp, "Evaluation of islanding detection methods for photovoltaic utility-interactive power systems", International Energy Agency Implementing Agreement on Photovoltaic Power Systems, March 2002.
  9. S. Yuyama, T. Ichinose, K. Kimoto, T. Itami, T. Ambo, C.Okado, K. Nakajima, S. Hojo, H. shinohara, S. Ioka, M. Kuniyoshi, "A high-speed frequency shift method as a protection for islanding phenomena of utility interactive PV system", Solar Energy Materials and Solar Cells, vol. 35, 1994, pp. 477-486.
  10. Energy for the Future: Renewable Sources of Energy - White Paper for a Community Strategy and Action Plan, pp. 599, 26 November 1997
  11. O. Wasynczuk, "Modeling and dynamic performance of a self-commutated photovoltaic inverter system," IEEE Trans. on Energy Conversion, Vol. 4, No. 3, pp. 322-328, September 1989
  12. O. Wasynczuk, "Modeling and dynamic performance of a line-commutated photovoltaic inverter system," IEEE Trans. on Energy Conversion, Vol. 4, No. 3, pp. 337-343, September 1989
  13. L.Wang, Y.H. Lin, " Dynamic stability analysis of a photovoltaic array connected to a large utility grid, " IEEE PES Winter Meeting, 2000 Vol. 1, pp. 476-480

## References

---

14. M. Calais, H. Hinz, "A ripple-based maximum power point tracking algorithm for a single-phase, grid connected photovoltaic system," *Solar Energy*, Vol. 63, No. 5, pp. 277-282, 1998
15. K.H. Hussein, L. Muta, T. Hoshino, M. Osakada, "Maximum photovoltaic power tracking: an algorithm for rapidly changing atmospheric conditions," *IEE Proc. Generation, transmission and distribution.*, Vol 142, No. 1, January 1995
16. J.H.R Enslin, M.S. Wolf, D.B. Snyman, W Swiegers, "Integrated photovoltaic maximum power point tracking converter," *IEEE Trans. on Industrial Electronics*, Vol. 44, No. 6, December 1997
17. C. Hua, J. Lin, C. Shen, "Implementation of a DSP-controlled photovoltaic system with peak power tracking," *IEEE Trans. on Industrial electronics*, Vol. 45, No. 1 February 1998
18. S.W.H. de Hann, H. Oldenkamp, C.F.A. Frumau, W. Bonin, "Development of a 100 W resonant inverter for ac modules" *Proceedings of the 12<sup>th</sup> European Photovoltaic Solar Energy Conference*, Amsterdam 1994.
19. Hiyama, S.Kouzuma, T.Imakubo, "Identification of optimal point of PV modules using Neural Network for real time maximum power tracking control," *IEEE Trans. On Energy Conversion*, Vol. 10, No. 2, pp. 360-367, March 1995

## References

---

20. K.Ro, Saifur Rahman, "Two-loop controller for maximizing performance of a grid-connected photovoltaic fuel cell hybrid power plant", IEEE Trans. On Energy Conversion, Vol. 13, No. 3, pp. 276-281, September 1998
21. J.Y. Astic, A. Bihain, M. Jerosolimski, " The mixed Adams-BDF variable step size algorithm to simulate transient and long term phenomena in power systems", IEEE Trans. On Power Systems, Vol. 9, Issue 2, pp.929-935, May 1994
22. B. H. Chowdhury, "Effect of central station photovoltaic plant on power system security", Photovoltaic Specialists Conference, 1990, Conference Record of the Twenty-First IEEE, Vol. 2, 21-25 May 1990, pp. 831-835.
23. E. C. Kern, E. M. Gulachenski, G.A. Kern, "Cloud Effects on Distributed Photovoltaic Generation: Slow Transients at the Gardner, Massachusetts Photovoltaic Experiment", IEEE Transaction on Energy Conversion, Vol. 4, No. 2, June 1989, pp. 184-190.
24. K. Firor, C. M. Whitaker, C. Jennings, "Utility use of PV system ratings", Photovoltaic Specialists Conference, 1990, Conference Record of the Twenty-First IEEE, Vol. 2, 21-25 May 1990, pp. 932-936.
25. W. T. Jewell, T. D. Unruh, "Limits on cloud-induced fluctuation in photovoltaic generation", IEEE Transaction on Energy Conversion, Vol. 5, No. 1, March 1990, pp. 8-14.

## References

---

26. W. T. Jewell, R. Ramakumar, S. R. Hill, "A study of dispersed photovoltaic generation on the PSO system", IEEE Transactions on Energy Conversion, Vol. 3, No. 3, September 1998, pp. 473-478.
27. B. H. Chowdhury, A. W. Sawab, "Evaluating the value of distributed photovoltaic generations in radial distribution systems", IEEE Transaction on Energy Conversion, Vol. 11, No. 3, September 1996, pp. 595-600.
28. J. Ramachandran, N. M. Pearsall and G. A. Putrus, "Reduction in solar radiation fluctuation by spatial smoothing effect" was accepted and to be published in 19<sup>th</sup> European Photovoltaic Solar Energy Conference and Exhibition
29. D. L. Garrett, S. M. Jeter, "A photovoltaic voltage regulation impact investigation techniques: Part I - Model development", IEEE Transaction on Energy Conversion, Vol. 4, No. 1, March 1989, pp. 47-52.
30. L. Wang, Y. H. Lin, "Random fluctuations on dynamic stability of a grid-connected photovoltaic array", Power Engineering Society Winter Meeting, 2001, IEEE, Vol. 3, 28 Jan - 1 Feb 2001, pp. 985-989.
31. F. Giraud, Z. M. Salameh, "Analysis of the effects of a passing cloud on a grid-interactive photovoltaic system with battery storage using neural networks", IEEE Transaction on Energy Conversion, Vol. 14, No. 4, December 1999, pp. 1572-1577.

## References

---

32. F. M. A. Ghali, H. A. El-Khashab, M. S. Abdel-Motaleb, "Dynamic stability analysis of PV-injected power into a parallel AC-DC power system", IEEE, Photovoltaic Specialists Conference - 1994, Vol. 1, 5-9 Dec 1994, pp. 1056 - 1059.
33. R. Ramakumar, J. E. Bigger, "Photovoltaic Systems", Proceedings of the IEEE, Vol. 81, Issue. 3, March 1993, pp. 365-377.
34. P. Kundur, "Power System Stability and Control", McGraw-Hill Inc., 1994.
35. K. Pandiaraj, B. Fox, "Novel voltage control for embedded generation in rural distribution networks", Proceedings PowerCon 2000 International Conference on Power System Technology, vol. 1, 4-7 Dec 2000, pp. 457-462.
36. A. R. Wallace, A. E. Kiprakis, "Reduction of voltage violations from embedded generators connected to the distribution network by intelligent reactive power control", Fifth International Conference on Power System Management and Control, 2002, 17-19 April 2002, pp. 210 - 215.
37. N. G. Hingorani, L. Gyugyi, "Understanding FACTS concepts and technology of flexible ac transmission system", (Book), IEEE Power Engineering Society, New York, 1999.
38. H. Tyll, K. Bergmann, "Use of Static VAR Compensator (SVCs) in high voltage systems", SRBE-KBVE Studiedag, 22<sup>nd</sup> March 1990, Brussels, pp. 1-24.

39. M. Manjrekar, G. Venkataramanan, " Control strategies for a hybrid static reactive compensator", Canadian Conference on Electrical and Computer Engineering, 1996, vol. 2, 26-29 May 1996, pp. 834-837.
40. G. Welsh, K. Bergmann, D. Retzmann, M. Schmidt, "Transient AC/DC simulator and field tests of the closed loop control of the Pelham SVCs", 5<sup>th</sup> European Conference on Power Electronic and Applications, 1993, 13-16 September 1993, vol. 8, pp. 7-12.
41. K. T. G. Wong, "The role of static VAR compensators in staving off voltage collapse", IEE Colloquium on Voltage Collapse (Digest No: 1997/101), 24 April 1997, pp. 5/1-5/5.
42. S. K. Salman, F. Jiang, W. J. S. Rogers, "Investigation of the operating strategies of remotely connected embedded generators to help regulating local network voltage", International Conference on Opportunities and Advances in International Electric Power Generation, 18-20 March 1996, pp. 180-185
43. H. S. Kim, N. Okada, K. Takigawa, "Advanced grid connected PV system with functions to suppress disturbance by PV output variation and customer load change", Solar Energy Material and Solar Cells, vol. 67, issues 1-4, March 2001, pp. 559-569.

## References

---

44. N. Okada, K. Takigawa, "A voltage regulation method for dispersed grid-connected PV system under high-density connection", *Solar Energy Material and Solar Cells*, vol. 75, issues 3-4, 1 February 2003, pp. 637-646.
45. J. G. Slootweg, "Wind Power: Modelling and impact on power system dynamics", PhD Thesis submitted to Delft University of Technology, Delft, The Netherlands, 2003.
46. M.A. Pai, *Energy function analysis for power system stability*, Boston, US: Kluwer Academic Publishers 1989.
47. J. B. Ekanayake, L. Holdsworth, N. Jenkins, "Control of DFIG wind turbines", *IEE Power Engineer*, vol. 17, issue 1, February 2003, pp.28-32.
48. 2. J. B. Ekanayake, L. Holdsworth, N. Jenkins, "Power system frequency response from fixed speed and doubly fed induction generation based wind turbines", *Wind Energy Journal*, vol. 7, issue 1, March 2004, pp. 21-35.
49. 3. "Our energy future – creating a low carbon economy", DTI Energy White Paper, February 2003, [www.dti.gov.uk/energy/whitepaper/ourenergyfuture.pdf](http://www.dti.gov.uk/energy/whitepaper/ourenergyfuture.pdf).
50. The National Grid Company PLC – "Seven Year Statement", May 2001.
51. 4. I. A. Erinmez, D. O. Bickers, G. F. Wood, W. W. Hung, "NGC experience with frequency control in England and Wales – provision of frequency response

## References

---

by generators”, IEEE PES Winter Meeting, 31 January – 4 February 1999, New York, USA.

## List of Publications

1. Y. T. Tan, D. S. Kirschen, N. Jenkins, "Impact of a large penetration of photovoltaic generation on the power system", CIRED 17<sup>th</sup> International Conference on Electricity Distribution, Barcelona, Spain, 12<sup>th</sup>-15<sup>th</sup> May 2003, Session 4, paper no 84.

**The following paper has been accepted for publication but has not yet appeared in print:**

1. Y. T. Tan, D. S. Kirschen, N. Jenkins, "A model of PV generation suitable for stability analysis", accepted for publication in the IEEE Transaction on Energy Conversion

# APPENDICES

## A1 TEST SYSTEM DATA

*Transmission lines (R, X and B in p.u on 100 MVA base)*

Line	R	X	B
5-6	0.0000	0.0040	0.0000
6-7	0.0015	0.0288	1.1730
9-10	0.0010	0.0030	0.0000

*Transformers (R and X in p.u on 100 MVA base)*

Transformer	R	X	Ratio
1-5	0.0000	0.0020	0.9260
2-6	0.0000	0.0045	0.9200
3-7	0.0000	0.0125	0.9107
7-8	0.0000	0.0030	1.0256
7-9	0.0000	0.0026	1.0152
10-11	0.0000	0.0010	0.9350

*Loads*

Bus	P (MW)	Q (Mvar)	
8	3271	1015	(load level 1)
	3320	1030	(load level 2)
	3345	1038	(load level 3)
11	3384	971	(load level 1)
	3435	985	(load level 2)
	3460	993	(load level 3)

## Appendices

### *Shunt capacitors*

Bus	MVar
7	763
8	600
9	1710

### *Generation*

Bus	$P$ (MW)	$V$ (p.u)	
1	4004	0.9800	(load level 1)
	4125	0.9800	(load level 2)
	4189	0.9800	(load level 3)
2	1736	0.9646	(load level 1)
	1736	0.9646	(load level 2)
	1736	0.9646	(load level 3)
3	1154	1.0400	(load level 1)
	1154	1.0400	(load level 2)
	1154	1.0400	(load level 3)

### *Machine parameters*

Machine 1: Infinite bus

Machine 2:  $H = 2.09$ , MVA rating = 2200 MVA

Machine 3:  $H = 2.33$ , MVA rating = 1600 MVA

The following are the parameters of machine 2 and machine 3 on their respective MVA ratings:

$$\begin{array}{llll}
 R_a = 0.0046 & X_l = 0.155 & X''_d = 0.215 & T'_{q0} = 0.56 \\
 X_d = 2.07 & X'_d = 0.28 & X''_q = 0.215 & T''_{d0} = 0.033 \\
 X_q = 1.99 & X'_q = 0.49 & T'_{d0} = 4.10 & T''_{q0} = 0.062
 \end{array}$$

### *Exciters:*

Both machine 2 and machine 3 have thyristor exciters with a gain of 400 and the sensing circuit-time constant of 0.02 seconds.

Overexcitation limiter for machine 3:

$$I_{fd\ max1} = 3.02\ \text{p.u}$$

$$I_{fd\ max2} = 4.60\ \text{p.u}$$

$$K_2 = 12.6\ \text{p.u}$$

$$I_{LIM} = 3.85\ \text{p.u}$$

$$K_1 = 0.248\ \text{p.u}$$

The OXL is included for generator 3 only. The block diagram of the OXL is shown in Figure A1.1.

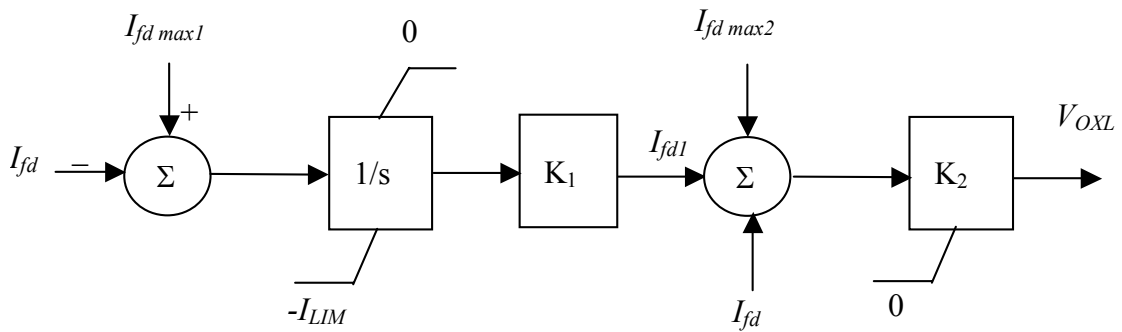


**Figure A1.1: Block Diagram of OXL**

**B1 IEEE-39 Bus Test System Load Flow Data**

*Transmission lines (R, X and B in p.u)*

Line	R	X	B
1-2	0.0035	0.0411	0.699
1-39	0.001	0.025	0.75
2-3	0.0013	0.0151	0.2572
2-25	0.007	0.0086	0.146
3-4	0.0013	0.0213	0.2214
3-18	0.0011	0.0133	0.2138
4-5	0.0008	0.0128	0.1342
4-14	0.0008	0.0129	0.1382
5-6	0.0002	0.0026	0.0434
5-8	0.0008	0.0112	0.1476
6-7	0.0006	0.0092	0.113
6-11	0.0007	0.0082	0.1389
7-8	0.0004	0.0046	0.078
8-9	0.0023	0.0363	0.3804
9-39	0.001	0.025	1.2
10-11	0.0004	0.0043	0.073
10-13	0.0004	0.0043	0.073
13-14	0.0009	0.0101	0.1723
14-15	0.0018	0.0217	0.366
15-16	0.0009	0.0094	0.171
16-17	0.0007	0.0089	0.1342
16-19	0.0016	0.0195	0.304
16-21	0.0008	0.0135	0.2548
16-24	0.0003	0.0059	0.068
17-18	0.0007	0.0082	0.1319
17-27	0.0013	0.0173	0.3216
21-22	0.0008	0.014	0.2565
22-23	0.0006	0.0096	0.1846
23-24	0.0022	0.035	0.361
25-26	0.0032	0.0323	0.513
26-27	0.0014	0.0147	0.2396
26-28	0.0043	0.0474	0.7802
26-29	0.0057	0.0625	1.029
28-29	0.0014	0.0151	0.249

## Appendices

---

### *Transformers (R and X in p.u)*

Transformer	<i>R</i>	<i>X</i>	Ratio
2-30	0	0.0181	0.975
6-31	0	0.025	0.91
10-32	0	0.02	0.93
11-12	0.0016	0.0435	0.97
12-13	0.0016	0.0435	0.97
19-20	0.0007	0.0138	0.97
19-33	0.0007	0.0142	0.95
20-34	0.0009	0.018	0.991
22-35	0	0.0143	0.975
23-36	0.0005	0.0272	1
25-37	0.0006	0.0232	0.985
29-38	0.0008	0.0156	0.975

---

### *Loads*

Bus	<i>P</i> (MW)	<i>Q</i> (Mvar)
1	966	109
3	322	2
4	500	184
7	234	84
8	522	176
9	138	16
12	9	88
15	320	153
16	329	32
18	158	30
20	680	103
21	274	115
22	247	85
24	309	-92
25	224	47
26	139	17
27	281	75
28	206	28
29	284	27

---

## Appendices

---

### *Generation*

Bus	$P$ (MW)	$V$ (p.u)
30	250	1.04
31	581	0.98
32	650	1.03
33	632	1.00
34	508	1.01
35	650	1.02
36	560	1.02
37	540	1.03
38	830	1.03
39	1000	1.03

---

### **B2 IEEE-39 Bus Test System Load Flow Results**

Bus	$V$ (p.u)	$Angle$ (p.u)
1	1.01	-14.9
2	1.04	-9.5
3	1.03	-11.6
4	1.01	-11.4
5	1.02	-9.6
6	1.02	-8.9
7	1.01	-10.8
8	1.01	-11.4
9	1.03	-8.5
10	1.04	-6.9
11	1.03	-7.6
12	1.04	-7.7
13	1.03	-7.7
14	1.02	-9.5
15	1.01	-10.3
16	1.02	-9.0
17	1.02	-10.3
18	1.02	-11.2
19	1.03	-4.2
20	1.00	-5.6
21	1.01	-6.8
22	1.02	-2.3

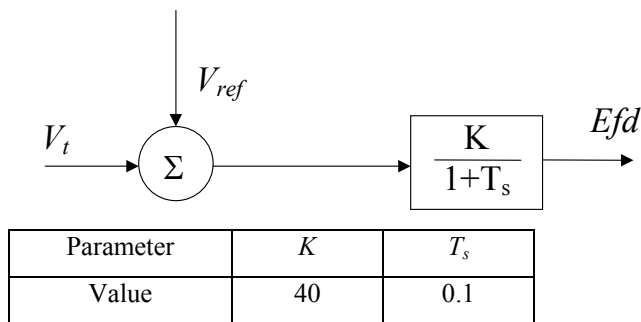
## Appendices

Bus	$V$ (p.u)	$Angle$ (p.u)
23	1.02	-1.4
24	1.02	-8.8
25	1.05	-8.0
26	1.04	-8.8
27	1.03	-10.7
28	1.05	-5.3
29	1.05	-2.5
30	1.04	-7.0
31	0.98	0.0
32	1.03	0.5
33	1.00	1.0
34	1.01	-0.4
35	1.02	3.0
36	1.02	7.0
37	1.03	-1.2
38	1.03	4.6
39	1.03	-4.9

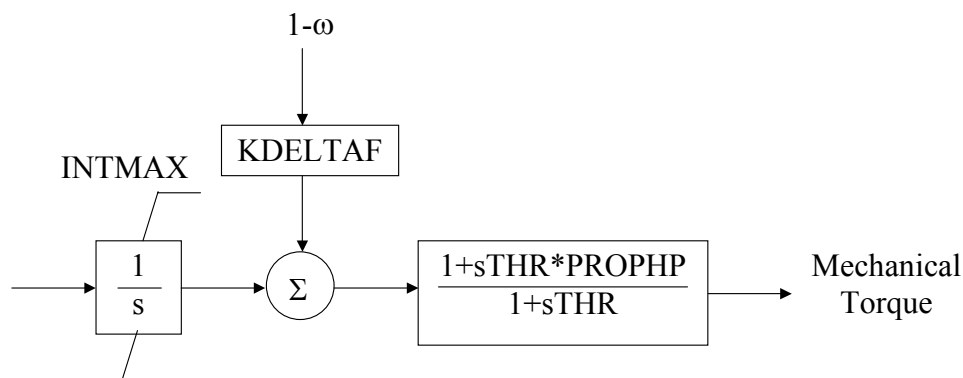
### B3 IEEE-39 Bus Test System Dynamic Data

GEN	$R_a$ (p.u)	$X_l$ (p.u)	$X_d$ (p.u)	$X_q$ (p.u)	$X_d'$ (p.u)	$X_q'$ (p.u)	$H$ (MWs/MVA)
Bus-30	0	0.0001	0.31001	0.31001	0.31	9999	3.5
Bus-31	0	0.0001	0.69701	0.69701	0.697	999	2.525
Bus-32	0	0.0001	0.53101	0.53101	0.531	999	2.98333
Bus-33	0	0.0001	0.43601	0.43601	0.436	9999	2.38333
Bus-34	0	0.0001	1.32001	1.32001	1.32	9999	2.16667
Bus-35	0	0.0001	0.5001	0.5001	0.5	9999	2.9
Bus-36	0	0.0001	0.49001	0.49001	0.49	9999	2.2
Bus-37	0	0.0001	0.57001	0.57001	0.57	9999	2.025
Bus-38	0	0.0001	0.57001	0.57001	0.57	9999	2.878
Bus-39	0	0.0001	0.06001	0.06001	0.06	9999	41.66667

Exciters:



Governor Model:



Parameter	$INTMAX$	$THR$	$PROPHP$	$KDELTA F$
Value	1.1	10	0.3	25

**B4 Amount of PV Generation Injected at Each Bus for Section 6.4.2.1**

Bus	$P$ (MW): Shaded regions represent PV generation				
	Figure 6.4 (10.48%)	Figure 6.5 (20.96%)	Figure 6.6 (29.16%)	Figure 6.7 (37.86%)	Figure 6.8 (41.9%)
30	250	250	250	250	250
31	581	581	581	581	581
32	650	650	650	650	650
33	632	632	632	632	632
34	508	508	508	508	508
35	650	650	650	650	650
36	560	560	560	560	560
37	540	540	540	540	540
38	830	830	830	830	830
39	1000	1000	1000	1000	1000